

University of Nevada, Reno

**Modeling the Effect of Riparian Shading on Water Temperature
for Portions of the Carson River, Western Nevada, USA**

A thesis submitted in partial fulfillment of the
requirements for the degree of Master of Science in
Hydrology

by:

Christopher B. Garner

Kenneth C. McGwire/Thesis Advisor

May, 2007



University of Nevada, Reno
1950

THE GRADUATE SCHOOL

We recommend that the thesis
prepared under our supervision by

CHRISTOPHER B. GARNER

Entitled

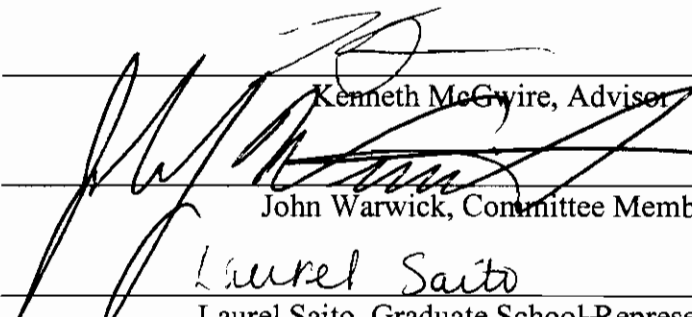
Modeling The Effect Of Riparian Shading On Water Temperature For Portions Of The
Carson River, Western Nevada, USA

be accepted in partial fulfillment of the
requirements for the degree of

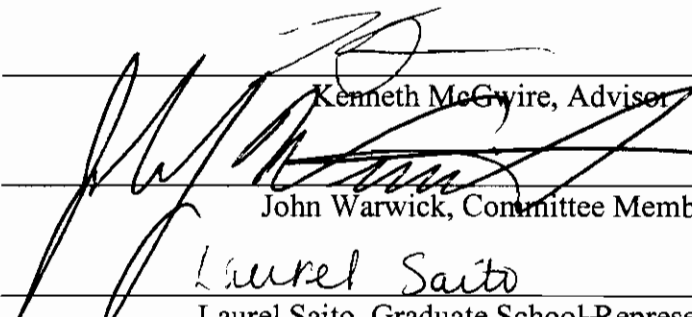
MASTER OF SCIENCE


Kenneth McGwire, Advisor

John Warwick, Committee Member


Laurel Saito

Laurel Saito, Graduate School Representative


Marsha H. Read, Ph. D., Associate Dean, Graduate School

May, 2007

ACKNOWLEDGEMENTS

It is difficult to overstate my gratitude to my advisor, Dr. Kenneth C. McGwire. With his enthusiasm, inspiration, patience, and his great efforts to explain things clearly and simply, he helped to make this thesis an exciting and valuable scientific learning experience. Without his expertise and guidance, many of the complex modifications to the HEATSOURCE model code would not have been possible.

I'd like to acknowledge my committee members Dr. John Warwick and Dr. Laurel Saito for their contributions. Dr. Warwick contributed his experience with the hydraulics of the Carson River, and his knowledge of water quality modeling and uncertainty analysis. Dr. Saito was an asset for her knowledge and experience with temperature and water quality modeling studies. I thank you both for your guidance.

I would also like to thank the United States Environmental Protection Agency for funding this research. Alan McKay of DRI laid much of the groundwork in securing funding for the project by corresponding with Nevada's Congressional Delegation who served with Congressman Jim Gibbons.

Paul Pugsley of the Carson Valley Conservation District was instrumental in getting access to many private properties in our study area. His knowledge and understanding of the geographical, historical, and political aspects of the Carson River were invaluable. Without Paul's efforts, the spatial density with which we sampled our system would not have been possible.

Randy Pahl of the Nevada Division of Environmental Protection conveyed NDEP's needs in terms of what the project should accomplish, the potential uses for our

model, as well as contributing information regarding the water quality issues on the Carson River. Randy also contributed field assistance during the acquisition of our PAR survey.

There were many people at the Desert Research Institute, other than those I've already mentioned, who should be acknowledged for their contributions. I'd like to thank Zach Latham for passing on the experience and knowledge he gained while modeling dissolved oxygen processes in the Carson River. I'd like to thank Dr. Richard Susfalk for his assistance with field monitoring equipment and for contributing water temperature data from his turbidity stations in our study area. I'd like to thank Dr. Gayle Dana for allowing us to use her meteorological equipment for two field seasons. I'd like to thank Jim Brock for his encouragement, and for passing on his experience with stream temperature modeling. Dr. Christian H. Fritsen was always available to make sure I understood the fundamentals of hydrologic optics and stream ecology. Dr. Fritsen also allowed us the use of streamflow and PAR measuring equipment, which facilitated the development of rating curves and modifications to the model code. I'd like to thank Jeramie Memmott for his ability to make ideas reality and Clint Davis for opening my eyes to the amazing microscopic world of living organisms in a single drop of Carson River water. I'd like to thank Brian Fitzgerald for downloading two field seasons of meteorological data at the Genoa Golf Course station and for helping me disassemble that bulky piece of equipment. I'd like to thank Mitch Goldfin for making our temperature stake design a reality and Alex Kameda for her encouragement.

Doug Maurer of the USGS was a big help in getting access to groundwater wells adjacent to the Carson River and also in giving us insight into the ground-surfacewater exchange processes in our study area.

Last but definitely not least, I'd like to thank my family for being so supportive of me during the completion of this project, and throughout the more difficult times in my life.

ABSTRACT

The HEATSOURCE 7.0 temperature model was modified to test whether hypothesized revegetation strategies could reduce water temperatures to 20°C along a portion of the Carson River in western Nevada. Modifications to the HEATSOURCE model made use of high-resolution LIDAR and image data of the study area to improve the representation of channel morphology and to better disaggregate parameters relating to energy balance. The model was modified to work with the Multi-Objective Complex global optimization algorithm. A simulation of riparian zone revegetation was performed by transplanting the vegetation attributes from a reach of substantial riparian tree cover to a sparsely vegetated 14 km long reach in the study area. Results showed that the maximum revegetation simulation produced measurable reductions in stream temperature. However, there were no days over the entire validation period when the maximum daily stream temperature would be expected to meet the 20°C threshold in the revegetated reach.

TABLE OF CONTENTS

MODELING THE EFFECT OF RIPARIAN SHADING ON WATER TEMPERATURE FOR PORTIONS OF THE CARSON RIVER, WESTERN NEVADA, USA.....	I
ACKNOWLEDGEMENTS.....	I
ABSTRACT.....	IV
LIST OF FIGURES.....	VII
LIST OF TABLES.....	XI
1 INTRODUCTION.....	1
2 BACKGROUND.....	8
2.1 STUDY AREA.....	
2.2 GEOSPATIAL DATA.....	17
3 METHODS.....	18
3.1 FIELD DATA COLLECTION.....	18
3.1.1 <i>Measurement Station Type 1: Inflow / Outflow /Streamflow</i>	19
3.1.2 <i>Measurement Station Type 2: In-Stream Conditions</i>	20
3.1.3 <i>Measurement Station Type 3: Air Temperature / Relative Humidity</i>	21
3.1.4 <i>Measurement Station Type 4: Solar Radiation / Wind Speed</i>	22
3.2 DATA SUMMARY.....	23
3.2.1 2005.....	23
3.2.2 2006.....	24
3.3 HEATSOURCE TEMPERATURE MODEL.....	25
3.3.1 <i>Hydrodynamics</i>	26
3.3.2 <i>Flow Routing</i>	27
3.3.3 <i>Shading Methodology</i>	28
3.3.4 <i>Heat Transfer Components</i>	32
3.4 MODIFICATIONS TO HEATSOURCE.....	35
3.4.1 <i>Channel Modifications</i>	35
3.4.2 <i>Modulation of Wind Velocity</i>	40
3.4.3 <i>Wind Shelter Coefficient and Canopy Shade Factor</i>	42
3.4.4 <i>Conduction Flux</i>	42
3.4.5 <i>Spatially Distributed Alluvium Temperature</i>	44
3.4.6 <i>Topographic Sampling</i>	45
3.4.7 <i>LIDAR-Derived Shading Attributes</i>	45
3.5 HEATSOURCE PROGRAMMING ERRORS.....	46
3.5.1 <i>Separation of Vegetation Shading From Fine Scale Topographic Shading</i>	46
3.5.2 <i>Evaporative flux calculation</i>	47
3.6 MODEL CALIBRATION.....	47
3.6.1 <i>Manual Calibration</i>	47
3.6.2 <i>Parameter Estimation</i>	58
3.7 MODEL VALIDATION.....	64
3.8 SIMULATING REVEGETATION SCENARIOS.....	67
3.9 INCREASED STREAMFLOW SCENARIOS.....	68
4 RESULTS.....	69
4.1 CALIBRATION RESULTS.....	69
4.1.1 <i>MOCOM Results</i>	69
4.1.2 <i>Daily Maximum Predictions</i>	69
4.2 VALIDATION RESULTS.....	73

4.2.1	<i>Daily Maximum Predictions</i>	73
4.2.2	<i>Longitudinal Profiles</i>	77
4.2.3	<i>Thermal Infrared Survey</i>	79
4.3	SIMULATING REVEGETATION SCENARIOS.....	81
4.3.1	<i>Change in Energy Components-Post Revegetation</i>	82
4.4	INCREASED STREAMFLOW SCENARIOS	85
5	DISCUSSION	87
6	LITERATURE CITED	99
7	APPENDIX A-FIGURES FROM PARAMETER ESTIMATION PROCEDURE	103
8	APPENDIX B-WATER AND STREAMBED TEMPERATURE DATA (2005)	111
9	APPENDIX C-WATER TEMPERATURE DATA (2006)	125

LIST OF FIGURES

FIGURE 1-LOCATION OF THE CARSON RIVER BASIN AND LOCATION OF STUDY AREA	9
FIGURE 2-CARSON RIVER STUDY AREA AND SAMPLING LOCATIONS.	10
FIGURE 3-STATION TYPE 2A AND 2B, WATER COLUMN AND STREAMBED TEMPERATURE	22
FIGURE 4-MEASUREMENT STATION TYPE 3, AND STATION TYPE 4	23
FIGURE 5-WATER TEMPERATURE MONITORING DESIGN FOR 2006 SAMPLING PERIOD	25
FIGURE 6-LANDCOVER POLYGONS (BOYD AND KASPER, 2004).....	29
FIGURE 7-SCHEMATIC OF LANDCOVER ZONES (BOYD AND KASPER, 2004).....	30
FIGURE 8-LANDCOVER RADIAL SAMPLING PATTERN (BOYD AND KASPER, 2004).....	30
FIGURE 9-EFFECTIVE SHADE DEFINED (BOYD AND KASPER, 2004).....	31
FIGURE 10-SCHEMATIC OF CHANNEL MODIFICATIONS	36
FIGURE 11-SIMBANKS MAIN-CHANNEL	38
FIGURE 12-SCHEMATIC OF FLOW DIFFERENCING FOR SUB-CHANNEL DEVELOPMENT	39
FIGURE 13-WIND SPEED REGRESSION	42
FIGURE 14-EIGHT ACCRETION ZONES.....	52
FIGURE 15- WATER AND STREAMBED TEMPERATURE FOR LAST LOW HEAD DAM SITE	53
FIGURE 16-STREAMFLOW RATING CURVE FOR SITE 9.....	53
FIGURE 17-CARSON CITY GAUGE PREDICTED AND OBSERVED STREAMFLOW (CALIBRATION PERIOD).	54
FIGURE 18-DEER RUN ROAD GAUGE PREDICTED AND OBSERVED STREAMFLOW (CALIBRATION PERIOD)	54
FIGURE 19-COMPARISON OF ORIGINAL HEATSOURCE SOLAR FLUX PREDICTED VS. OBSERVED	56
FIGURE 20-COMPARISON OF MODIFIED HEATSOURCE SOLAR FLUX PREDICTED VS. OBSERVED.....	56
FIGURE 21-STREAMFLOW RATING CURVE FOR SITE 19.....	65
FIGURE 22-CARSON CITY GAUGE PREDICTED AND OBSERVED STREAMFLOW (VALIDATION PERIOD)	66
FIGURE 23-DEER RUN ROAD GAUGE PREDICTED AND OBSERVED STREAMFLOW (VALIDATION PERIOD).....	67
FIGURE 24-DIEL TEMPERATURE PROFILE FOR SITE 10 (CALIBRATION PERIOD).....	70
FIGURE 25-DIEL TEMPERATURE PROFILE FOR SITE 14 (CALIBRATION PERIOD).....	70
FIGURE 26-DIEL TEMPERATURE PROFILE FOR SITE 21 (CALIBRATION PERIOD).....	71
FIGURE 27-99% CONFIDENCE INTERVAL FOR THE CALIBRATION PERIOD (GLUE METHOD).....	72

FIGURE 28-DIEL TEMPERATURE PROFILE FOR SITE 10 (VALIDATION PERIOD)	74
FIGURE 29-DIEL TEMPERATURE PROFILE FOR SITE 15 (VALIDATION PERIOD)	75
FIGURE 30-DIEL TEMPERATURE PROFILE FOR SITE 19 (VALIDATION PERIOD)	75
FIGURE 31-DIEL TEMPERATURE PROFILE FOR SITE 22 (VALIDATION PERIOD)	76
FIGURE 32-BOX PLOTS OF THE DAILY MAXIMUM TEMPERATURE RANGE FOR THE FOUR VALIDATION SITES...	77
FIGURE 33-LONGITUDINAL PROFILE (BEST-FIT SCENARIO).....	78
FIGURE 34-LONGITUDINAL PROFILE (WORST-FIT SCENARIO)	79
FIGURE 35-COMPARISON OF PREDICTED STREAM TEMPERATURES AND THE TIR SURVEY TEMPERATURES....	80
FIGURE 36-COMPARISON OF PREDICTED STREAM TEMPERATURES FOR EXISTING VEGETATION (RED DOTS) AND SIMULATED VEGETATION (BLUE Xs).....	82
FIGURE 37-SHORTWAVE FLUX FOR EXISTING AND SIMULATED VEGETATION	84
FIGURE 38- LONGWAVE FLUX FOR EXISTING AND SIMULATED VEGETATION.....	84
FIGURE 39- EVAPORATIVE FLUX FOR EXISTING AND SIMULATED VEGETATION.....	84
FIGURE 40- CONVECTIVE FLUX FOR EXISTING AND SIMULATED VEGETATION	85
FIGURE 41- CONDUCTIVE FLUX FOR EXISTING AND SIMULATED VEGETATION	85
FIGURE 42- TOTAL HEAT FLUX FOR EXISTING AND SIMULATED VEGETATION	85
FIGURE 43-LONGITUDINAL PROFILES FOR EXISTING VEGETATION WITH ACTUAL FLOW (RED DOTS), EXISTING VEGETATION WITH HIGH FLOW (BLACK DOTS), AND SIMULATED VEGETATION WITH HIGH FLOW (PURPLE DOTS).....	87
FIGURE 44-SENSITIVITY OF WIND COEFFICIENT A	103
FIGURE 45-SENSITIVITY OF WIND COEFFICIENT B	103
FIGURE 46-SENSITIVITY OF WIND SHELTER COEFFICIENT.....	104
FIGURE 47-SENSITIVITY OF CANOPY SHADE FACTOR	104
FIGURE 48-SENSITIVITY OF CONDUCTION LAYER DEPTH.....	105
FIGURE 49-SENSITIVITY OF ALLUVIUM TEMPERATURE UPPER #1	105
FIGURE 50-SENSITIVITY OF ALLUVIUM TEMPERATURE UPPER #2	106
FIGURE 51-SENSITIVITY OF ALLUVIUM TEMPERATURE LOWER	106

FIGURE 52-MOCOM SOLUTION FOR WCA AND WCB.....	107
FIGURE 53-SENSITIVITY OF WIND SHELTER COEFFICIENT (2 ND SENSITIVITY)	107
FIGURE 54-SENSITIVITY OF CANOPY SHADE FACTOR (2 ND SENSITIVITY)	108
FIGURE 55-SENSITIVITY OF CONDUCTION LAYER DEPTH (2 ND SENSITIVITY)	108
FIGURE 56-SENSITIVITY OF ALLUVIUM TEMPERATURE UPPER #1 (2 ND SENSITIVITY)	109
FIGURE 57-SENSITIVITY OF ALLUVIUM TEMPERATURE UPPER #2 (2 ND SENSITIVITY)	109
FIGURE 58-SENSITIVITY OF ALLUVIUM TEMPERATURE LOWER (2 ND SENSITIVITY).....	110
FIGURE 59- FINAL MOCOM CALIBRATION SOLUTION (CIRCLED)	110
FIGURE 60-WATER AND STREAMBED TEMPERATURES FOR GENOA GOLF COURSE (SITE 4).....	111
FIGURE 61-WATER AND STREAMBED TEMPERATURES FOR LAST LOW HEAD DAM (SITE 8).....	112
FIGURE 62-WATER AND STREAMBED TEMPERATURES FOR LIPPENCOTT SKI RANCH(SITE 10).....	113
FIGURE 63-WATER AND STREAMBED TEMPERATURES FOR AMBROSETTI CREEK INLET (SITE 11)	114
FIGURE 64-WATER AND STREAMBED TEMPERATURES FOR CRADLEBAUGH BRIDGE (SITE 12).....	115
FIGURE 65-WATER AND STREAMBED TEMPERATURES FOR SUN RIDGE GOLF COURSE (SITE 13).....	116
FIGURE 66-WATER AND STREAMBED TEMPERATURES FOR VNT (SITE 14).....	117
FIGURE 67-WATER AND STREAMBED TEMPERATURES FOR MCTARNAHAN (SITE 15)	118
FIGURE 68-WATER AND STREAMBED TEMPERATURES FOR FOERSCHLER RANCH (SITE 17).....	119
FIGURE 69-WATER AND STREAMBED TEMPERATURES FOR MEXICAN DAM (SITE 18).....	120
FIGURE 70-WATER AND STREAMBED TEMPERATURES FOR RIVERVIEW PARK (SITE 19)	121
FIGURE 71-WATER AND STREAMBED TEMPERATURES FOR RIVERVIEW PARK RETURN FLOW (UPSTREAM OF SITE 19).....	122
FIGURE 72-WATER AND STREAMBED TEMPERATURES FOR EMPIRE GOLF COURSE (SITE 20).....	123
FIGURE 73-WATER AND STREAMBED TEMPERATURES FOR MORGAN MILL ROAD (SITE 21).....	124
FIGURE 74-WATER TEMPERATURES FOR GENOA GOLF COURSE (SITE 4).....	125
FIGURE 75-WATER TEMPERATURES FOR LAST LOW HEAD DAM (SITE 8).....	126
FIGURE 76-WATER TEMPERATURES FOR LIPPENCOTT SKI RANCH (SITE 10).....	127
FIGURE 77-WATER TEMPERATURES FOR AMBROSETTI CREEK INLET (SITE 11)	128

FIGURE 78-WATER TEMPERATURES FOR MCTARNAHAN (SITE 15) 129

FIGURE 79-WATER TEMPERATURES FOR FOERSCHLER RANCH (SITE 17)..... 130

FIGURE 80-WATER TEMPERATURES FOR MEXICAN DAM (SITE 18) 131

FIGURE 81-WATER TEMPERATURES FOR RIVERVIEW PARK RETURN FLOW (DOWNSTREAM OF SITE 19)..... 132

FIGURE 82-WATER TEMPERATURES FOR RIVERVIEW PARK (SITE 19)..... 133

FIGURE 83-WATER TEMPERATURES FOR DEER RUN ROAD (SITE 22)..... 134

LIST OF TABLES

TABLE 1-EXISTING TEMPERATURE STANDARDS (NAC) FOR GENOA GAUGE TO CARSON GAUGE	12
TABLE 2-EXISTING TEMPERATURE STANDARDS (NAC) FOR CARSON GAUGE TO DEER RUN ROAD GAUGE ...	12
TABLE 3-SAMPLING LOCATIONS INDICATING WHAT TYPE DATA WAS COLLECTED IN 2005 AT EACH SITE	20
TABLE 4-STREAMBED THERMAL PROPERTIES.....	55
TABLE 5-PARAMETER RANGES FOR INITIAL SENSITIVITY ANALYSIS (EIGHT PARAMETERS).....	63
TABLE 6-MOCOM CALIBRATION RESULTS	69
TABLE 7- STATISTICS FOR MAXIMUM DAILY STREAM TEMPERATURE PREDICTIONS (CALIBRATION PERIOD)..	71
TABLE 8-STATISTICS FOR MAXIMUM DAILY STREAM TEMPERATURE PREDICTIONS (VALIDATION PERIOD).....	74

1 INTRODUCTION

Stream water temperature is one of the more important parameters in understanding stream ecosystem dynamics because many of the physical, chemical, and biological properties of water are a function of temperature. Thus, the thermal condition of a stream has a considerable impact on the ability of aquatic organisms to feed, metabolize, reproduce, and survive (Coutant, 1976). This is especially true for coldwater aquatic species, such as trout, that have physiological optima $\leq 20^{\circ}\text{C}$ (Eaton et al., 1995). In the Carson River, high water temperature is a concern with respect to the river's existing classification as a coldwater fishery from the California-Nevada state line to the Deer Run Road gauge in Nevada (Figure 1). Irrigation withdrawals in the basin, coupled with the absence of near-stream shade producing vegetation, have contributed to daily maximum water temperatures near 30°C .

Quantifying the effect of riparian shading on stream water temperature plays a crucial role in developing potential stream revegetation plans. Of all the heat fluxes to a stream, the dominant flux is solar radiation (Sinokrot and Stefan, 1993; Marcott and Duong, 1973). Solar heating of rivers is controlled at multiple spatial scales. At a coarse scale, the topography of the region controls the potential duration of sun exposure along different stretches of the river. At a finer scale, solar heating will depend on channel morphology and shading from vegetation and other structures in the riparian zone. The amount of riparian shading in near stream environments is important because it intercepts a fraction of the total incoming shortwave radiation, alters wind, humidity, and air temperature conditions, and emits longwave radiation. Such changes in the stream's

microclimate modify the various heat fluxes at the air-water interface, which can produce fluctuations in discharge and temperature. To understand the complex interactions of these factors and make informed decisions regarding stream ecosystem management, natural resource managers can use computer simulations to model stream temperature. Depending on the desired model output and the complexity of the system, stream water temperature is usually predicted using one of three types of models: regression; stochastic; or deterministic.

The purpose of regression models is to develop a statistical relationship between an independent predictor variable and a dependent response variable(s). Single and multiple parameter linear regression are the most commonly used methods for predicting water temperature, although logistic regressions have also been applied. Single parameter linear regression models have the advantage of requiring only daily, weekly, or monthly average air temperature as the input variable and have been used in numerous stream temperature modeling studies (Johnson, 1971; Smith, 1981; Crisp & Howson, 1982; Stefan and Preud'homme, 1993; Webb & Nobilis, 1997). Johnson (1971) fitted a sine function to observed monthly mean stream temperature and determined that a linear relationship existed between the phase angle and annual mean stream temperature. Smith (1981) used average monthly minimums and maximums of air temperature as well as monthly means for developing monthly air-water temperature regressions. Crisp and Howson (1982) developed linear regressions using 5 and 7 day mean air and water temperatures. Stefan and Preud'homme (1993) demonstrated that the correlation of air-water linear regressions increases as the temporal scale of input data increases from hourly to daily to weekly. However, a study by Webb and Nobilis (1997) found the

regression between monthly mean values of air temperature and water temperature was better correlated ($r^2 > 0.95$) than those developed for annual mean values ($r^2 < 0.55$).

Multiple linear regression techniques incorporate additional stream parameters such as discharge, channel depth, or solar radiation. For example, Neumann et al. (2003) developed a stepwise multiple regression to select the most statistically significant input parameters for predicting water temperature on the Truckee River at Reno, Nevada. The stepwise procedure selected daily maximum air temperature and average daily flow as the best subset of regression parameters by minimizing the residual error between observed and predicted data. The model showed good correlation to observed stream temperature data ($r^2 = 0.90$). Using a prediction confidence distance, which is a function of the model uncertainty, the model was able to estimate the additional flow necessary to meet temperature criteria (Neumann et al., 2003). Other multiple regression models have been used with similar input parameters to predict stream temperature. Jeppesson and Iverson (1987) used solar radiation along with channel depth and air temperature as input variables, whereas Jourdonnais et al. (1992) developed a multiple regression that was based on stream discharge and the mean, maximum, and minimum air temperature from the present and previous day.

Logistic regressions are used in favor of linear regression when air-water temperature relationships are non-linear. In strongly gaining streams, groundwater discharge can reduce the daily maximum water temperature, which gives the system a non-linear behavior (Caissie, 2006). For example, Smith (1981) attributed the poor correlation of predictions to observed data for linear regressions at one site to a large amount of groundwater discharge. At sites where this is the case, a logistic regression can

be used to fit the non-linearity of the system. Mohseni et al. (1998) developed a four parameter logistic regression based on weekly air temperatures for 584 United States Geological Survey (USGS) streamflow gauging stations.

Stochastic methods are used in modeling stream temperature by separating an observed water temperature time series into a long term component and a short term component. In this process, the long term component which captures the annual fluctuations in temperature is isolated from the short-term residual component. The short term residuals are an expression of the divergence from the annual component. Caissie et al. (1998) used this approach to predict maximum daily water temperatures in a relatively small stream using air temperature as the input variable. Their methodology used the short term residuals to model water temperatures using a multiple regression, second order Markov process analysis, and a Box-Jenkins time series model (Cassie et al., 1998). The three methods produced similar results; however, the second order Markov analysis was favored “based on its simplicity in development” (Cassie et al., 1998).

Stochastic and regression models have the advantage of being computationally simple and applicable to locations where air temperature or streamflow data are available. While regression or stochastic models can be used effectively to predict water temperature at discrete locations, they have problems with extrapolation when trying to project such empirical relationships into the future or to locations where measurements were not actually made. This level of predictive capability calls for a deterministic model that represents the processes influencing water temperature in a realistic, though tractable, manner.

Deterministic models simulate heat transfer by accounting for the various fluxes of energy to the stream. Excluding advection, heat transfer in streams is driven by the following fluxes: diffuse and direct shortwave radiation ($\Phi_{\text{shortwave}}$), longwave radiation (Φ_{longwave}), evaporation ($\Phi_{\text{evaporation}}$), convection at the air-water interface ($\Phi_{\text{convection}}$), and streambed conduction ($\Phi_{\text{conduction}}$). The total net heat flux (Φ_{total}) into or out of a stream is the sum of the above components ($\text{W} \cdot \text{m}^{-2}$) (1).

$$\Phi_{\text{total}} = \Phi_{\text{shortwave}} + \Phi_{\text{longwave}} + \Phi_{\text{evaporation}} + \Phi_{\text{convection}} + \Phi_{\text{conduction}} \quad (1)$$

Each of these components can be affected by anthropogenic activities, atmospheric conditions, hydrology, topography, riparian vegetation, and substrate conditions. Studies that have used deterministic models include Sinokrot and Stephan (1993), Gu et al. (1998), Morin and Couillard (1990), and Brock and Caupp (2004). Sinokrot and Stephan (1993) used a modified version of the dynamic stream water temperature simulation model, MNSTREM to solve the one-dimensional unsteady heat advection-dispersion equation. Using a steady flow assumption, MNSTREM accounts for the energy exchange at the air-water interface as well as heat conduction to the streambed. Output predictions for hourly and daily water temperature were accurate in the range of 0.2°C to 1°C, respectively. Analysis of the relative importance of the energy components showed solar radiation to be the most important heat flux across the stream atmosphere boundary. Streambed conduction was shown to be an important component in shallow streams. Gu et al. (1998) used the water temperature equilibrium concept and the bulk heat exchange coefficient to obtain a discharge threshold at which the rate of water temperature increase begins to dramatically increase. Morin and Couillard (1990) adapted the CEQEAU hydrological model to incorporate a temperature model based on

an energy budget approach. Brock and Caupp (2004) adapted the DSSAMt model to assess the environmental impacts of the Truckee River Operating Agreement (TROA), which included water allocation, protection of wetlands, and settlement of tribal claims. DSSAMt features a one-dimensional steady-state model that solves the transport and exchange equation for temperature.

Deterministic models such as those mentioned above are better suited to scenario analysis than regression or stochastic models because their formulation is based on the mechanisms that drive the system. In the case of stream temperature models, they consider the underlying physical processes that influence the heat status of the river. For this reason, deterministic models can overcome the dimensional limitations of empirical models. They have the ability to simulate temperature at high spatial and temporal scales, and can be implemented in a one-dimensional mode on the assumption that rivers are vertically and laterally well mixed. The main problems with a deterministic approach are substantial input data requirements and computational burden, but the ability to represent the temporal and spatial variability of the system often outweighs these disadvantages. Overall, the model's intended purpose will be the primary factor in determining what type of water temperature model is used.

In this study, a model was needed that incorporated the effects of riparian shading on water temperatures. Deterministic models have been used to evaluate the impact of different restoration scenarios on stream temperature. For example, SNTEMP has been applied in evaluating the thermal habitat conditions of coldwater fish species (Bartholow, 1991), in analyzing the effect of riparian vegetation removal (Sullivan et al., 1990; Bartholow, 2000), and in channel restoration scenarios (Bartholow, 1991, 1993). Chen et

al. (1998) built upon the experience of several other investigators in developing the SHADE-HSPF model that incorporated information on the effect of shading from vegetation adjacent to the stream for a forested watershed in Oregon. The DSSAMt model (Brock and Caupp, 2004) was modified to include a shading component that took the coordinates of ridgelines from topography and streamside vegetation as input. In the shade model STREAMLINE, Rutherford et al. (1997) showed that in small pasture streams, shade fractions of 50% were able to maintain daily maximum water temperatures at 25°C, but to reduce maximum daily water temperatures below 20°C, shade fractions of 70% were necessary.

The deterministic models described above simulate streamflow in a steady state mode on the assumption that substantial variations in flow do not occur over the modeled period. However, on the Carson River, irrigation withdrawals, low head dams, and return flows produce dynamic variation in discharge over small temporal scales. Further contributing to flow variations is the Alpine Decree, which stipulates that California and Nevada alternate irrigation withdrawals from the river on a weekly basis. Thus, when trying to understand riparian shading effects in a river like the Carson, where fluctuations in discharge occur over small temporal periods, streamflow and heat exchange processes are characterized best using a dynamic approach.

With this in mind, the primary goal of the study was to develop a physically-based characterization of the selected portion of the Carson River that would form the basis of temperature modeling and revegetation analysis. To satisfy this goal, an existing stream temperature model (HEATSOURCE 7.0) was selected for its ability to simulate dynamic streamflow and open channel heat transfer processes, its ability to quantify the

effect of riparian shading on stream temperature, and the availability of its source code for modifications. HEATSOURCE is a one-dimensional, physically based deterministic model that was developed by Matt Boyd and Brian Kasper of Oregon State University to aid the Oregon Department of Environmental Quality (ODEQ) in setting its temperature TMDLs for rivers in Oregon. An external peer review of the model can be found at:

<http://www.deq.state.or.us/wq/HeatSource/HeatSource.html>,

where reviewer questions along with ODEQ responses are presented. Loheide and Gorelick (2006) used the HEATSOURCE 7.0 model to quantify stream-aquifer interactions in a 1.7 km reach of Cottonwood Creek in Plumas National Forest, CA. For our project, the HEATSOURCE model was modified and calibrated to test whether hypothesized re-vegetation strategies along a selected portion of the Carson River in western Nevada could reduce water temperatures to ≤ 20 °C.

2 Background

2.1 Study Area

The Carson River Basin is located in eastern California and western Nevada (Figure 1). With its headwaters in the Sierra Nevada of eastern California, and its terminus in the Carson Sink, the Carson River Basin is an endorheic system that covers an area of approximately 10,272 km².

The Upper Carson River Watershed (UCRW), which extends from the headwaters in California to Deer Run Road in Carson City, Nevada, is classified as a cold-water fishery. The study area, which is a portion of the UCRW, covers a distance of 31.35 river

Carson River Basin

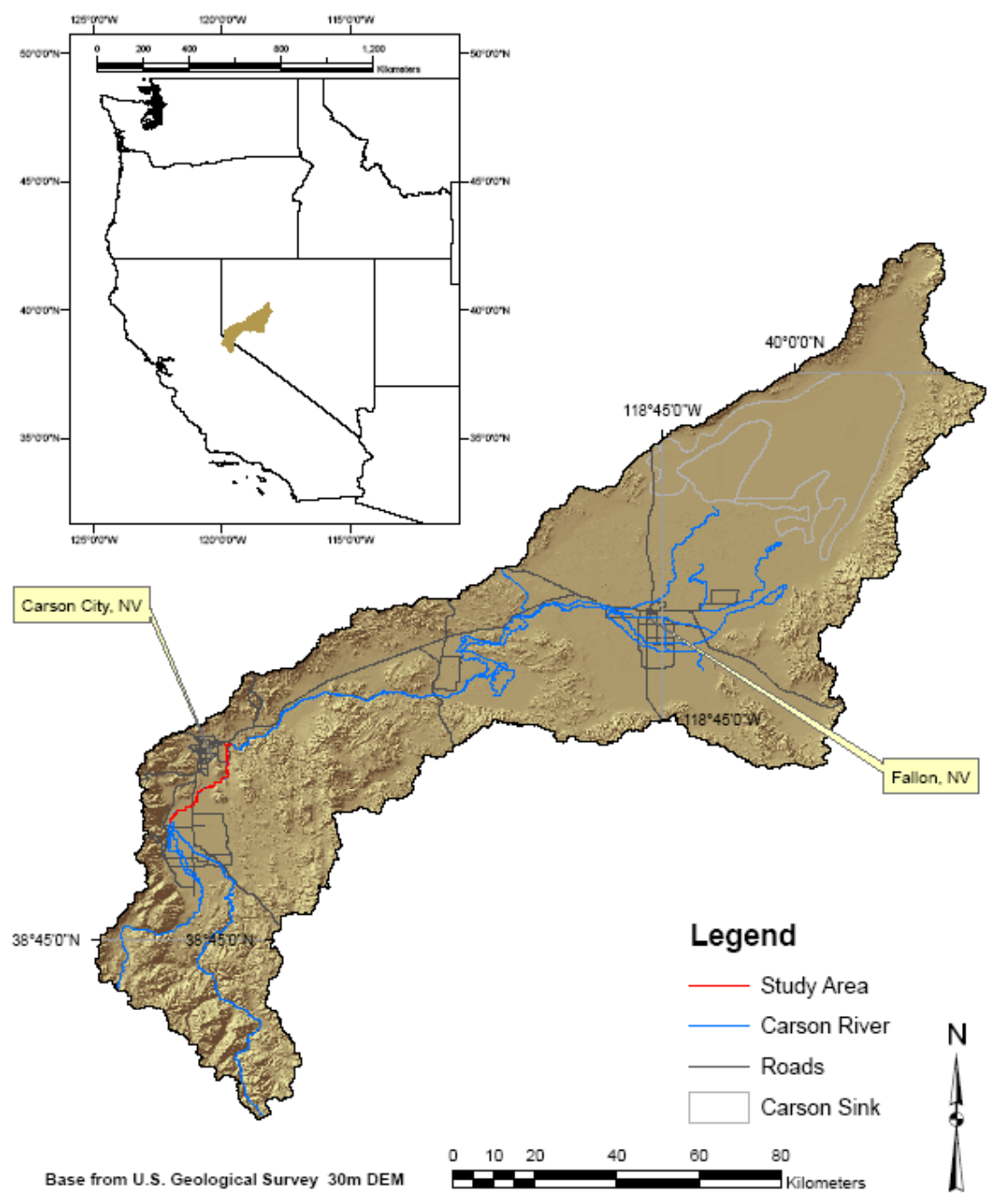


Figure 1-Location of the Carson River Basin and location of study area.

Carson River Study Area (Vegetation Zones)

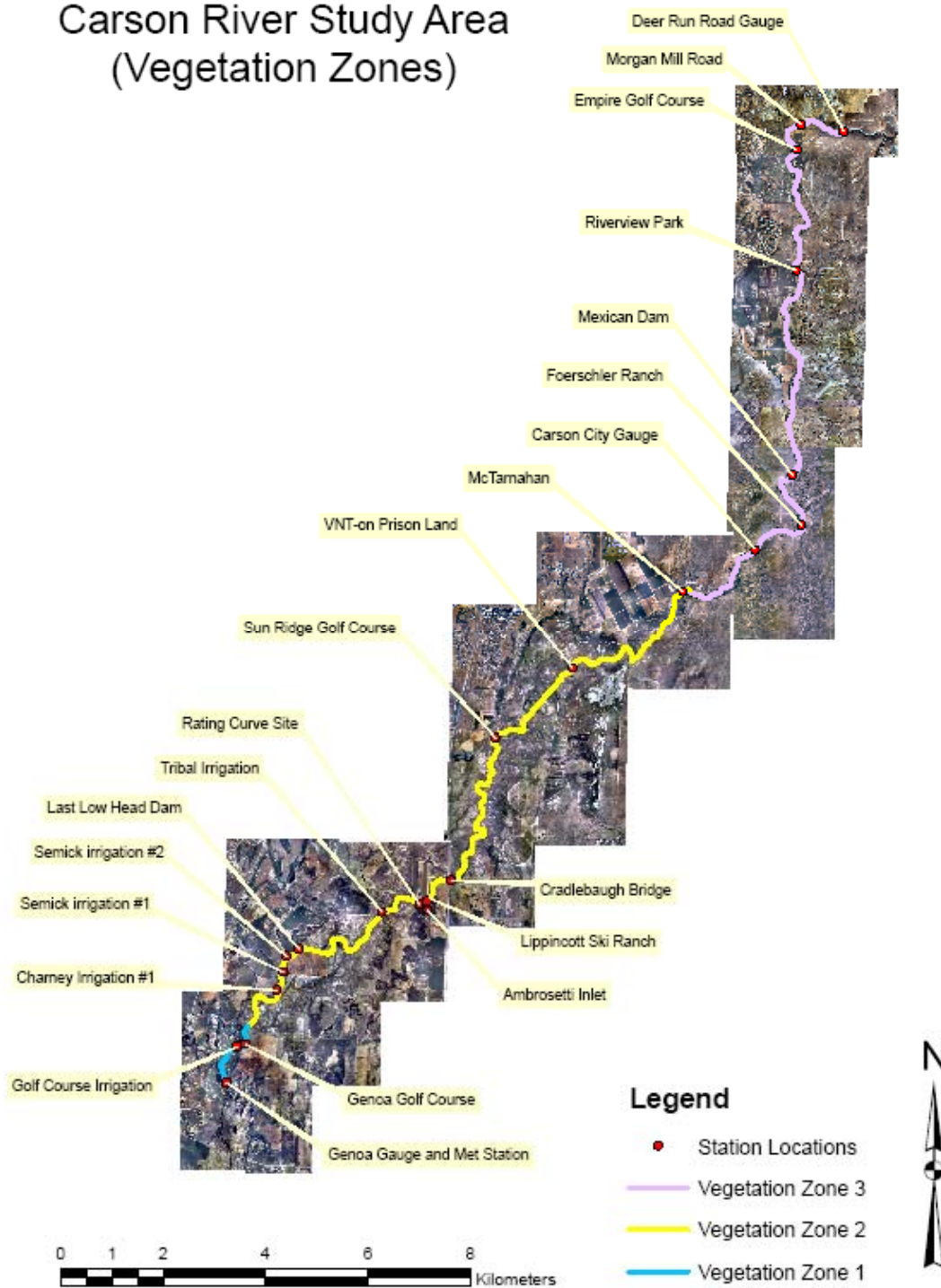


Figure 2-Carson River study area and sampling locations.

km from the USGS Genoa gauge near the confluence of the East and West Forks of the Carson River with the Brockliss Slough, downstream to the USGS Deer Run Road gauge. Irrigation withdrawals from the East Fork and West Fork are extensive in the portion of the basin between the state line and our study area. A large portion of the diverted streamflow ends up in the Brockliss Slough. The large number of diversions and the high volume of diverted water contribute to very low-flow reaches below diversion dams on the East and West forks of the Carson River.

While much of the lower Carson River is used to support recreational uses at Lahontan Reservoir or agricultural activities in the Lahontan Valley, upstream portions in Nevada and California (East Fork; West Fork; and main stem) that are designated as a coldwater fishery have associated water quality standards designed to support this beneficial use. These include standards for nutrients (N and P); total suspended solids (TSS), dissolved oxygen (DO), and temperature.

Presently, portions of the UCRW in Nevada are impaired due to high levels of nutrients (N and P); total suspended solids (TSS), dissolved oxygen (DO), and temperature (T). In response, the Nevada Division of Environmental Protection (NDEP) designated the Carson as a “Focus Watershed” within its 2003 Non-Point Source Management Plan (NDEP, 2003). An outgrowth of this priority status has been the direction of programmatic resources towards addressing one or more of the aforementioned water quality issues. In particular, recently completed, ongoing or pending studies relating to phosphorous source assessment, dissolved oxygen dynamics, and TSS reflect NDEP’s commitment to bringing the Carson River into compliance with the CWA.

The Clean Water Act (CWA) requires States to adopt water quality standards for regulated water bodies (USEPA, 1972). In accordance with the CWA, the state of Nevada has developed its own set of temperature regulations prescribed in the Nevada Administrative Code (NAC). In the study area, temperature standards set by the NAC are defined for the reach from Genoa gauge to Carson City gauge, and the reach from Carson City gauge to Deer Run Road gauge (Figure 2) (Pahl, 2004). The standards are dependent on the time of year for each respective reach (Tables 1 and 2). Although these are the current temperature regulations for the study area, the 20°C limit identified by Eaton et al. (1995) is used here because it provides a better indication of the river's potential to function as a true coldwater fishery.

Table 1-Existing temperature standards (NAC) for Genoa gauge to Carson gauge

Reach	November - April	May - June	July - October
Genoa gauge - Carson gauge	≤ 13°C	≤ 17°C	≤ 23°C

Table 2-Existing temperature standards (NAC) for Carson gauge to Deer Run Road gauge

Reach	November - May	June - October
Carson gauge - Deer Run Road gauge	≤ 18°C	≤ 23°C

In the past, water quality regulation has been based primarily on controlling point source pollution and the use of “effluent-based water quality standards” that were outlined in the CWA. For the most part, this stance has succeeded in improving the quality of our nation’s waters as generators of wastewater have complied with the regulations established in the National Pollution Discharge Elimination System (NPDES). The NPDES has improved water quality, but it has not enabled all waters to be deemed of high ecological integrity (i.e. waters that are “fishable and swimmable”),

mostly because non-point source pollution was not regulated in the 1970's and 80's (NRC, 2001).

In July of 2000, the United States Environmental Protection Agency (USEPA) implemented the TMDL approach to water quality control to minimize the continued degradation of surface waters produced by leaving non-point source pollution unchecked. A TMDL is the total maximum daily load that a water body can receive while remaining in compliance with a state's water quality standard for that pollutant. Before setting a TMDL, the beneficial uses for the water resource of concern must be evaluated, and the problems that threaten that use must be understood. NDEP has instituted a three phase plan for developing its TMDLs for the Carson River (NDEP, 2004):

1. Decide whether a particular beneficial use is appropriate;
2. Confirm impairment of beneficial use;
3. Develop TMDLs for the pollutants of concern.

In recognition that thermal loading in various portions of the Basin leads to periodic exceedances of existing temperature standards, the Desert Research Institute (DRI), in cooperation with the USEPA and NDEP, developed a project for a portion of the Carson River Basin aimed at improving the understanding of those processes controlling stream temperature dynamics within the study area (Figures 1 and 2). Specifically, information from the project should yield a fundamental understanding of the thermal regime of the study area and aid in possible reevaluation of beneficial uses.

In the study area, fish species of concern are listed as rainbow trout (*Oncorhynchus mykiss*), brown trout (*Salmo trutta*), catfish (*Ictalurus*), and smallmouth bass (*Micropterus dolomieu*). According to the Nevada Department of Wildlife (NDOW),

there is no indication of a self-propagating trout population in the study area portion of the Carson River. NDOW has been performing surveys of fish population since 1994. Records of these surveys show low population densities and small fish size, which supports the contention that there is no viable reproducing trout population in the river. Since 1879, NDOW has been stocking the Carson River with non-native trout (rainbow and brown), and catfish were first planted in the Carson in the late 1870's (NDOW, 2000). Historical newspaper records compiled by NDOW suggest prior to the 1870's the native Lahontan Cutthroat Trout (*Oncorhynchus clarki henshawi*) fishery in the Carson River was healthy, but the indigenous fishery was degraded in the late 1800's (NDOW, 1999).

Mean annual flow, taken from a 50-year USGS record at the Carson City gauge (Figure 2), is approximately $11 \text{ m}^3/\text{sec}$. However, temporal and spatial fluctuations can be extreme, owing primarily to a combination of climatic variability and anthropogenic activities that include withdrawals for agricultural, municipal, and industrial uses. One by-product of these fluctuations can be seasonally low flows in the 0 to $1.0 \text{ m}^3/\text{sec}$ range.

Precipitation in the watershed varies based on year, elevation, and season with most occurring at high elevation during the months of November and March. The average annual precipitation from 1948 to 2005 at Carson City is 267 mm, which is near the 300 mm/year often used to define the upper limit for a desert climate (Strahler and Strahler, 1973). At Carson City, daily maximum air temperature can exceed 38°C in the summer with possible daily minimums less than 0°C in the winter. Since 1982, the wettest year (1983) was 206% of average and the two driest years were 36% (1988) and

37% (1992) of average annual precipitation, based on measurements of the Sierra snowpack by the USDA Natural Resources Conservation Service (NRCS).

The general types of vegetation present in the study area are native phreatophytes such as rabbitbrush and greasewood, native nonphreatophytes such as bitterbrush and sagebrush, irrigated crops such as alfalfa and pasture grasses, cottonwood, and willow (Maurer et al., 2006). In terms of riparian vegetation, the study area can be divided into three zones, each with its own gross vegetation characteristics. The upper zone (Figure 2-light blue) is partly comprised by agricultural lands and an irrigated golf course. In the middle agricultural zone (Figure 2-yellow), irrigated alfalfa and pasture grasses dominate, although some areas in this zone are composed of bitterbrush-sagebrush, rabbitbrush-greasewood vegetation. In the lower more heavily vegetated zone (Figure 2-purple), extensive cottonwood canopies and willows are present.

Topographically, the study extent is defined by three different regimes. The first is a flat valley floor regime between the Genoa gauge (Site 1) and the McTarnahan site (Site 15); the second is a more topographically complex canyon regime extending downstream from the McTarnahan site to about 1.4 km downstream of Mexican Dam (Site 18) in Figure 2. A third regime extending from the end of regime 2 downstream to the Deer Run Road gauge (Site 22) is comprised by high topographic relief on the east bank and flat floodplain morphology on the west bank. The study area geology is comprised of unconsolidated Quaternary basin-fill deposits (Maurer et al., 2006). Streambed sediments in the upstream valley floor regime are comprised mostly of silty sands, whereas in the middle topographic regime substrate conditions are more dominated by gravels as a result of the surrounding granitic geology. Streambed

conditions in the third regime are more variable with the percentage of sand and silt increasing and gravel decreasing as distance downstream increases.

Stream-aquifer interactions can be an important process influencing the energy balance of a stream. Traditionally, ground and surfacewater resources have been treated as separate entities, with one or the other often being ignored in water-management decisions. As more scientific work has focused on the interactions of these two components, hydrologists have realized that surface and groundwater components are part of a single hydrologic system (Winter et al., 1998). In our study area, streamflow differentials between the three gauging stations during 2005 and 2006 indicated the river to be gaining. A USGS report published in 2006 examined the surface-groundwater exchange processes in the UCRW using water temperature-streambed profiles to determine streamflow infiltration and seepage (Maurer et al., 2006). The study did not cover the full extent of the study area for this project, but it did identify two locations (in our study area) just upstream of Charney Irrigation #1 (Site 5) to be strongly gaining, and another near Cradlebaugh Bridge (Site 12) to be a losing site (Figure 2). However, the authors reported a high degree of uncertainty associated with the determination of streamflow seepage and infiltration rates due to panel-temperature effects, the potential for changes in hydraulic conditions over time, and the small temperature fluctuations for losing sites (Maurer et al., 2006).

2.2 Geospatial Data

Six sources of geospatial data were available for model parameterization;

1. A high-resolution LIDAR survey (1 meter X/Y, 18.3cm Z) from 2004 (Leica ALS50 LIDAR Sensor, BAE systems)
2. Hyperspectral imagery (1 meter X/Y) from 2004 (Aurora Sensor, BAE systems)
3. High resolution digital color ortho-photography (0.3048 meter X/Y) from 2003
4. USGS Digital Elevation Model (DEM) (30meter X/Y, ± 7 to 15 meter Z)
5. Water mask raster
6. Thermal Infrared Radiometry Survey (1.2 meter X/Y, 0.1°C resolution) from 2006 (Firemapper 2.0 Sensor, Watershed Sciences)

The LIDAR dataset consisted of a filtered ground surface component that provided information on the topography of the land surface and the gradient of the river, and a first return component, which supplied information on the elevation of vegetation and other structures in the riparian zone. Hyperspectral imagery, which was acquired concurrently with the LIDAR, aided in quantifying the river's low-flow wetted channel dimensions. Digital color ortho-photography assisted in determining which locations were used in sampling field data for model calibration and validation. The 30m USGS DEM was used in quantifying the coarse scale topographic shading attributed to ridge lines. The "water mask" raster layer was digitized in ArcGis 9.0 to cover the wetted surface area of the river at the time of the acquisition of LIDAR and hyperspectral imagery. The water mask enabled calculation of wetted channel widths used in characterizing the channel geometry. As a second validation component, a thermal infrared survey was collected in the summer of 2006. The survey covered a length of 117

stream km from the California-Nevada state line on the east and west forks, including the Brockliss Slough and main stem, to the downstream extent of the study area. The availability of these data sources facilitated detailed characterization of streamside vegetation, channel geometry, and enabled improvements to the HEATSOURCE model code.

3 METHODS

3.1 Field Data Collection

In 2005, twenty-two sampling locations were used as summarized in Table 3. The stations are numbered consecutively in the downstream direction and the location of each station in the study area is shown in Figure 2. Each location was selected to provide the best opportunity of capturing the spatial variability of model parameters (i.e. different vegetation, topographical, meteorological, temperature, and streamflow regimes) while maintaining site accessibility. The data loggers at these sites were periodically downloaded and repositioned as required by changing water levels. All data for 2005 were acquired at a 10 minute temporal resolution and were used in model calibration.

In 2006, an independent set of water temperature data was collected for the purpose of model validation. We did not collect streambed temperature data in 2006, and we collected meteorological data only at site 10. Sites 9, 10, 12, 13, 14, 20, 21 were not used due to limited resources, and the sampling resolution of temperature data loggers was reduced to 30 minutes. These changes were made to decrease the frequency of data downloads and conserve available resources. Other changes in 2006 included duplicate water temperature data loggers at all sites, to reduce the possibility of data loss.

Otherwise, the sampling protocol was the same as in 2005. For both years, four types of field measurement stations were used.

- 1) Stations for monitoring stream flow, inflows, and irrigation pumping diversions (including water temperature for inflows).
- 2) In-stream stations for water temperature and streambed temperature.
- 3) In-channel meteorological stations for air temperature and relative humidity.
- 4) In-channel meteorological stations for solar radiation and wind speed.

3.1.1 Measurement Station Type 1: Inflow / Outflow /Streamflow

Streamflow data was obtained from existing USGS monitoring locations at the four sites identified in Table 3. A flow rating curve was developed in 2005 using an Onset[®] HOBO U20 water level logger, at site 9 (Figure 2), to allow recalibration of streamflow, and aid in developing accretion zones. In 2006, a second rating curve for a return flow just downstream of Riverview Park (Site 19) was developed in an effort to understand and quantify major return flows not monitored during the 2005 field season. The Ambrosetti Creek gauge and Genoa gauge provided information on boundary condition flows, while the Carson City gauge and Deer Run Road gauge allowed recalibration of flow levels. Irrigation water is diverted into Mexican Ditch (at the Mexican Dam, upstream of site 18) and diversions are measured on a weekly to biweekly interval. Withdrawals from the Mexican Ditch were acquired from the Carson City watermaster's office, and remaining streamflow data were acquired from the USGS on a 30 minute basis. Withdrawals via irrigation pumps were monitored using Onset[®] Hobo motor on/off sensors. Permission to monitor the tribal irrigation site shown in Figure 2

could not be obtained. The information from motor on/off sensors was combined with pump flow rates to estimate pumping withdrawals. For inflows, water temperature was measured using Dallas Semiconductor iButtons (specifications below).

Table 3-Sampling locations indicating what type data was collected in 2005 at each site

Site #	Location	Stream km	Station Type	Flow/ Divert	Water Temp.	Bed Temp.	AT/RH	SW	WS
1	Genoa Gauge (USGS)	31.35	1	Flow					
2	Genoa Met Station	31.35	3, 4				X	X	X
3	Golf course irrigation	30.48	1	Divert					
4	Genoa Golf Course	30.24	2, 3		X	X	X		
5	Charney Irrigation #1	28.65	1	Divert					
6	Semick Irrigation #1	28.23	1	Divert					
7	Semick Irrigation #2	27.93	1	Divert					
8	Last Low Head Dam	27.63	2, 3		X	X	X		
9	Rating Curve Site (2005)	24.21	1	Flow					
10	Lippincott Ski Ranch	24.06	2, 3, 4		X	X	X	X	X
11	Ambrosetti Inlet Gauge (USGS)	23.97	1	Flow	X				
12	Cradlebaugh Bridge	23.28	1		X				
13	Sun Ridge Golf Course	19.38	2, 3		X	X	X		
14	VNT-on Prison Land	17.07	2, 3, 4		X	X	X	X	X
15	McTarnahan	13.68	2, 3		X	X	X		
16	Carson City Gauge (USGS)	11.70	2, 3, 4	Flow					
17	Foerschler Ranch	10.47	2, 3, 4		X	X	X	X	X
18	Mexican Dam	9.18	1, 2, 3	Divert	X	X	X		
19	Riverview Park	4.68	2, 3, 4		X	X	X	X	X
20	Empire Golf Course	1.71	2, 3, 4		X	X	X	X	X
21	Morgan Mill Road	0.93	2		X	X	X		
22	Deer Run Road Gauge (USGS)	0	1, 2	Flow					

Station Type 1 = streamflow, inflow, diversions

Station Type 2 = Water (Water Temp.) and Streambed temperature (Bed Temp.)

Station Type 3 = Air Temperature (AT) and Relative Humidity (RH)

Station Type 4 = Shortwave (SW) radiation and Wind Speed (WS)

Flow = streamflow gauge

Divert = diversion from the river

3.1.2 Measurement Station Type 2: In-Stream Conditions

In 2005, Station type 2 consisted of a 2.5' solid PVC stake (containing temperature data loggers) that was partially driven into the streambed so that water temperature and streambed temperature could be measured simultaneously from one location (Figure 3).

- a.) Water Temperature: Dallas Semiconductor iButton[®] Thermochron data logger (Model DS1922L-F5). The data logger was attached to a fob which was housed inside a white PVC tube (Figure 3) to ensure that the data logger was not exposed to direct solar radiation. The PVC tube was attached to the stake so that the datalogger was situated approximately 10-15cm above the channel bottom. Absolute accuracy for the Thermochron data loggers is advertised as $\pm 0.5^{\circ}\text{C}$. Testing of iButton[®] model DS1922L-F5, suggested absolute accuracy was well within manufacturers listed accuracy of $\pm 0.5^{\circ}\text{C}$.
- b.) Streambed Temperature: Dallas Semiconductor iButton[®] Thermochron data logger (Model DS1922L-F5). The data logger was housed in a slot inside the 2.5' PVC stake that allowed direct contact to subsurface flow at a depth of approximately 30-35 cm into the channel alluvium (Figure 3). Stakes were partially driven into the streambed at locations that were 1/2 the maximum water depth and repositioned periodically through the season to accommodate changes in flow and morphology.

3.1.3 Measurement Station Type 3: Air Temperature / Relative Humidity

Air Temperature / Relative Humidity: Onset[®] HOBO H-08 air temperature/RH data logger. Absolute accuracy for the H-08 is advertised as $\pm 0.2^{\circ}\text{C}$ / $\pm 3\%$ RH. Station 3 was configured to monitor air temperature and relative humidity at in-channel locations. The sensor was located in a radiation shield mounted on a galvanized steel pole driven into streambed as near to the water surface as possible (Figure 4). Twelve stations collected data on air temperature and relative humidity.

3.1.4 Measurement Station Type 4: Solar Radiation / Wind Speed

Six measurement stations collected data on wind speed and incoming shortwave energy. At the Genoa Meteorological station (Site 2 and Figure 2), a 2-meter tripod was erected using Campbell Scientific sensors. In addition, five other locations were instrumented with a portable configuration of wind speed and solar radiation sensors and data loggers from Onset[®] Corporation (Figure 4). These five stations were used to characterize wind speed for more versus less locally sheltered portions of the upstream (low overall tree cover) versus downstream reaches (high overall tree cover and higher topographic relief). The sensors were also mounted on a galvanized steel pole driven into streambed as near to the water surface as possible (Figure 4).

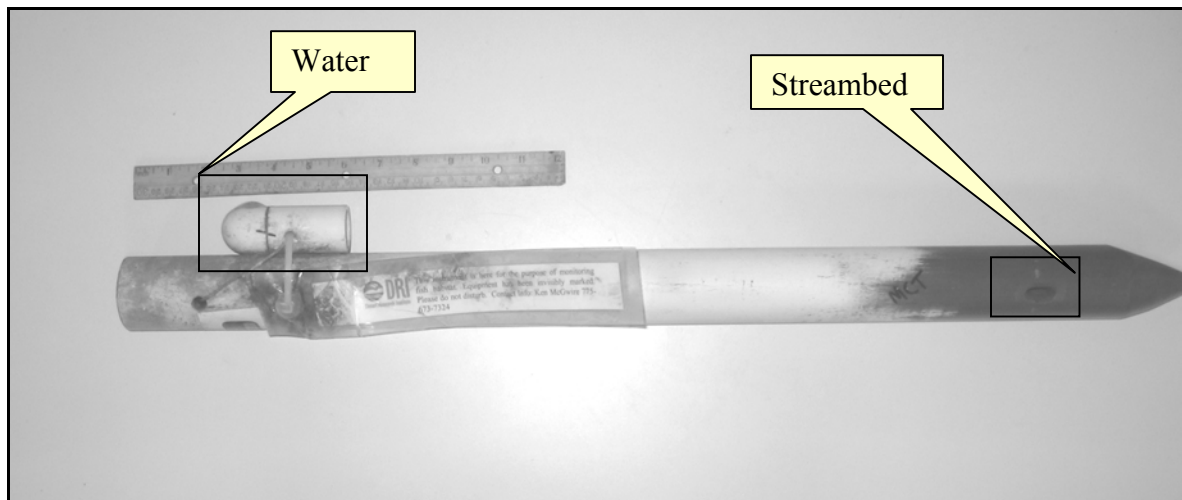


Figure 3-Station type 2a and 2b, water column and streambed temperature

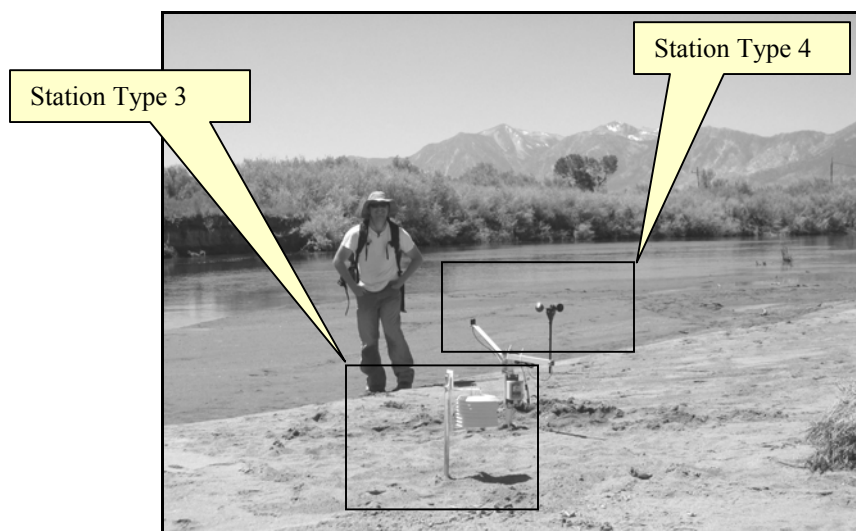


Figure 4-Measurement station type 3, and station type 4

3.2 Data Summary

Due to higher than average flows in 2005 and 2006, we were unable to deploy the in-stream and in-channel equipment until mid-late July for both years. Once deployed, the in-stream data loggers and other in-channel equipment performed reasonably well, although iButton[®] data loggers did exhibit an average failure rate (25%) over the two years of data collection. Water and streambed temperature data for the 2005 collection period are shown in Figures 60 - 73 of Appendix B, and water temperature data from 2006 are shown in Figures 74 - 83 of Appendix C. Below is a summary of the extent of data available for model calibration and validation.

3.2.1 2005

In the study area, the Carson River's streambed is composed of fine sands and silts that are easily mobilized at high flow and deposited at low flow. Due to depositional events in 2005, some water temperature stakes were buried, which resulted in data gaps at some sites, prompting field visits every 1 to 2 weeks to minimize burials. In addition to

sensor burial, eight of the original 32 iButtons failed entirely, and two of the irrigation pump monitors for Simeck Irrigation #1(Site 6) and Charney Irrigation #1 (Site 5) sites did not log any data. One Onset[®] air temperature/relative humidity station was vandalized at the Morgan Mill Road (Site 21), and one solar radiation/wind speed station at VNT (Site 14) was vandalized, but because of dense spatial sampling, these data losses were not critical. As a result of the iButton[®] failures, sensor burials, and lack of redundancy at sites, some water temperature data loss occurred at the upstream boundary site at the Genoa Golf Course (Site 4) and at Ambrosetti Inlet (Site 11). The data gaps for these important boundary condition sites reduced the length of available data for calibration. After compiling data from the 2005 field season, the longest continuous time series available for model calibration spanned a 17 day period from 8/21/05-9/7/05.

3.2.2 2006

We developed a new water temperature monitoring design in 2006 that eliminated the problems associated with burial. The new design utilized an anchor and float, with the iButton[®] temperature data logger tethered to the float such that the temperature could be measured at approximately 20 cm from the top of the water column (Figure 5).

Streambed temperature data were not collected in 2006. IButton[®] temperature data loggers for 2006 performed slightly better in terms of failure rate, but water temperature data loggers at Mexican Dam (Site 18) were vandalized on multiple occasions. Pump monitors in 2006 all functioned as planned resulting in continuous monitoring of pumping withdrawals for the validation period. Data available for validation spanned a

period of 30 days from 8/6/06-9/5/05. The period coincided with the acquisition of the TIR survey.

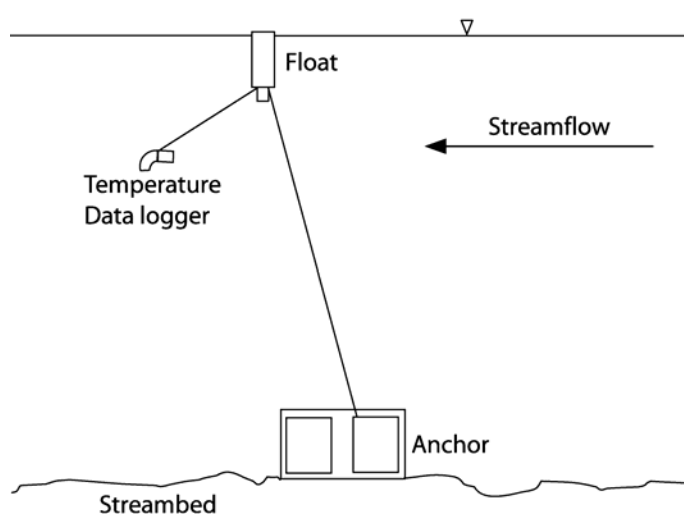


Figure 5-Water temperature monitoring design for 2006 sampling period

3.3 HEATSOURCE Temperature Model

Hydrodynamics, flow routing, heat transfer, and re-vegetation were simulated using a modified version of the one dimensional HEATSOURCE 7.0 temperature model. Through most of the study area, the Carson River is a shallow, well-mixed body, so the one-dimensional modeling approach was deemed suitable. The model's algorithms are coded in Microsoft Visual Basic with a Microsoft Excel user interface. The methodology described below is representative of the original HEATSOURCE operation prior to modifications. Modifications to the model are discussed in a subsequent section. For a more detailed explanation of the model's functionality, the reader is referred to Boyd and Kasper (2004).

By standard HEATSOURCE methods, model inputs are developed in Arcview 3.3 using TTools 7.21(an Arcview extension developed by the Oregon Department of Forestry). TTools is not a part of the HEATSOURCE model code, but is preprocessing

software that is used in preparing input data for the model. In TTools, a stream centerline is digitized for the entire length of the study area and the modeling nodes are created by segmenting the stream centerline into point features based on a user specified nodal spacing. The bankfull channel dimensions, approximated by the near-stream disturbance zone (Figure 6), are digitized using available digital ortho-photography. At each node, TTools calculates stream direction, bankfull channel width, elevation, gradient, topographic shade, and riparian vegetation attributes. These river characteristics are stored in an attribute table that is used as input for the HEATSOURCE model. For further explanation of TTools methodology, the reader is referred to Boyd and Kasper (2002).

3.3.1 Hydrodynamics

HEATSOURCE uses Manning's equation (2), a single trapezoid channel geometry, bankfull width, channel side slope, longitudinal slope, width to depth ratio, discharge, and Manning's roughness coefficient to estimate the wetted channel dimensions. The method assumes steady flow and uniform conditions over the length of a model segment, but when combined with the flow routing methods below, unsteady flows and non-uniform conditions can be simulated.

$$Q = \frac{A_x}{N} \cdot R_h^{\frac{2}{3}} \cdot S_o^{\frac{1}{2}} \quad (2)$$

Where:

Q = discharge, (m³·sec⁻¹)

A_x = cross sectional area, (m²)

N = Manning's roughness coefficient (unitless)

R_h = hydraulic radius (m)

S_o = channel bottom slope (unitless)

3.3.2 Flow Routing

Dynamic routing of flow through the model domain is based on the simultaneous solution of the St. Venant equations of continuity (3) and the one-dimensional momentum equation (4).

$$\frac{\partial d_w}{\partial t} + d_w \cdot \frac{\partial U}{\partial x} + U \cdot \frac{\partial d_w}{\partial x} = 0 \quad (3)$$

$$\frac{\partial U}{\partial t} + U \cdot \frac{\partial U}{\partial x} + g \cdot \frac{\partial d_w}{\partial x} = g \cdot (S_o - S_f) \quad (4)$$

Where:

U = water velocity, ($m \cdot sec^{-1}$)

d_w = average water column depth (m)

t = time, (sec)

x = distance along channel, (m)

g = acceleration of gravity ($m \cdot sec^{-2}$)

S_o = bed slope (unitless)

S_f = friction slope (water surface slope) (unitless)

HEATSOURCE allows for the use of two separate numerical methods to approximate the solution of (3) and (4): the Muskingum-Cunge method, and an explicit finite difference method. The Muskingum-Cunge method, which makes assumptions about wedge storage in order to estimate the storage terms in the continuity equation, was used for flow routing. The method is computationally efficient, and numerically stable.

3.3.3 Shading Methodology

HEATSOURCE has a solar shade subroutine that calculates the solar position for any given date/time, and accounts for both topographic shading and riparian shading. In order to quantify the patterns of shading on the river and its banks, landcover attributes of the canopy height, density, and distribution of streamside vegetation are normally estimated from ortho-photography and field surveys. In the modeling framework, the coarse and fine scale topographic shading, along with the riparian landcover, determine the amount of shortwave energy reaching the water surface.

3.3.3.1 Topographic Shading

Regional topographic shading from ridgelines and fine scale topographic shading resulting from stream banks or other near-stream topographic features are sampled in TTools using a 10m or 30m USGS DEM in three principal directions (W, S, and E) and angles between these directions are estimated using a weighted average of the neighboring directions. The relationship between solar altitude and the view to horizon determines coarse scale topographic shading. The view to horizon is the angle between the model node and the elevation of the highest topographic feature between the node and the sun. If the solar altitude is greater than the view to horizon, then the stream is not shaded by the coarse scale topography at that time step. If the stream is being shaded by topography, then the direct solar component is completely attenuated before reaching the water surface.

3.3.3.2 Riparian Shading

Before sampling of the riparian features is performed, a suggested 300 ft riparian buffer zone is digitized along both banks of the river from the near stream disturbance zone outward (Figure 6). Landcover polygons are digitized between the outer edge of the buffer zone and the channel edges using digital ortho-photography. Each of the landcover polygons is characterized as a region of similar density and height to which a distinct landcover code is assigned. Around each model node, the riparian landcover polygons are sampled by TTools in four zones of distance (Figure 7) for seven radial lines (NE, E, SE, S, SW, W, and NW) (Figure 8), and the associated codes are stored in a table. A landcover attribute table relates the landcover codes to their corresponding height and density values for vegetation.

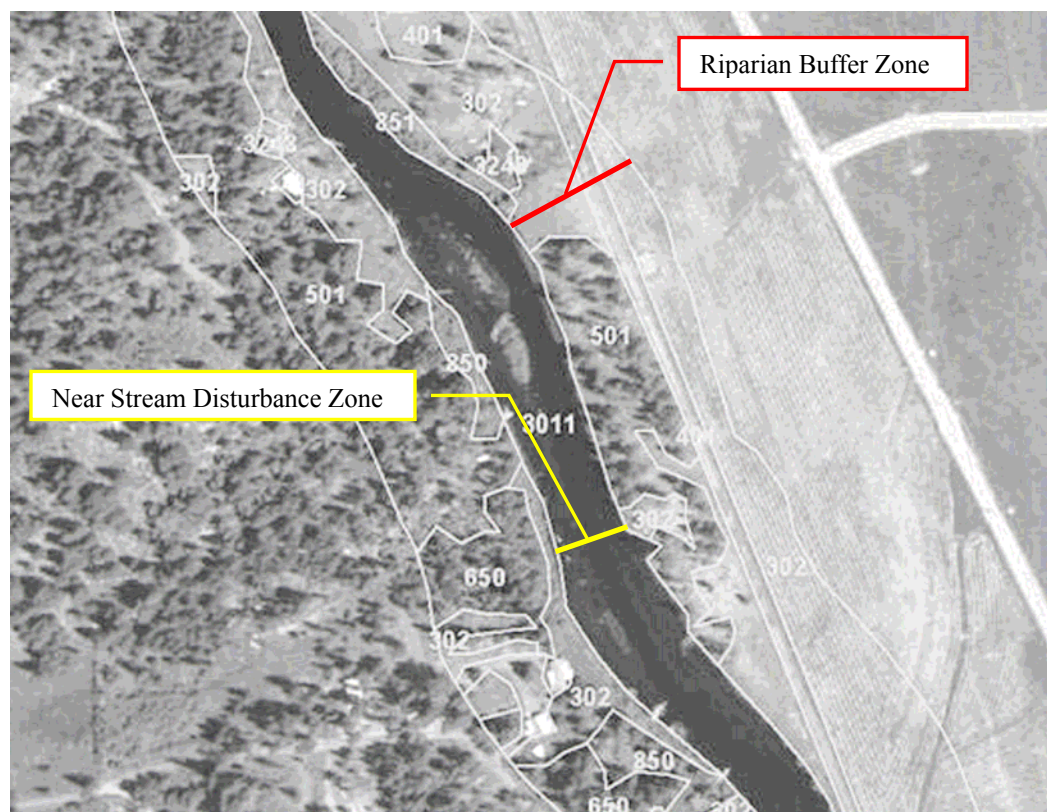


Figure 6-Landcover polygons (Boyd and Kasper, 2004)

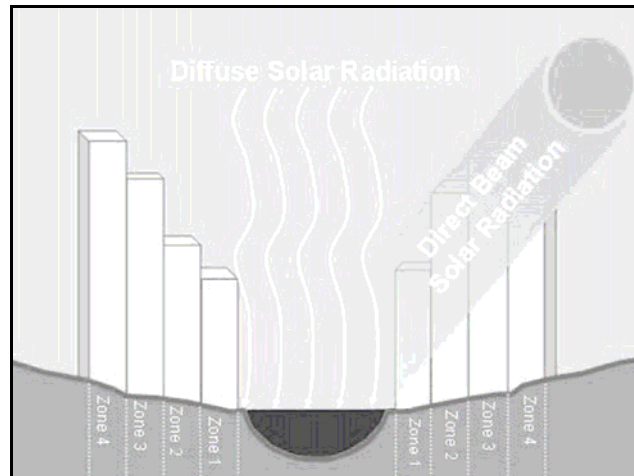
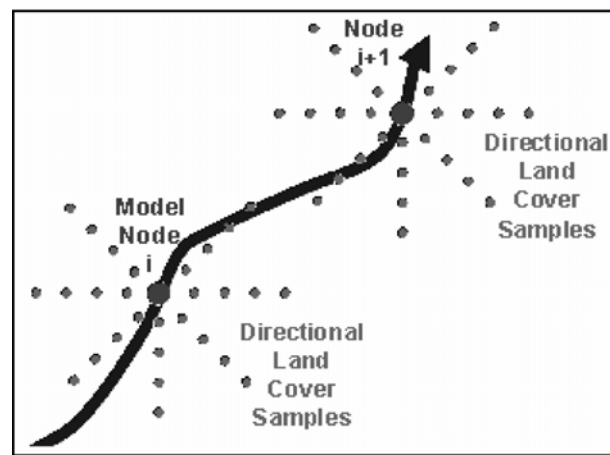


Figure 7-Schematic of landcover zones (Boyd and Kasper, 2004)



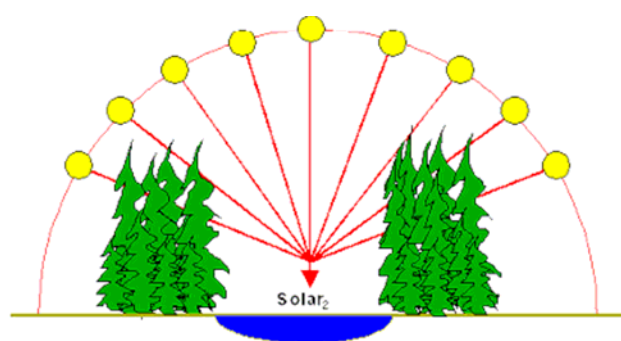
Example of land Cover Sampling Performed by TTools and Used as Model Input in Heat Source

Figure 8-Landcover radial sampling pattern (Boyd and Kasper, 2004)

Once the landcover attributes have been derived, the resulting information is moved into the HEATSOURCE model, where a routine called *vegematic* calculates the average landcover height and density on the left and right banks for each zone.

Shade-a-lator, an empirical routine contained in HEATSOURCE, simulates the potential solar flux component, and a cloudiness factor, ranging from 0 to 1, incorporates the effect

of clouds in modulating the shortwave component. *Shade-a-lator* also calculates effective shade (Figure 9), and determines how much shortwave energy reaches the stream surface. The direct and diffuse solar radiation components are routed through the canopy based on the height and density characteristics that are assigned to each zone. Routing occurs consecutively from the 4th and outermost zone to the 1st innermost zone. Shadowing is calculated as a function of solar altitude and azimuth. If the shadow length is greater than the distance from a particular zone to the stream center point, then shading is occurring. If shading is occurring, direct beam radiation is attenuated as a function of the light extinction coefficient and the path length through the land cover zone, which is a function of solar position and land cover zone width. Using vegetation density and height, attenuation is calculated using Beer's Law and the direct solar radiation passing through a zone is then routed to the next zone (Oke, 1978). After passing through all 4 landcover zones, the remaining direct solar radiation component is routed to the stream surface. The diffuse solar component filters through the canopy based on canopy density values for each node.



$$\text{Effective Shade} = \frac{(\text{Solar}_1 - \text{Solar}_2)}{\text{Solar}_1}$$

Where,

Solar₁ Potential Daily Direct Beam Solar Radiation Load

Solar₂ Daily Direct Beam Solar Radiation Load Received at the Stream Surface

Figure 9-Effective Shade Defined (Boyd and Kasper, 2004)

3.3.4 Heat Transfer Components

3.3.4.1 *Shortwave Radiation ($\Phi_{shortwave}$)*

Once the solar radiation has reached the water surface, there are several heat transfer processes controlling the amount of energy that is absorbed and reflected. Stream surface albedo, which is calculated as a function of the angle of incoming radiation, controls how much shortwave radiation is reflected. Of the shortwave energy that is not reflected, a portion is absorbed by the water column and the streambed, while any remaining portion is proportionately reflected back and absorbed by the water column. The radiation absorbed by the streambed becomes part of the streambed conduction flux calculation.

3.3.4.2 *Longwave Radiation ($\Phi_{longwave}$)*

Longwave radiation has been noted as an important heat transfer process for stream environments. Parker and Krenkel (1969) suggested that back radiation component is the single most important component in a stream's ability to dissipate heat. The longwave radiation flux is made up of a positive component (atmospheric and land cover) and a negative (back-radiation) component. Back-radiation is calculated using the Stefan-Boltzman Fourth Power radiation law for a blackbody.

3.3.4.3 *Evaporation ($\Phi_{evaporation}$)*

In HEATSOURCE, the evaporative heat flux is a function of the latent heat of vaporization, the evaporation rate, and the density of water. Evaporation has also been noted as a primary process in dissipating heat energy from the stream system (Parker and Krenkel, 1969). The rate of evaporation can be calculated using two methods: mass

transfer method, or Penman method. In both evaporation routines, a wind function is used to estimate the adiabatic part of evaporation. The wind function has the form:

$$f(\bar{W}) = A + B \cdot \bar{W} \quad (5)$$

where, A and B are unitless wind coefficients often defined using values from the literature. \bar{W} is the wind velocity (m/s) measured at 2m above the water surface. The mass transfer evaporation method was selected for use.

3.3.4.4 Convection ($\Phi_{convection}$)

The convective flux, also known as the sensible heat exchange, results from a combination of turbulent and molecular heat exchange at the air water interface. The convective flux is calculated as the product of the Bowen Ratio and the evaporative heat flux.

3.3.4.5 Streambed Conduction ($\Phi_{conduction}$)

While conduction at the streambed term may be 500 to 3500 times higher than that for the air (Halliday and Resnik, 1988), it is difficult to quantify, and the streambed component is not even included in older versions of the HTRCH temperature modeling component of the oft-used HSPF model. In developing their HSPF-SHADE model, Chen et al. (1998) dealt with the influence of thermal conductance between river water and adjacent bed material by adapting an analytical approach by Jobson (1977). As noted by Sinokrot and Stefan (1993), accounting for streambed conduction is critical in shallow streams, conditions regularly observed within the Carson River. HEATSOURCE uses a three-component system comprised by the water column, a shallow conduction layer, and

the deeper alluvium to conceptualize heat conduction at the water-streambed interface. The size and conductance properties of the conduction layer/alluvium, the properties of water, and the heat gradient between the mediums control the rate at which heat is transferred through system.

3.3.4.6 Stream Temperature Simulation

HEATSOURCE uses a finite difference approximation to solve the second order parabolic partial differential equation below for water temperature. Equation (6) allows for unsteady flows and non-uniform conditions.

$$\frac{\partial T_w}{\partial t} = -U \cdot \frac{\partial T_w}{\partial x} + D_L \cdot \frac{\partial^2 T_w}{\partial x^2} + \frac{\Phi_{total}}{c_{H_2O} \cdot \rho_{H_2O} \cdot \bar{d}_w} \quad (6)$$

Where:

- T_w = water temperature, ($^{\circ}\text{C}$)
- t = time, (sec)
- x = distance along channel, (m)
- U = water velocity, ($\text{m}\cdot\text{sec}^{-1}$)
- D_L = longitudinal dispersion coefficient, ($\text{m}^2\cdot\text{sec}^{-1}$)
- Φ_{total} = net surface heat flux, ($\text{kcal}\cdot(\text{m}^2\cdot\text{day}^{-1})$)
- ρ_{H_2O} = density of water, ($\text{kg}\cdot\text{m}^{-3}$)
- c_{H_2O} = specific heat of water, ($1 \text{ kcal}\cdot(\text{kg}\cdot^{\circ}\text{C})^{-1}$)
- \bar{d}_w = average water column depth, (m)

3.4 Modifications to HEATSOURCE

Many of the subroutines in the HEATSOURCE model were calibrated for rivers in Oregon, where conditions can be different from those observed in the study area. Multiple modifications were made to the HEATSOURCE code to improve its ability to operate under the conditions observed in the study area and to make use of detailed geospatial data. The changes included:

- 1) channel modifications
- 2) modulation of wind velocity
- 3) addition of a wind shelter coefficient and canopy shade factor
- 4) accretion effects on conduction flux
- 5) spatially distributed alluvium temperature zones
- 6) LIDAR derived shading attributes
- 7) improved topographic sampling methods

3.4.1 Channel Modifications

The original version of HEATSOURCE assumes a single trapezoid channel geometry when calculating hydraulics. By standard HEATSOURCE methods, the dimensions of the single channel (Figure 10a), are estimated from ortho-photography and field surveys. In the Carson River, there is a large disparity in discharge between spring runoff and summertime low-flow conditions. At high flow the river expands to fill the entire bankfull channel, but at low flow the Carson River recedes into a low-flow thalweg channel (Figure 10b), which is not represented well by a single trapezoid. If a single channel was used, unrealistic wetted channel dimensions and associated hydraulics would result in unrealistic heat exchange fluxes. As an alternative, a two-channel geometry was

written into the HEATSOURCE model code (Figure 10b) that allowed the model to maintain numerical stability, and simulate realistic wetted channel dimensions.

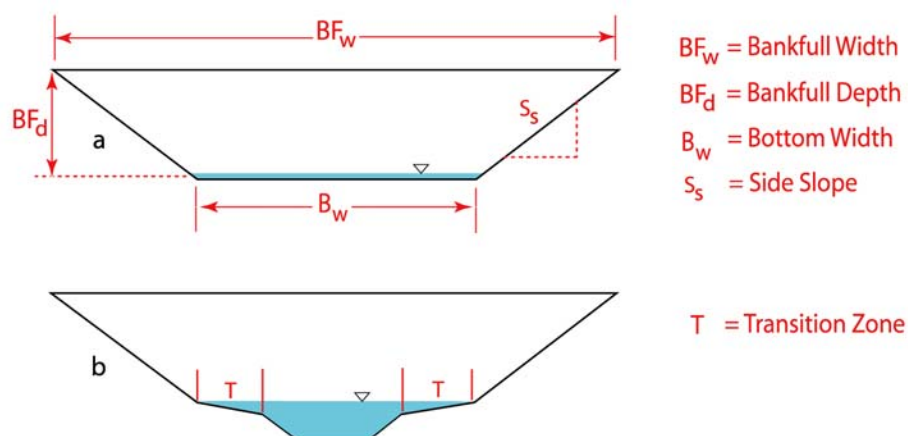


Figure 10-Schematic of channel modifications

For the channel modifications, the available high resolution LIDAR and hyperspectral imagery were used to parameterize the two-channel configuration. The bare ground LIDAR data was used to quantify the channel geometry above the low-flow water surface at the time of the LIDAR acquisition; this channel will be referred to as the main-channel. The below water surface geometry was developed using the hyperspectral imagery in combination with a field survey of maximum depth; this second channel will be called the sub-channel.

Hourly water temperature data (USGS Genoa gauge 2004 and 2005) collected by Dr. Richard Susfalk of DRI were used to evaluate the potential flow regimes in which a temperature limit was exceeded. A temperature limit of 20°C, cited by Eaton et al. (1995) as the optimal upper temperature limit for coldwater species, was selected as a threshold for determining the range of flow conditions over which the model might feasibly be applied. The time of year at which temperature limits were exceeded was dissimilar between the two years of data, but the flow regime in which they occurred was similar

(approximately $15 \text{ m}^3\text{s}^{-1}$). For our purposes the $15 \text{ m}^3\text{s}^{-1}$ flow threshold indicated that it was not necessary to model the entire bankfull channel because we were only concerned with the flow regime at which temperature criteria were exceeded.

A program called *simbanks* was developed by Dr. Kenneth McGwire of DRI to take advantage of our high resolution geospatial datasets by not fitting a coarse trapezoid to the bankfull channel geometry. The *simbanks* channel geometry (Figure 11), produced wetted dimensions and cross sections that were generally more representative of the main-channel than simply connecting the bankfull edges to the edges of the water mask product (refer to geospatial data section for water mask definition). In calculating the channel dimensions, *simbanks* proceeds to each of the model nodes, steps out to the edge of the water mask, and incrementally steps outward on the LIDAR channel surface until a pre-specified height above the water mask has been achieved on each bank. For a given height, the area of the tan rectangle in Figure 11 is known. The cross sectional areas of the two regions shown in green were calculated from the LIDAR data and a trapezoid of equivalent area (blue dashed lines) was calculated. Since each cross section was unique, this process was iterated using Manning's equation to ensure that the cross section could accommodate a flow of $15 \text{ m}^3\text{s}^{-1}$. The modified HEATSOURCE code assumes a symmetrical trapezoid, so *simbanks* calculates the equivalent side slope for a symmetrical trapezoid. The program also resolved problems in using a trapezoidal main-channel associated with in-channel islands (localized in-channel highs), and braided sections of river, by skipping over islands in the water mask when extracting the LIDAR transect. With the help of *simbanks*, the available LIDAR was able to produce a more realistic characterization of the main-channel geometry, but it provided no bathymetry

information on the wetted channel dimensions for the sub-channel. This is because the laser used by the LIDAR sensor could not penetrate the water.

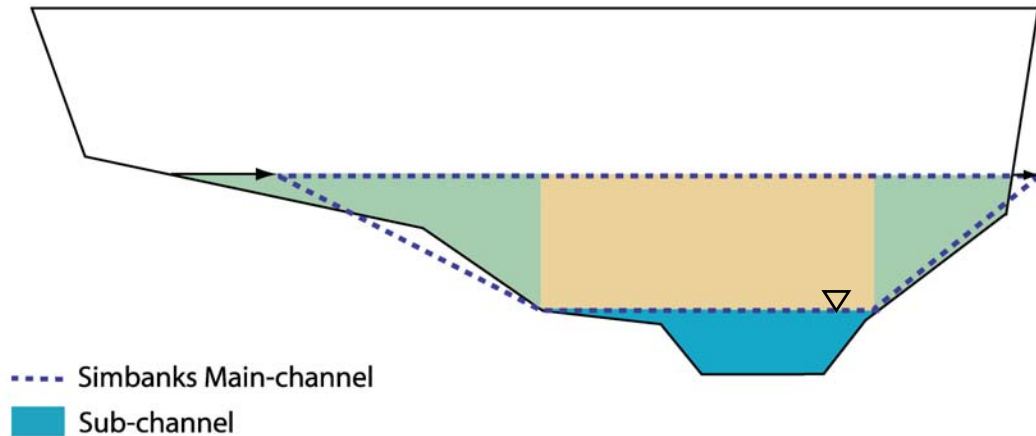


Figure 11-Simbanks main-channel

The low flow bathymetry information needed for the sub-channel was derived from the hyperspectral imagery by relating pixel brightness to depth. Extracting this information was problematic for several reasons:

1. The imagery was acquired in 2004, the year prior to the calibration period (2005);
2. Depth information was not surveyed during image acquisition; and
3. Hyperspectral flight lines occurred at different times with different lighting conditions

A method was developed to overcome these problems by linking a GPS survey of river depths to pixel brightness for a selected water penetrating wavelength (460 nm) in the hyperspectral imagery. The survey consisted of a canoe traverse over the 31.35 stream km study area with a depth finder (Eagle[®] CUDA 242) linked to a GPS. The survey was completed in the summer of 2006 over three days (7/15, 7/16, 7/25) at an

average flow of $7.5 \text{ m}^3\text{s}^{-1}$. During hyperspectral image acquisition (6/24, 6/26, 6/27) in the summer of 2004, the average flow was approximately $2.8 \text{ m}^3\text{s}^{-1}$. Ideally, the survey would have taken place at a flow regime identical to the streamflow during image acquisition. However, streamflow was unpredictable, and $7.5 \text{ m}^3\text{s}^{-1}$ was the minimum flow to allow an end to end canoe traverse. Even at $7.5 \text{ m}^3\text{s}^{-1}$, multiple portages were required. During the survey, we attempted to maintain a steady velocity over the deepest part of the channel so that we would be recording estimates of maximum depth. Performing the depth survey two years after image acquisition assumed that the channel morphology had remained relatively constant over that period. To compensate for movement of the channel that occurred since image acquisition, the surveyed depth values were manually edited to better match observed morphology in the 2004 imagery.

The higher flow rate during the depth survey necessitated back calculations of the depth discrepancy (yellow in Figure 12) to subtract from field measurements. For each day of image acquisition and each day of the depth survey, the difference in average daily streamflow was calculated. The flow differencing was possible because streamflow was relatively static during both the survey and hyperspectral acquisition.

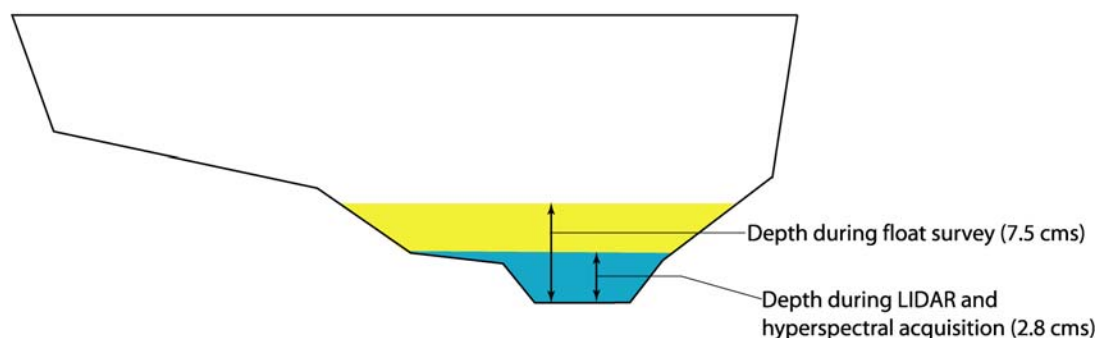


Figure 12-Schematic of flow differencing for sub-channel development

The unknown depth was back calculated at each model node using Manning's equation and the differenced flow rate. Travel time studies performed by Latham et al. (2006) and Horvath et al. (1998) indicated a Manning's roughness coefficient of 0.35 was appropriate for the study area. The Newton-Raphson solver routine in HEATSOURCE was adapted to perform the back calculations by using the main-channel dimensions, the differenced flow rate, and Manning's equation. The back calculated depth was subtracted from the original float survey depth to estimate the low flow depth (blue Figure 12) used for the sub-channel.

The top width of the trapezoid used for the sub-channel was determined from the water mask and reliable LIDAR measurements of the land surface. To derive the remaining sub-channel dimensions, the maximum low flow depth from the field survey was assigned to the darkest pixel in the hyperspectral imagery, and zero depth was assigned to the brightest pixel within the water mask. This allowed calculation of a gradient of brightness to depth along a cross section at each node. The depth values along each cross section were sorted and fitted to a trapezoidal geometry using either a logistic curve or linear fit to estimate the sub-channel dimensions, based on which had a better r^2 . Since multiple images were acquired over multiple days (resulting in different lighting conditions), each model node required a unique relation of brightness to depth.

3.4.2 Modulation of Wind Velocity

For revegetation simulations, we needed a method for relating the effect that riparian vegetation has on wind speed, so that wind speed measurements from a single exposed location could be related to the remaining model nodes during testing and

scenario analysis. During revegetation simulations, we also needed to be able to translate the sheltering effect of tree cover with the vegetation attributes to the reach targeted for revegetation.

In the original HEATSOURCE code, atmospheric data from meteorological stations are assigned to model nodes in a consecutive downstream direction until the model encounters the next meteorological station. After analyzing the wind speed data from the five in-channel meteorological stations from 2005, it was clear that in-channel wind speed was dependent on the amount of riparian vegetation around a particular station. To incorporate this dependence, we regressed wind speed (as a percent of speed at the most exposed location) to a log transform of the average height of tree cover (from LIDAR) in a 150m radius around each model node. The 150m radius was chosen after trials of several radii. The regression shown in Figure 13 is based on the average wind speeds of each station over the entire 2005 field season. Modulation of the wind speed based on tree cover did not incorporate wind direction; however, winds were predominantly from the west or southwest through the period of observation. Consequently, in reaches that have patchy vegetation or strong local topography, wind speed may be poorly estimated on days when wind direction deviates from the average.

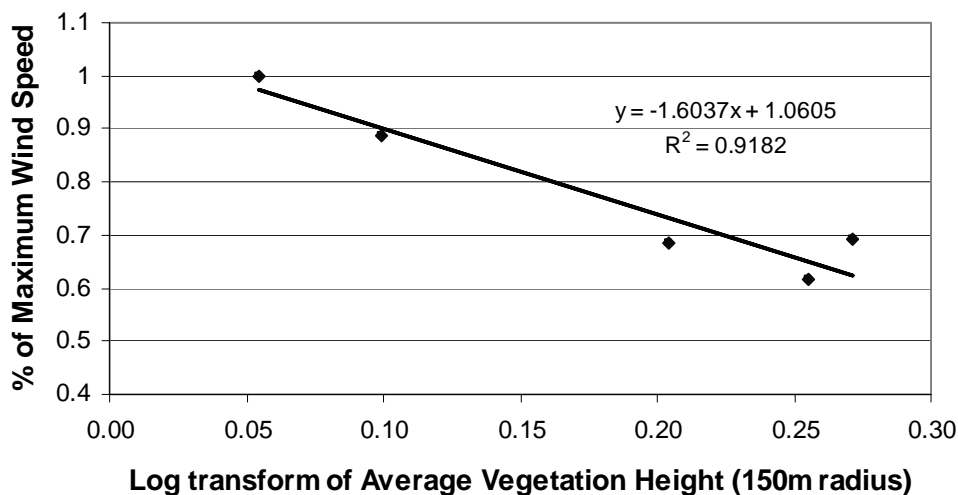


Figure 13-Wind speed regression

3.4.3 Wind Shelter Coefficient and Canopy Shade Factor

A wind shelter coefficient and canopy shade factor were added to the model code to give the user flexibility in controlling the effect of the riparian vegetation on wind and incoming solar radiation. These were simple multipliers that allowed tuning of empirical relationships in the model calibration process.

3.4.4 Conduction Flux

The original conduction flux methods in HEATSOURCE accounted for the advection of groundwater into the channel, but they did not account for the actual movement of this water through the conduction layer. Rather, the advected water was simply added to the water column at the alluvium temperature. In order to better represent the energy balance, a simple method was adopted to account for streambed heating/cooling effects due to advection. Conceptually, when a model segment is gaining or losing, a volume of water is displaced from the conduction layer, but is replaced by an

amount from the alluvium or water column respectively. At each time step, the adapted code deals with this in a four step process.

- 1) Determine initial temperature of the accreted volume based on whether the model segment is gaining (alluvium temperature) or losing (surface water temperature).
- 2) Calculate heat flux to/from sediment (as shown in equations 7-10) at each time step based on the amount of pore space displaced in the conduction layer.

$$\rho_{\text{remaining}} = \frac{\rho_{\text{H}_2\text{O}} \cdot \text{VR}_{\text{H}_2\text{O}} + \rho_{\text{sed}} \cdot \text{V}_{\text{sed}}}{\text{VR}_{\text{H}_2\text{O}} + \text{V}_{\text{sed}}} \quad (7)$$

$$\text{C}_{\text{remaining}} = \frac{\text{C}_{\text{H}_2\text{O}} \cdot \text{VR}_{\text{H}_2\text{O}} + \text{C}_{\text{sed}} \cdot \text{V}_{\text{sed}}}{\text{VR}_{\text{H}_2\text{O}} + \text{V}_{\text{sed}}} \quad (8)$$

$$E = \rho_{\text{H}_2\text{O}} \cdot \text{VA} \cdot \text{C}_{\text{H}_2\text{O}} \cdot (\text{T}_{\text{acc}} - \text{T}_{\text{sed}}) \quad (9)$$

$$\text{T}_{\text{sednew}} = \frac{\text{T}_{\text{sed}} + E \cdot \frac{\text{C}_{\text{remaining}}}{\text{C}_{\text{H}_2\text{O}}}}{\rho_{\text{remaining}} \cdot \text{V}_{\text{remaining}} \cdot \text{C}_{\text{remaining}}} \quad (10)$$

Where:

$\rho_{\text{H}_2\text{O}}$ = density of water ($\text{kg} \cdot \text{m}^{-3}$)

$\text{VR}_{\text{H}_2\text{O}}$ = volume of pore water remaining after accretion step (m^3)

ρ_{sed} = sediment density ($\text{kg} \cdot \text{m}^{-3}$)

V_{sed} = volume of sediment in conduction layer (m^3)

$\rho_{\text{remaining}}$ = density of water and sediment after accretion step ($\text{kg} \cdot \text{m}^{-3}$)

$\text{C}_{\text{H}_2\text{O}}$ = heat capacity of water ($\text{J} \cdot (\text{kg} \cdot ^\circ\text{C})^{-1}$)

C_{sed} = heat capacity of sediments in conduction layer ($\text{J} \cdot (\text{kg} \cdot ^\circ\text{C})^{-1}$)

$C_{\text{remaining}}$ = heat capacity of water-sediment after accretion step ($\text{J}\cdot(\text{kg}\cdot^{\circ}\text{C})^{-1}$)

VA = volume accreted (m^3)

T_{acc} = temperature of the accretion ($^{\circ}\text{C}$)

T_{sed} = temperature of the sediment prior to accretion ($^{\circ}\text{C}$)

E = energy gained or lost in the conduction layer (J)

$V_{\text{remaining}}$ = volume remaining in conduction layer after accretion step (m^3)

T_{sednew} = new conduction layer temperature ($^{\circ}\text{C}$)

- 3) Assume accreted water and conduction layer sediments reach thermal equilibrium in that time step.
- 4) If accretion is positive, then accretion is added to the surface water at the new conduction layer temperature.

3.4.5 Spatially Distributed Alluvium Temperature

The original HEATSOURCE code characterized the temperature of the alluvium using a constant value for all model nodes. We adapted the code to use three alluvium temperature zones that allowed a higher degree of spatial variability. The three geographic zones were delineated based primarily on the observed streambed temperature data. Each of the zones showed distinctly different streambed temperature on average. Streambed temperatures acquired at 30 cm depth were assumed to approximate the temperature of shallow groundwater at the boundary between alluvium zone and conduction layer. The three alluvium zones were used in the automated parameter estimation for model calibration.

3.4.6 Topographic Sampling

The original HEATSOURCE routine calculated coarse scale topographic shading from ridgelines in only three directions (W, S, and E). The routine was adapted to calculate the coarse topographic shading using the same seven directions (NE, E, SE, S, SW, W, and NW) used in the calculation of riparian and fine scale topographic features. This modification was made because a portion of this reach of the Carson River flows through an area of relatively steep topography.

3.4.7 LIDAR-Derived Shading Attributes

Standard HEATSOURCE and TTools methods quantify the existing riparian vegetation by digitizing a riparian buffer zone and vegetation polygons in TTools. Although the method is suitable for that type of data, it was not able to fully utilize the LIDAR data because it assumes that vegetation has been aggregated to polygons in a map. The LIDAR imagery has an x/y resolution of 1m, and when aggregated to detailed polygons that represented variations in vegetation height, TTools struggled with the spatial density of the LIDAR input because the spatial analyst extension in ArcView has a limited capacity. The method was bypassed and a program was coded to sample the vegetation attributes directly from the LIDAR imagery to derive a higher resolution representation of riparian tree cover. Preliminary testing of shading routines indicated that the averaging of tree height based on tree density within the recommended 300 foot buffer zone was underemphasizing the effect of near-stream tall cottonwoods, as most of the highest, densest vegetation on the Carson River is within 60 meters of the channel edge. The new program was setup to use a 60m buffer zone instead of the suggested 300 feet. For each model node, the algorithm proceeded outward to each of the 4 landcover

zones, but instead of sampling in radial lines as TTools does (Figure 6), the new algorithm exhaustively sampled the landcover zones in triangular sectors corresponding to each direction to estimate the average height and density of vegetation that should be visible from the channel. This visibility constraint only included LIDAR values exceeding a threshold of 10 degrees above horizontal. This provided a threshold for estimating the density of that portion of the vegetation corresponding to a shade-producing canopy and ensured that the use of vegetation density to provide an average height did not unduly depress the estimated canopy height.

3.5 HEATSOURCE Programming Errors

While making the modifications to the HEATSOURCE code we corrected two programming errors. The corrections were:

- 1) separation of vegetation shading from fine scale topographic shading
- 2) a correction to the calculation of evaporative flux

3.5.1 Separation of Vegetation Shading From Fine Scale Topographic Shading

In the original HEATSOURCE code, near-stream shading from fine scale topographic features and shading from riparian vegetation were not treated as separate components. The height of the stream bank and vegetation were summed and multiplied by the density of the vegetation in order to provide the average height of shade cover. This was a logical error, as this approach applied the vegetation density to the solid land component of the shade as well. The HEATSOURCE code was modified to correct the error by calculating average height of the vegetation (density * height), and then adding it to the height of the fine-scale topography. As this error affects the dominant heat flux of

shortwave radiation and the purpose of the study was to quantify the effects of near-stream vegetation, this error was a substantial problem.

3.5.2 Evaporative flux calculation

In the original model code, the amount of evaporative loss during a time step is calculated before the evaporative rate is calculated. This was possible because the model uses a zero evaporative rate for the first time step at the first model node, and subsequent time steps use the evaporative rate from the previous node (or the last node's previous time step at the upper boundary condition). This error is likely to have a small effect because when running the model at a small time step the evaporative rate is not expected to vary substantially over such small temporal scales. However, when running the model with larger time steps the problem could become more considerable.

3.6 Model Calibration

Some HEATSOURCE parameters were calibrated in a manual mode, while other more poorly defined parameters were calibrated using parameter estimation routines.

3.6.1 Manual Calibration

Model input data were developed for a 30m node spacing to take advantage of the high resolution geospatial data sources. However, due to high velocity reaches of the river, the smallest model spacing that allowed complete mixing in a model time step was 240m. Model output was calculated at this nodal spacing.

3.6.1.1 Low Head Dam Hydraulics

Initial manual calibration revealed the model's inability to simulate the behavior of low head dams. As a simple way of representing dams, the model allows the user to set specific nodes as control depths. A control depth holds the depth in a model segment to the specified height, and the discharge out of the segment is such that the depth requirement is maintained. The three low head dams in the study area are rock low head dams constructed to maintain a greater water depth for pumping withdrawals. A low head dam is a constructed hydraulic barrier with a height not exceeding 25 feet. The three dams in the study area have a hydraulic height of approximately 1 meter. Model nodes were set up to coincide with the approximate location of each dam and each 240m model segment (upstream of the dams) was given a control depth based on the average maximum channel depth for that segment.

3.6.1.2 Control Temperatures

Control temperatures can be used to set individual model nodes to use observed temperature data during a model run. Water temperature was reset at the last low head dam site (Site 8-stream km 27.6) and the Mexican Dam (Site 18-stream km 9.12) to use observed data. This ensured that the calibration of reaches downstream of low head dams was not affected by uncertainty associated with dam hydraulics. With this approach, each of the two model nodes downstream of low head dams now become new temperature boundary conditions for the model.

3.6.1.3 Flow Balancing

A water balance for the study area was developed using USGS streamflow data in combination with the streamflow data obtained from the rating curve developed in 2005 to estimate streamflow infiltration and seepage between gauges. Based on the location of the rating curve site (Site 9), and existing USGS gauges (Table 3), the study area was divided into three reaches, each having its own water balance. The water balance equation (11) was used to calculate the flow differential between points of known streamflow:

$$\Delta Q = Q_{IN} + \text{INFLOW} - \text{OUTFLOW} - \text{PUMPS} - E - \text{PREC} - Q_{OUT} \quad (11)$$

Where:

- ΔQ = the differential of streamflow over a model segment $\text{m}^3 \text{s}^{-1}$;
- Q_{IN} = the streamflow at the upstream boundary of the reach $\text{m}^3 \text{s}^{-1}$;
- INFLOW = surface return flows to the river $\text{m}^3 \text{s}^{-1}$;
- OUTFLOW = ditch withdrawals from the river $\text{m}^3 \text{s}^{-1}$;
- PUMPS = the pumping withdrawals $\text{m}^3 \text{s}^{-1}$;
- E = evaporation $\text{m}^3 \text{s}^{-1}$;
- PREC = precipitation $\text{m}^3 \text{s}^{-1}$;
- Q_{OUT} = streamflow at the downstream end of the reach $\text{m}^3 \text{s}^{-1}$.

No precipitation was recorded during the model calibration period, so $\text{PREC} = 0$ and evaporation rates were obtained from the Western Nevada Community College (WNCC) meteorological station in Carson City. One water balance was developed for the reach between the Genoa gauge and the rating curve site (Site 9). Four pumping diversions are present in this reach and were monitored, but two of the four pump monitors were not

functioning correctly. Therefore, two of the pumps were assumed always on, which was later verified by the pump operator. Another water balance was developed for the reach between site 9 and Carson City gauge, and a third for the reach between Carson City gauge and Deer Run Road gauge. For each reach, the differential between gauges was attributed to groundwater accretion if negative and streamflow seepage if positive. This resulted in 3 preliminary accretion zones for the model domain that were all estimated to be gaining. Using the observed streambed temperature data, the 2006 TIR survey, and the locations of low head dams, the three preliminary accretion zones were further subdivided into eight different accretion zones (Figure 14). Zones immediately upstream of low head dams were hypothesized to be losing due to the head gradient resulting from ponded water behind dams. However, there was no quantitative data to indicate whether these locations were actually losing, so they were assumed neutral. Sediment temperatures downstream from the low head dams showed minimal daily variation in temperature, suggesting a gaining component to these sites (Figure 15). Therefore, they were assigned positive accretion values. The streamflow differentials from the three preliminary accretion zones were distributed among model nodes in the eight sub-divided accretion zones based on observed streambed temperature data and observable trends in the TIR survey.

In order to properly estimate the thermal balance, streamflow must be sufficiently calibrated to ensure proper representation of volumes and flow rates. Despite having streamflow data from the rating curve site (Figure 16), attempts to incorporate that data during flow calibration were problematic. For instance, when streamflow was calibrated between the Genoa gauge and the rating curve at site 9, the match to observed data was

acceptable. However, an acceptable calibration between site 9 and the Carson City gauge could not be obtained. It is not clear whether the uncertainty associated with the rating curve, pumping rates, problems with the low head dam hydraulics, or a combination of the three was producing the difficulties with streamflow calibration between the rating curve site and Carson City gauge (Site 16). Thus, for streamflow balancing, we disregarded the rating curve data and calibrated streamflow to the three existing USGS gauges in the study area. The eight accretion values, pumping rates, inflows and outflows were entered into the model. The flow balancing procedure was an iterative process that was completed in two stages.

First, the reach between Genoa gauge and Carson City gauge was balanced by adjusting the rate of withdrawal for unmonitored pumps until the predicted streamflow at Carson City gauge was sufficiently fitted to observations. Pumping withdrawals were not allowed to exceed the maximum rate of $0.1415 \text{ m}^3 \text{ s}^{-1}$ for the irrigation pumps. For the reach between Carson City gauge and Deer Run Road gauge, a high degree of uncertainty was associated with the withdrawal data for the Mexican Ditch in 2005 and the Riverview Park return flow (Site 19) (not monitored in 2005). To simplify the calibration procedure for this reach, streamflow was balanced by assuming a constant inflow rate for the Riverview Park return flow, and adjusting ditch withdrawal rates in a realistic range until the predicted flows at the Deer Run Road gauge matched the observations. The observed and predicted hydrographs for the calibration period are shown in Figures 17 and 18.

Carson River Study Area (Accretion Zones)

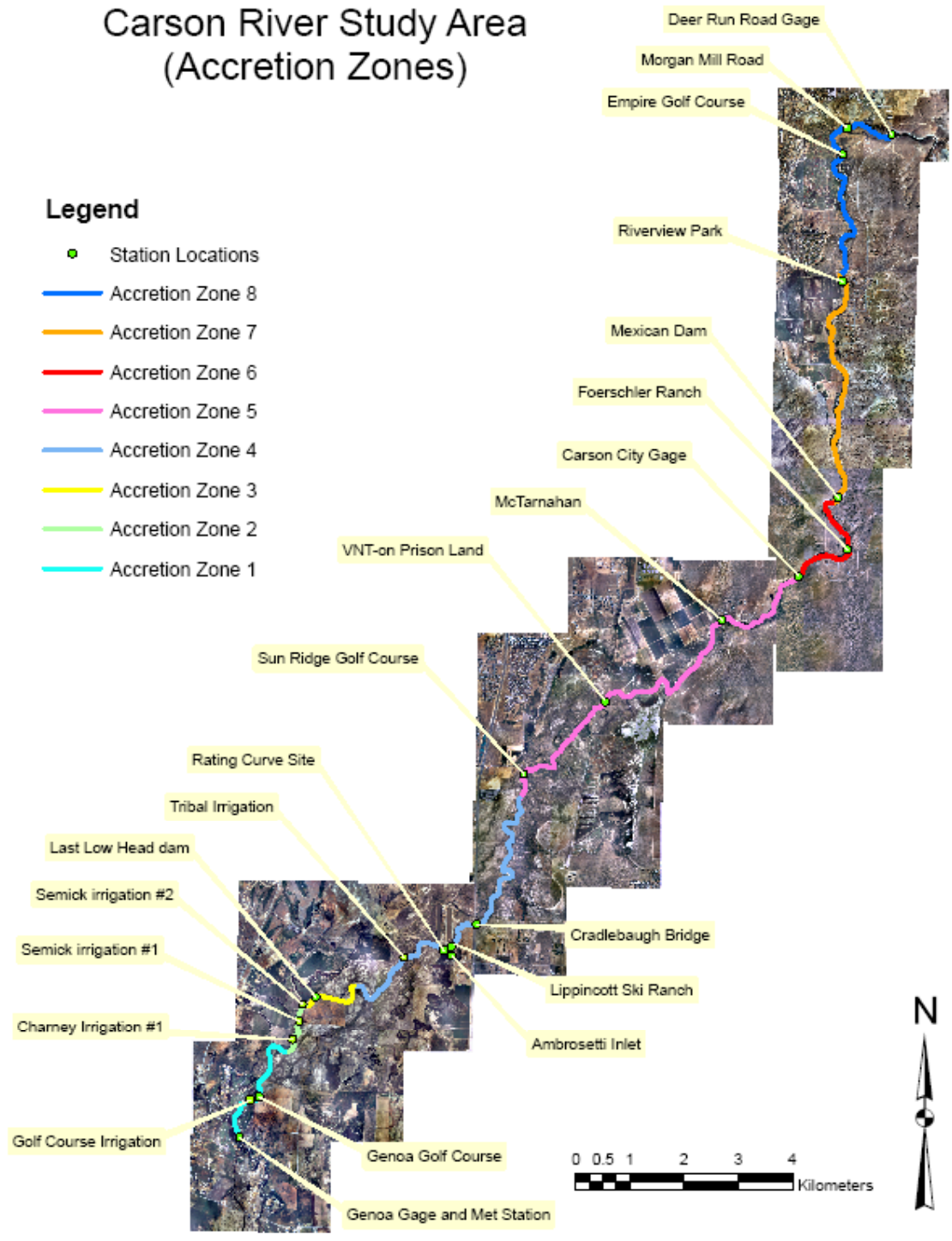


Figure 14-Eight accretion zones

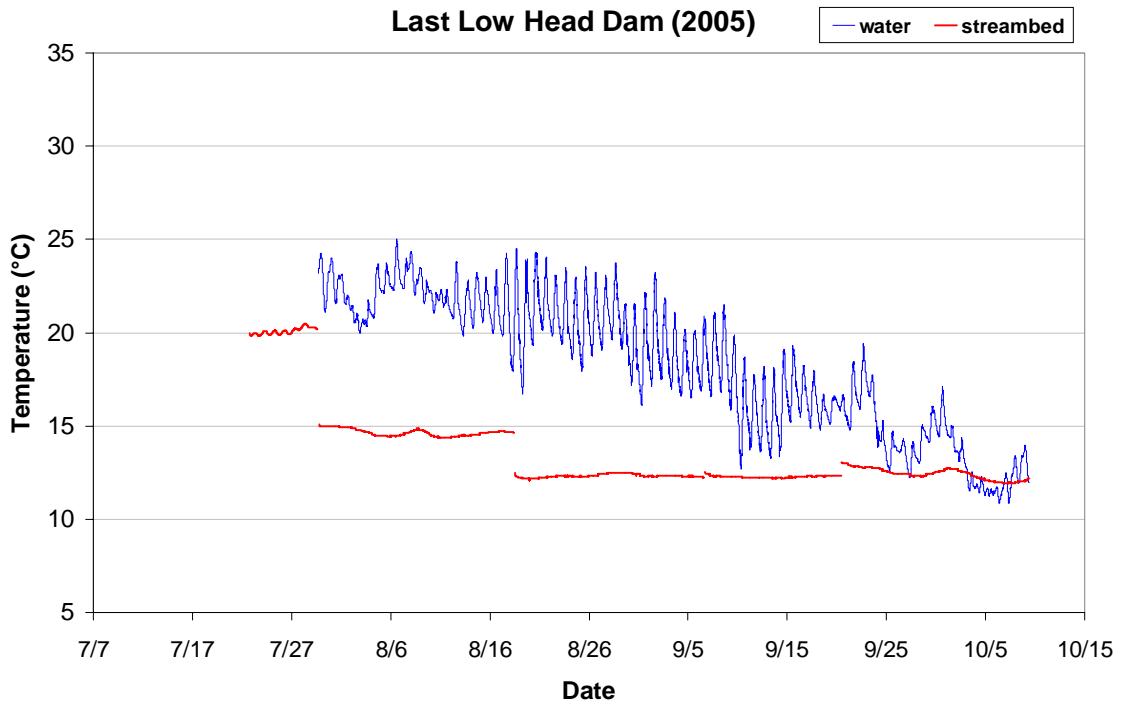


Figure 15- Water and streambed temperature for last low head dam site

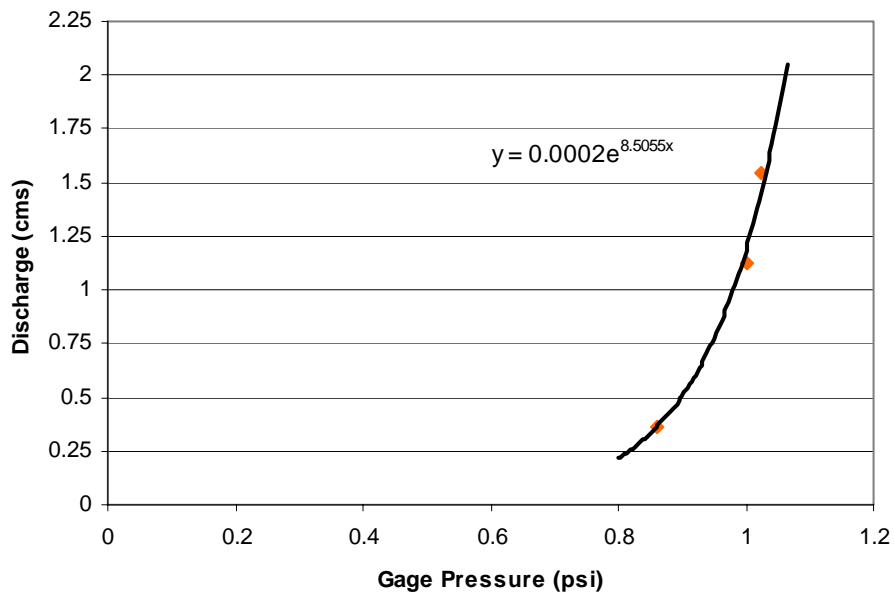


Figure 16-Streamflow rating curve for site 9

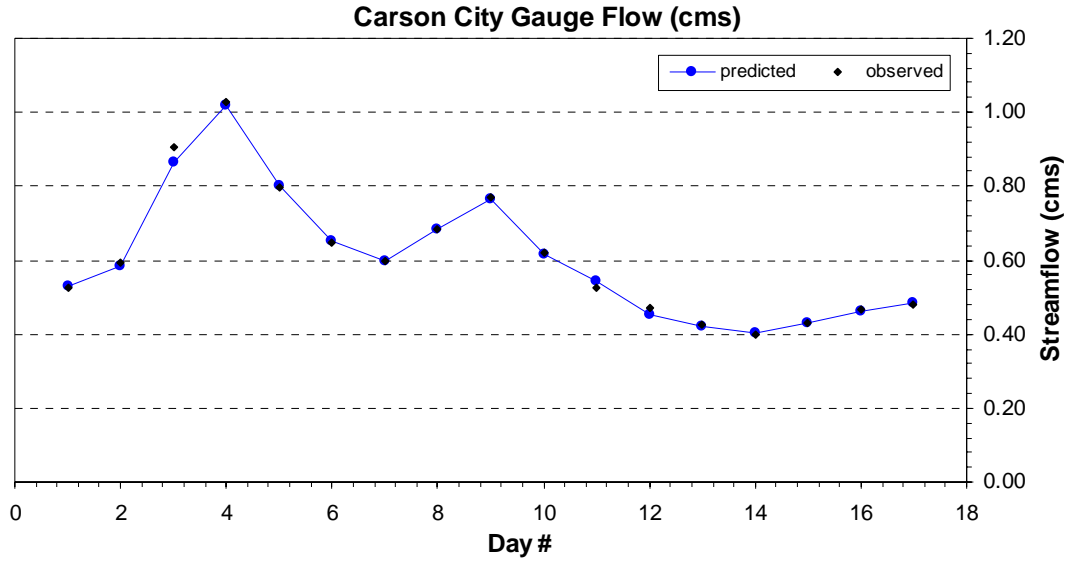


Figure 17-Carson City gauge predicted and observed streamflow (calibration period).

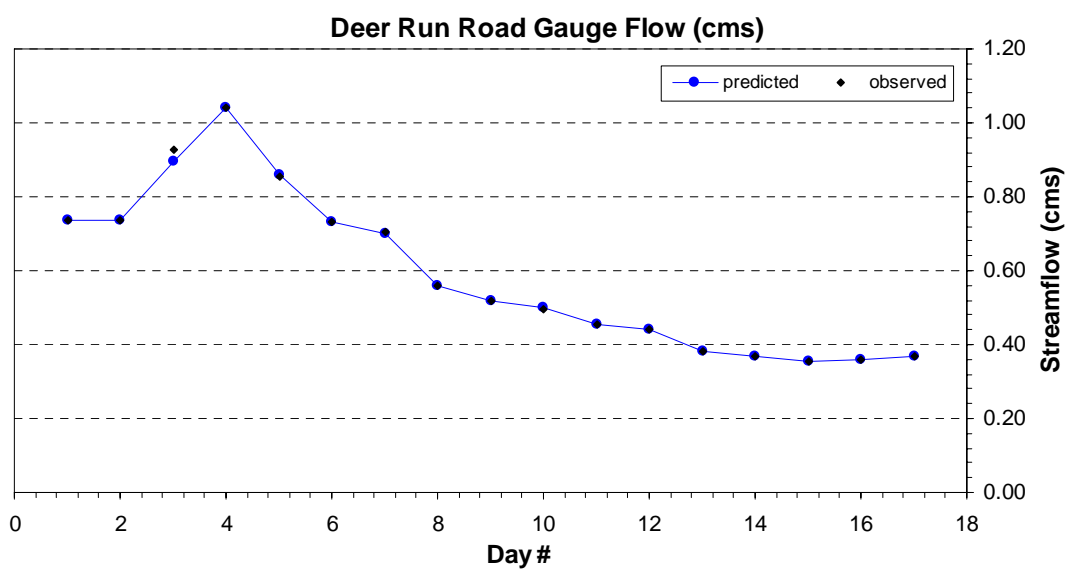


Figure 18-Deer Run Road gauge predicted and observed streamflow (calibration period)

3.6.1.4 Streambed Properties

The original model's thermal diffusivity and density terms for streambed sediments were not consistent with the streambed thermal properties in the Carson River.

The streambed sediment properties for the study area were not measured in the field because of limited resources, so the values in the modified model were subjectively assigned using Stonestrom and Constantz (2003), a number of online sources, and model default parameters. Thermal properties for saturated sandy sediments were used since sand is the dominant overall size fraction in study area (Table 4).

Table 4-Streambed thermal properties

Parameter	Value	Units
Sediment Density	2607.9	kg/m ³
Sediment Thermal Diffusivity	1.04 e-06	m ² /s

3.6.1.5 *Solar Radiation*

When compared to observed solar radiation data acquired in 2005, the equations in the model for estimating the amount of solar radiation reaching the water surface, were systematically overpredicting the observed data (Figure 19). This error was attributed to the model's empirical formula for solar radiation being developed for rivers in Oregon (i.e. different atmospheric conditions, elevation, and latitude). To account for the overprediction, a multiplier was developed using the ratio of observed to predicted solar radiation. The ratio corrected the solar flux reaching the water surface so that it better represented the observed pyranometer data (Figure 20). Note: The model's output for predicted solar flux is for a two hour time step and the observed data is plotted at an hourly scale. Thus, in the figure, predictions appear to have the tops of their daily peaks removed.

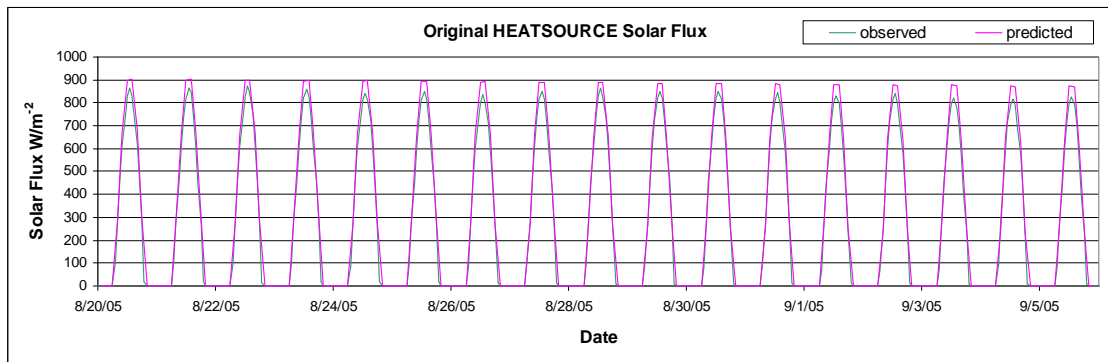


Figure 19-Comparison of original HEATSOURCE solar flux predicted vs. observed

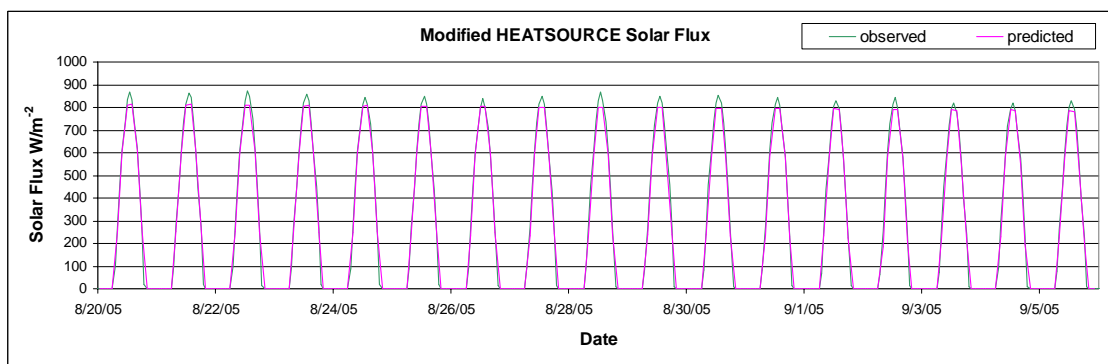


Figure 20-Comparison of modified HEATSOURCE solar flux predicted vs. observed

3.6.1.6 Cloudiness Factor

In HEATSOURCE, the influence of cloud cover on energy transmission in the atmosphere is included as a cloudiness factor that ranges from 0 (no cloud cover) to 1 (total cloud cover). Normally, qualitative observations (i.e. clear, scattered) of cloud cover are available to estimate this factor in the model. For the study area, no such data was readily available. The solar radiation data collected from pyranometers in 2005 and 2006 were used to develop a cloudiness factor that related solar radiation data to cloud cover. At each measurement in the time series, a clear-sky reference point was calculated by taking the median of the shortwave radiation at that time of day for the 5 days preceding and following that date. If the radiation value was $\leq 2/3$ the median value, that

site was given a cloudiness factor of 1 (total cloud cover) for that time interval. This procedure was repeated for the four remaining pyranometer sites and cloudiness was estimated by the proportion of cloudy sites. Thus, if 3 of the 4 sites showed cloudiness, the whole study area was assigned a cloudiness factor of 75% for that 10 minute measurement. The 10 minute cloudiness factors were then averaged to hourly values.

3.6.1.7 Radiation Attenuation in the Water Column and Streambed

Field measurements of surface PAR were made using a LICOR[®] LI-190SA Quantum Sensor. Downwelling PAR and upwelling PAR in the water column were measured using a submersible PAR sensor (LICOR[®] LI-192SA Underwater Quantum Sensor). Since water strongly attenuates shortwave radiation in the near to mid-infrared wavelengths, PAR is approximately equal to the shortwave energy absorbed or transmitted in the stream. The measurements were made at three representative locations in the study area: two upstream and downstream of the Last Low Head Dam (Site 8), and another upstream of Mexican Dam (Site 18). Based on the measurements, the empirical formulas in the original model code were adapted to estimate the transmittance and downward absorption (12) of radiation through the water column, as well as the shortwave energy absorbed in the streambed (13), reflection from the streambed (14), and upward transmittance and absorption in the water column (15). The adapted equations, listed below, were implemented in the model code to better represent the optical properties of water and substrate reflectivity in the Carson River.

$$\phi_{\text{TRD}} = 0.3763 \cdot e^{(-1.5584 \cdot \text{WP})} \quad (12)$$

$$\phi_{\text{BED}} = \cos(\theta_{\text{SA}}) \cdot (1 - 0.052) \quad (13)$$

$$\phi_{\text{BEDREF}} = 1 - \phi_{\text{BED}} \quad (14)$$

$$\phi_{\text{TRU}} = 0.3763 \cdot e^{(-1.5584 \cdot \text{Depth})} \quad (15)$$

Where,

ϕ_{TRD} = downward shortwave transmittance in water column (Wm^{-2})

WP = water path (m)

ϕ_{BED} = shortwave energy absorbed in streambed (Wm^{-2})

θ_{SA} = solar altitude (radians)

ϕ_{BEDREF} = shortwave energy reflected from streambed (Wm^{-2})

ϕ_{TRU} = Upward transmittance of shortwave in water column (Wm^{-2})

Depth = water column depth (m)

3.6.2 Parameter Estimation

When modeling complex systems, certain poorly understood model parameters will possess a fundamental uncertainty that often results from a lack of observed measurements to define their feasible range. Manually determining the appropriate values for such parameters can be difficult and time consuming, but the calibration procedure can be expedited through the use of parameter estimation routines. For the calibration of poorly defined HEATSOURCE model parameters, the Multi-Objective Complex (MOCOM) global optimization method was applied.

Yapo et al. (1998) developed the MOCOM global optimization method to have the benefits of controlled random search, competitive evolution, Pareto ranking, and a multi-objective downhill simplex search. The main problem with single objective

optimization methods is that no single objective measure is suitable to quantify the ability or inability of a model to fit the observed data (Yapo et al., 1998). The MOCOM algorithm overcomes this problem by calculating a set of Pareto optimal solutions based on multiple objective measures. For the HEATSOURCE calibration, two objective functions, Root Mean Squared Error (RMSE) (16) and the absolute value of percent bias (|%bias|) (17), were minimized simultaneously with MOCOM to develop a Pareto optimal solution set. These two objective measures were selected for their ability to evaluate different aspects of the model's error.

$$\text{RMSE} = \left[\frac{1}{N} \sum_{t=1}^N (T_t^{\text{pred}} - T_t^{\text{obs}})^2 \right]^{\frac{1}{2}} \quad (16)$$

$$|\% \text{bias}| = \left| \frac{\sum_{t=1}^N (T_t^{\text{pred}} - T_t^{\text{obs}})}{\sum_{t=1}^N (T_t^{\text{obs}})} \cdot 100\% \right| \quad (17)$$

Where,

T_t^{pred} = Predicted stream temperature at time t (°C)

T_t^{obs} = Observed stream temperature at time t (°C)

N = Number of observations

The main characteristic of a Pareto solution set is that the solutions are non-commensurate, that is, no one solution is objectively better than another (Yapo et al., 1998). For instance, with RMSE and |%bias| as objective measures (Figure 52) moving away from lowest RMSE results in improvement of |%bias| and deterioration of RMSE (Yapo et al., 1998). This gives the modeler an option to subjectively select the most

suitable parameter values from the Pareto solutions that minimizes the error in some kind of trade-off with respect to both objective functions. For a more detailed description of MOCOM operation the reader is referred to Yapo et al. (1998).

A MATLAB controller code (described below) was modified to execute the HEATSOURCE model, perform sensitivity analyses, operate the MOCOM algorithm, and assess model uncertainty. The observed water temperature data for the Lippencott Ski Ranch (Site 10), VNT (Site 14), and Empire Golf Course (Site 20) were selected for use in optimizing model parameters because of their contrast in vegetation, topography, temperature regime, and quality of data. Observations from remaining sites were omitted from parameter optimization because of their use as boundary conditions, questionable data quality (e.g. intermittent temperature sensor burial), or redundant coverage. Redundant coverage refers to sites that showed a very similar thermal behavior. During parameter fitting, these redundant sites would have over-represented certain hydrologic regimes in the study area. Since the project was focused toward understanding the thermal dynamics of the river as it relates to its classification as a coldwater fishery, and the goal of reducing daily maximum temperatures to $\leq 20^{\circ}\text{C}$, the model was calibrated only to a portion of the time series comprising the daily maximum water temperature (12:00-24:00 each day). This optimized model performance for the period of interest, but may have reduced the accuracy of predictions outside the calibration range.

In parameter estimation, the time required to complete a model run is important because it dictates the number of parameter sets that can feasibly be tested. Since the HEATSOURCE model is coded in Visual Basic, rather than a compiled language like FORTAN or C, the running time for a single simulation in the original code was more

than 5 minutes. Several changes were made to reduce the time required to run the model, including shortening of the simulation period from 17 days to 10, and precalculation of wetted channel geometries, evaporation, hydraulics, and solar position. When combined, the changes reduced the time required for one model simulation from 5 minutes to approximately 40 seconds, which allowed a larger number of parameter sets to be tested during sensitivity analysis, and reduced the time needed to complete the MOCOM calibration runs. The HEATSOURCE model was modified to read the selected parameter values from a text file that was generated for each iteration of the MOCOM procedure.

3.6.2.1 MATLAB Controller Development

A MATLAB controller code was adapted from preexisting MATLAB code (developed by Dr. Douglas Boyle of DRI) that used a Uniform Random Search (URS) algorithm to optimize curve number and lag time for the HEC-1 model. The controller was adapted to run the modified HEATSOURCE model, which required replacing the desired parameters in the model input file and making a system call to run a script that executed the model. Once the model was run, the predicted and observed data were loaded into MATLAB where the RMSE and $|\%bias|$ were computed for each realization. A MATLAB version (coded by Jasper A. Vrugt of the University of Arizona) of the MOCOM global optimization algorithm was integrated with the controller code. The basic functionality of the MOCOM algorithm was unaltered.

3.6.2.2 Calibration Procedure

For model parameters that were not measured directly or were poorly defined in the literature, a sensitivity analysis was used to determine which parameters had the

greatest effect on model output. The parameters used in the initial sensitivity analysis were the wind coefficients A and B (WCA and WCB), wind shelter coefficient (WSC), canopy shade factor (CSF), conduction layer depth (CLD), alluvium temperature for the upper reach #1 (ATU1), alluvium temperature for the upper reach #2 (ATU2), and alluvium temperature for the lower (ATL) reach (Table 5). The parameter values were generated from a uniform random distribution over their feasible range. The lower and upper bounds used for each calibration parameter are shown in Table 5. The bounds for WCA and WCB were selected to encompass the range of values cited in the HEATSOURCE model documentation (Boyd and Kasper, 2004). The CLD is conceptually defined by the thermal and hydraulic properties of streambed sediments and the heat gradient between mediums. Due to uncertainty associated with its value, we felt a wider range (0.05–1.2m) relative to default HEATSOURCE values, would allow a better chance of capturing the true sensitivity of this parameter. Later during MOCOM calibration runs, the upper bound for CLD was changed to 0.3m because MOCOM repeatedly got stuck in local minima. The ranges for the alluvium temperature parameters were guided by the maximum and minimum observed streambed temperature data in each alluvium zone. The model was executed for 1000 parameter iterations to determine which parameters were most sensitive. RMSE and $|\%bias|$ were used for objective functions as a measure of model sensitivity. Resulting dot plots (Appendix A: Figures 44 – 51) show the sensitivity of each parameter with respect to RMSE and $|\%bias|$ for the 1000 realizations. WCA and WCB showed sensitivity over their range, but any discernible sensitivity of the other parameters was obscured by the model response to WCA and WCB. In order to obtain a clearer picture of the sensitivity of the other 6

parameters, the MOCOM routine was used to obtain an initial estimate for WCA and WCB. This estimate (circled on Figure 52 in Appendix A) was selected to give the best trade off between RMSE and $|\%bias|$.

Table 5-Parameter ranges for initial sensitivity analysis (eight parameters)

Parameter	Lower Bound	Upper Bound
Wind Coefficient A (unitless)	1.0E-12	1.0E-08
Wind Coefficient B (unitless)	1.0E-10	1.0E-07
Wind Shelter Coefficient (unitless)	-0.2	1.00
Canopy Shade Factor (unitless)	0.25	1.20
Conduction Layer Depth (m)	0.05	1.2
Alluvium Temperature Upper Reach #1 (°C)	11	24
Alluvium Temperature Upper Reach #2 (°C)	11	24
Alluvium Temperature Lower Reach (°C)	11	24

A second sensitivity analysis was performed on the remaining 6 parameters using the initial estimate for WCA and WCB. Figures 53 to 58 in Appendix A show the sensitivity of the six parameters. From these figures it is apparent that 4 of the 6, including CLD, ATU1, ATU2, and ATL exhibited the most sensitivity over their range. Other temperature modeling studies have utilized a wind shelter coefficient to incorporate the sheltering effect that vegetation or topography has on wind speed. Brock and Caupp (2004) performed a sensitivity analysis on parameters for their DSSAMt temperature model and found that model response was highly sensitive to wind speed. Therefore, we retained the WSC as a MOCOM calibration parameter despite the fact that the sensitivity analysis indicated the model was insensitive to this parameter. Prior exploratory calibration runs were performed to determine the model's sensitivity to the CSF. The efforts indicated the model to be insensitive to this parameter, and no other temperature studies could be located that had used this parameter. Therefore, WSC, CLD, ATU1, ATU2, and ATL were retained for model calibration, whereas the CSF was eliminated

from the final MOCOM calibration run. When using parameter estimation methods it is desirable to obtain a simultaneous solution for the parameters of interest, so WCA and WCB were reinserted in the final MOCOM calibration run.

3.7 Model Validation

The HEATSOURCE model was validated using a combination of in-situ field data and the TIR survey collected in 2006. Accretion rates, WCA, WCB, alluvium zones, WSC, and CLD derived during model calibration in 2005 were held constant during the validation period. Microclimate data, including solar radiation, relative humidity, air temperature, and wind speed were collected at the Lippencott ski Ranch site (site 10) in 2006. A new series of cloudiness factors was developed based on the solar radiation data, this time relying solely on site 10. Data collected in 2005 from in-channel meteorological stations were used to develop regression equations that allowed us to relate the 2006 in-channel air temperature and relative humidity conditions at site 10 to the 4 remaining meteorological zones of the model. Air temperature regressions showed a range of r^2 from 0.954 to 0.980. Relative humidity regressions showed a range of r^2 from 0.842 to 0.943.

Streamflow was “recalibrated” to observed data during the validation period to isolate the error related to heat transfer simulations and reduce any error in the validated model that could be attributed to poor hydraulic representation. If the goal of the effort was specifically to test the robustness of the hydraulic representation, one would not usually recalibrate during validation. However, the primary goal of this study was to determine the change in thermal balance associated with possible revegetation, so

recalibration of streamflow reduced the uncertainty of temperature predictions for those revegetation scenarios. The streamflow recalibration was similar to the procedure used in the 2005 calibration period, except that information on pumping rates and the return flow at site 19 was more complete than in 2005. The return flow rates at site 19 were estimated from the rating curve shown in Figure 21. The rating curve developed for the return flow at the Riverview Park site (Site 19) exhibited a considerable degree of uncertainty at moderate to high flow. The uncertainty was attributed to scouring and depositional events which produced a variable cross section during two of the discharge measurements. In spite of this uncertainty, the information was used because it provided a better estimate of returns than simply assuming a constant rate as was done in 2005.

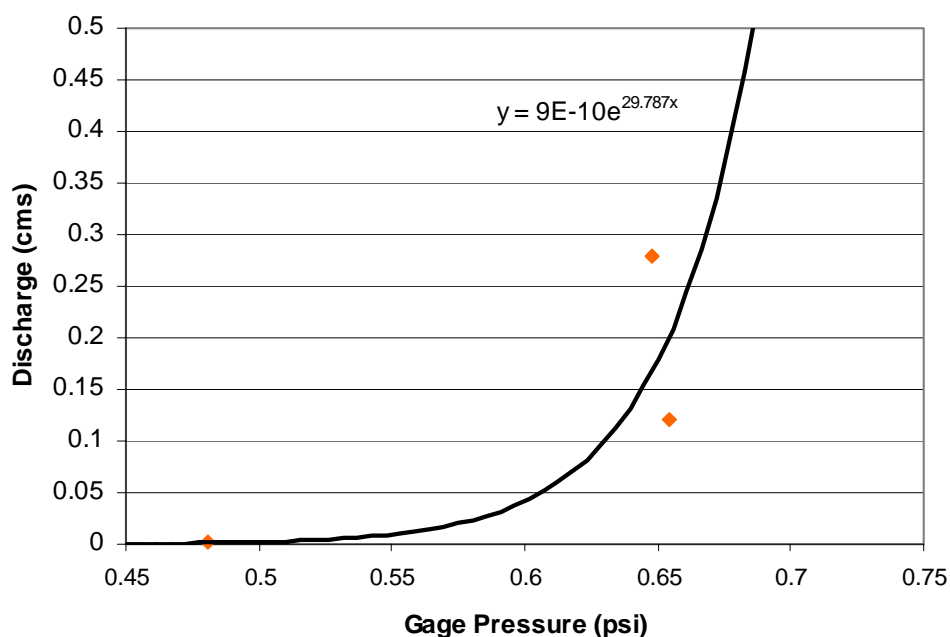


Figure 21-Streamflow rating curve for site 19

The pumping data was varied to balance streamflow between Genoa gauge and Carson City gauge. Estimates of 2006 withdrawals at Mexican Ditch were obtained from

the watermaster's office. To balance streamflow between Carson City gauge and Deer Run Road gauge, withdrawals at the Mexican ditch were increased if there was a surplus of water, and return flow rates were increased for streamflow deficits. The predicted and observed streamflow for the recalibration are shown in Figures 22 and 23.

The accuracy of temperature predictions was assessed by computing the daily maximum temperature range, the maximum over and underprediction, RMSE, and %bias for model predictions at four sites (Site 10, 15, 19 and 22). These four sites were selected for their quality (i.e. no apparent problems with burial or dam effects) and low overall uncertainty.

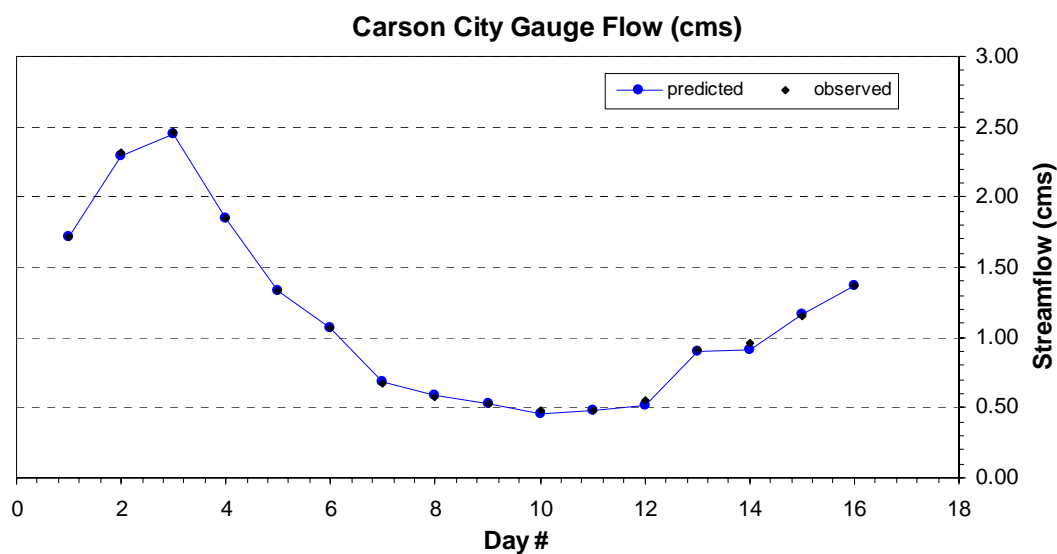


Figure 22-Carson City gauge predicted and observed streamflow (validation period)

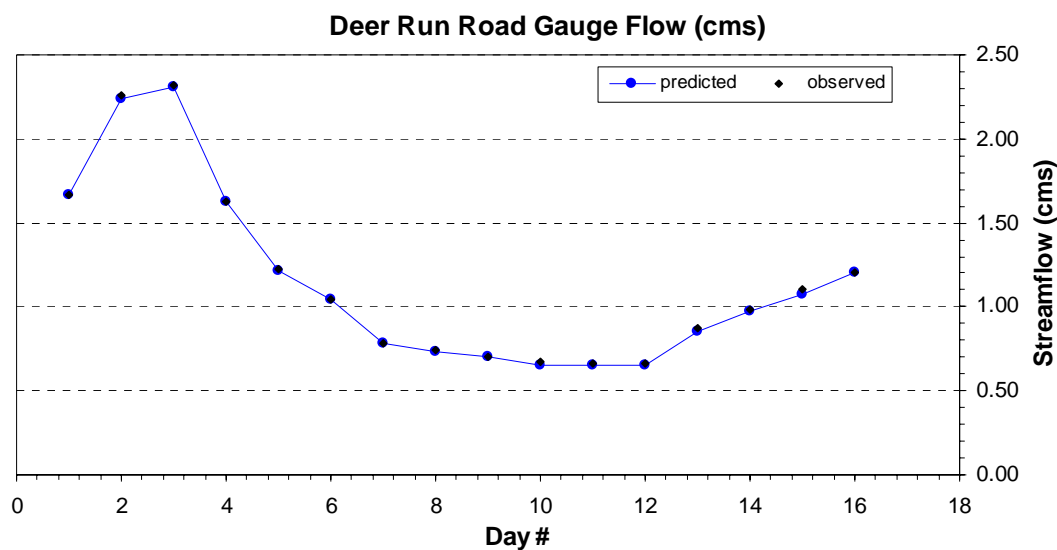


Figure 23-Deer Run Road gauge predicted and observed streamflow (validation period)

3.8 Simulating Revegetation Scenarios

The project was developed to test whether hypothesized revegetation strategies along the selected portion of the Carson River could reduce water temperatures to below 20°C, which is the optimal upper limit for coldwater fisheries (Eaton et al., 1995). Simulations of riparian revegetation were performed during the validation period by transplanting the vegetation attributes of the heavily vegetated zone 3 to the sparsely vegetated zone 2 (Figure 2). Six nodes in vegetation zone 3 were identified as having the densest mature cottonwood canopy in the entire study area. Vegetation surrounding these nodes was assumed to be the maximum possible native tree cover that could be expected in the revegetated reach. A program called *shadesim* was coded to sample existing LIDAR-derived vegetation attributes from the six nodes and randomly assign them to a series of user-defined destination nodes, correcting for differences in stream direction and channel width of the destination nodes. Vegetation attributes were transplanted only to

stream banks where the vegetation would actually provide shade (i.e. directional zones from 90° to 270°) since transpiration, longwave flux, and reduced evaporative cooling associated with unnecessary tree cover would be expected to offset some of the cooling from reductions in shortwave radiation. The simulated revegetation began downstream of the last low head dam (Site 8) and extended downstream to the McTarnahan site (Site 15), where the topographic shading and naturally occurring tree cover begin to increase.

3.9 Increased Streamflow Scenarios

Another question for the project was the relationship between streamflow and stream temperature reductions. Streamflow-temperature dynamics were evaluated by performing two model runs with an increased streamflow of $15\text{m}^3\text{ s}^{-1}$ at the Genoa gauge boundary condition site, one with existing vegetation and another with simulated revegetation. This was the upper flow limit of the model domain and the typical regime where 20°C is exceeded early in the summer. There is a large degree of uncertainty with these simulations, since there is no information for boundary condition stream temperatures that would occur if a discharge of $15\text{m}^3\text{ s}^{-1}$ could be maintained into the peak thermal stress of mid-late summer. It is also exceedingly unlikely that such conditions could be implemented given the status of negotiated water rights. Although flows of this magnitude never occur at the time of maximum annual stream temperature, we used this scenario to explore the importance of streamflow relative to revegetation. Given the uncertainties, all parameters except streamflow remained identical to those used in the validated model.

4 Results

4.1 Calibration Results

4.1.1 MOCOM Results

The MOCOM algorithm was run using an initial sample size of 25 points. The small sample size allowed the MOCOM routine to complete in a shorter amount of time. The resulting 25 Pareto optimal solutions are shown in Figure 59. The 25 solutions are shown, but only nine are visible because many of the solutions are overlapping. The solutions do not exhibit the typical Pareto curve shape that is typical for MOCOM solution sets and they span a very narrow range of $|\%bias|$ and RMSE. In this case, a trade-off solution is not as meaningful because moving from lowest to highest RMSE does not produce much deterioration of $|\%bias|$. Nevertheless, the parameter set circled in Figure 59 was selected as it gives the best trade-off between RMSE and $|\%bias|$. The parameter values and associated objective values for our final MOCOM solution are shown in Table 6.

Table 6-MOCOM calibration results

MOCOM							
Objective Measures	WCA (unitless)	WCB (unitless)	WSC (unitless)	CLD (m)	ATU1 (°C)	ATU2 (°C)	ATL (°C)
RMSE = 0.78 $ \%bias $ = 0.4E-03	8.11E-10	1.14E-08	0.034	0.27	20.45	17.68	23.86

4.1.2 Daily Maximum Predictions

During calibration, daily streamflow averaged $0.6 \text{ m}^3 \text{ s}^{-1}$ based on the three USGS gauging stations in the study area. The period contained a diverse range of hydraulic and atmospheric conditions representing the low flow condition. Figures 24, 25, and 26

compare observed water temperature data to the stream temperatures predicted by the calibrated model. Only the sites used directly in the parameter estimation methodology are presented (10, 14, and 21).

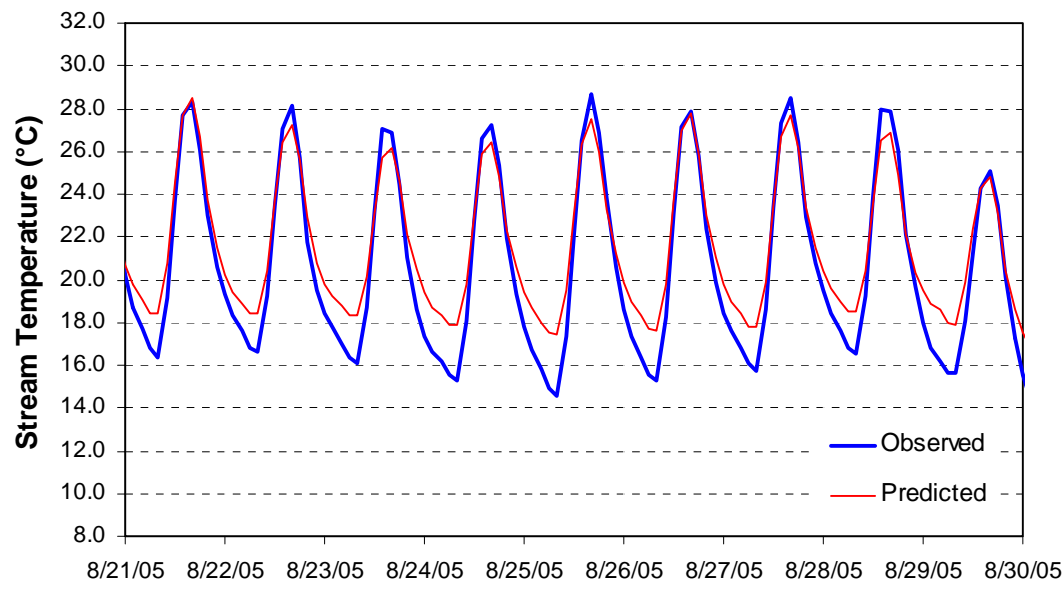


Figure 24-Diel temperature profile for site 10 (calibration period)

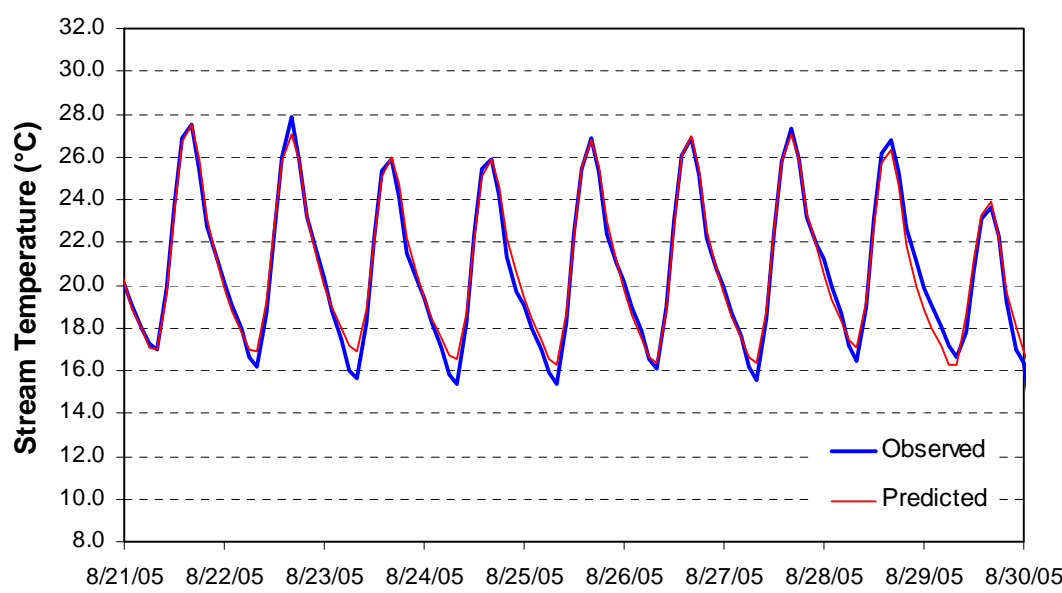


Figure 25-Diel temperature profile for site 14 (calibration period)

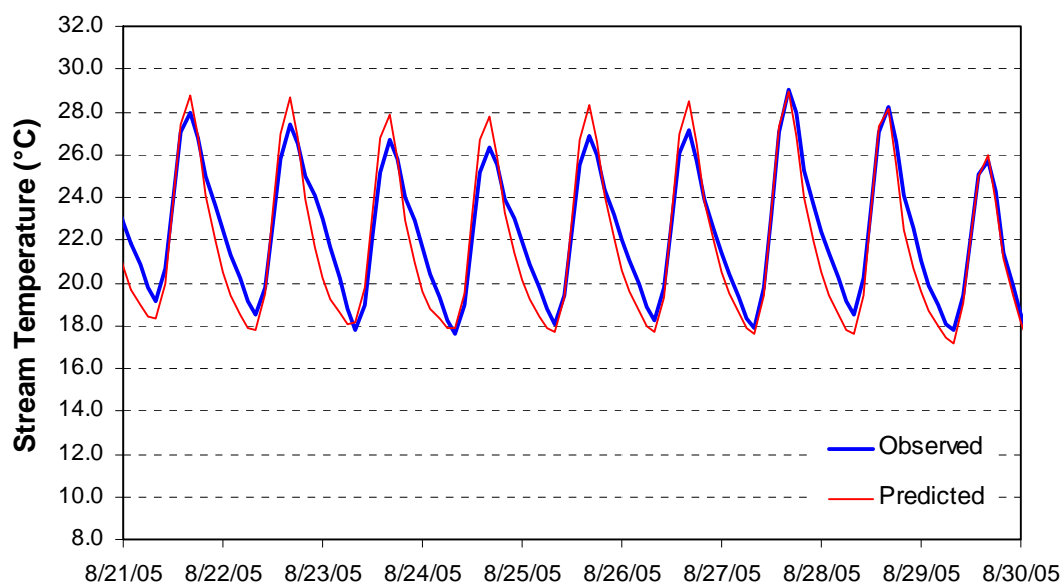


Figure 26-Diel temperature profile for site 21 (calibration period)

The RMSE, %bias, maximum overprediction (OP), maximum underprediction (UP), and average residual error between the predicted and observed daily maximum temperatures for the calibration period are presented in Table 7. Values for RMSE in Table 7 are larger than the MOCOM estimate because they were calculated for the daily maximum stream temperature, and MOCOM estimate was calculated using the period (12:00 – 24:00). Note: absolute percent bias was used for the MOCOM estimate, but in Table 7 percent bias is used.

Table 7- Statistics for maximum daily stream temperature predictions (calibration period)

Site #	RMSE (°C)	% Bias	Max-OP (°C)	Max-UP (°C)	Avg-residual (°C)
10	0.88	-2.51	0.35	-1.51	-0.69
14	0.79	0.41	2.32	-0.75	0.11
21	1.44	4.00	3.40	-0.10	0.83
mean	1.04	0.63	2.02	-0.79	1.07

To assess the ability of the model to represent a range of conditions, a 99% confidence interval was calculated using the Generalized Likelihood Uncertainty Estimation (GLUE) method. The GLUE method, which is based on Bayesian Monte Carlo theory, assigns weights to predictions as a function of their proximity to the observations. Those predictions that are closer to the observations receive a higher weight, while those further from observations receive a lower weight. Figure 27 shows the 99% confidence interval developed using the GLUE method with RMSE as a measure of model error. The upper and lower limits, shown with red dashed lines, delineate the interval in which 99% of the predictions will fall. The black line shows the observed series and the blue line represents the mean estimated response of the model to a random distribution of inputs. The range of confidence for the three sites is summarized below.

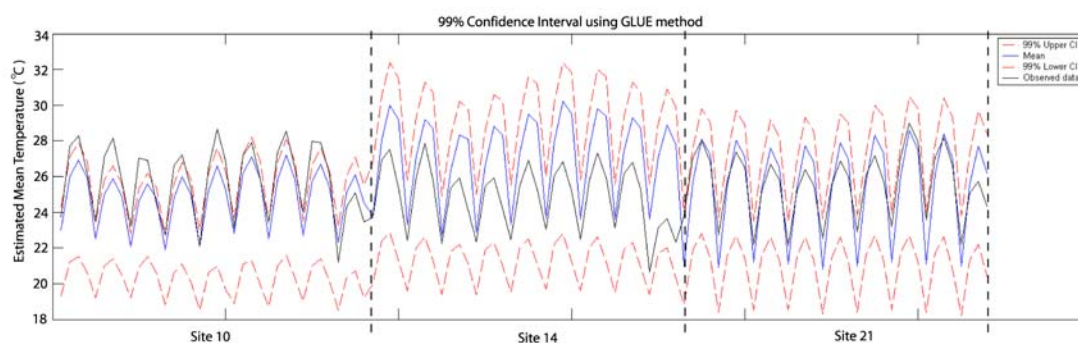


Figure 27-99% confidence interval for the calibration period (GLUE method)

For site 10, the cool 99% lower confidence limit indicates that the model has the capability to simulate much cooler conditions, but the maximum daily observed temperatures at this site often fall outside the upper 99% confidence interval. This shows there are some conceptual problems with the model design or with the manual calibration settings, and that the model will struggle to match conditions warmer than those observed

in 2005. In contrast to site 10, the confidence interval at sites 14 and 21 have a warmer lower confidence limit, a warmer upper confidence limit, and the observations are fully contained within the range of confidence. This shows the model has the ability to capture increased heating or cooling beyond that of the observed series for these sites.

4.2 Validation Results

During the model validation period, streamflow averaged $1.22 \text{ m}^3 \text{ s}^{-1}$ (two times higher than streamflow during the calibration period) based on the three USGS gauging stations in the study area. Streamflow was higher during the validation period because the simulation took place earlier in the month of August than during calibration. Otherwise the two water years (2005 and 2006) were similar. Error associated with the validation period was assessed by computing RMSE, %bias, maximum overprediction, maximum underprediction, and average residual error for the predicted versus observed daily maximum predictions. Longitudinal temperature profiles were compared to the observed data and the TIR survey to assess the spatial dynamics of model predictions.

4.2.1 Daily Maximum Predictions

For model validation, we compared the model's predicted daily maximum temperature to field data from four validation sites (10, 15, 19, and 22). Figures 28, 29, 30, and 31 compare the diel fluctuations in observed water temperature to those predicted by the model during the validation period. The error measures associated with the daily maximum stream predictions for each site are summarized in Table 8.

Table 8-Statistics for maximum daily stream temperature predictions (validation period)

Site #	RMSE (°C)	%		Max-UP (°C)	Avg-residual (°C)
		BIAS	Max-OP (°C)		
10	1.03	-1.84	0.98	-2.13	-0.48
15	1.24	-0.51	2.26	-2.33	-0.13
19	2.12	5.03	4.12	-1.66	1.29
22	1.48	2.43	3.76	-1.73	0.77
Mean	1.47	1.28	2.78	-1.96	0.36

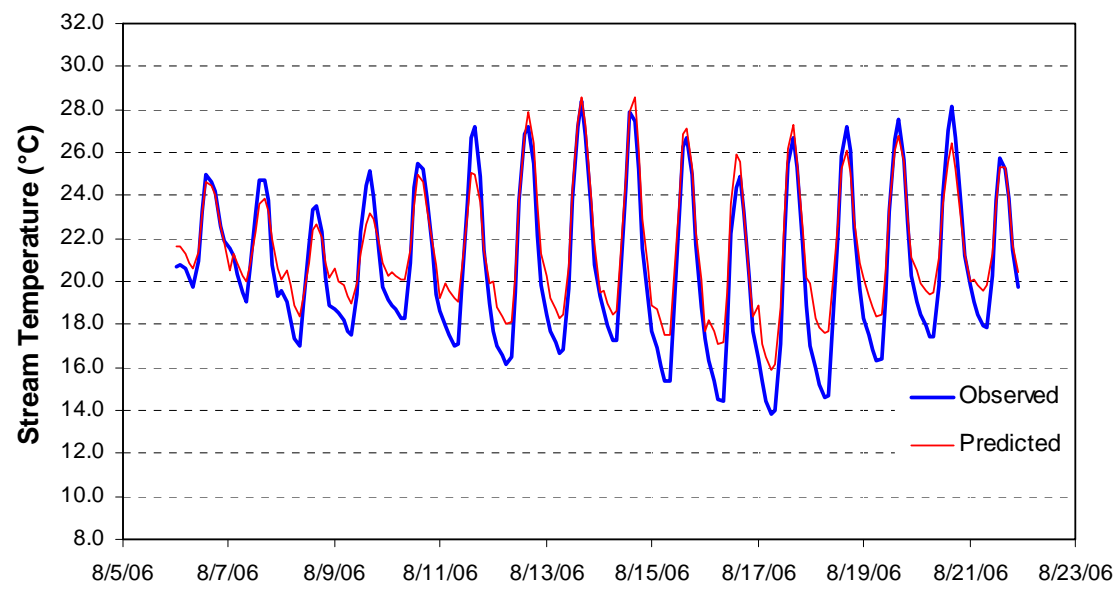


Figure 28-Diel temperature profile for site 10 (validation period)

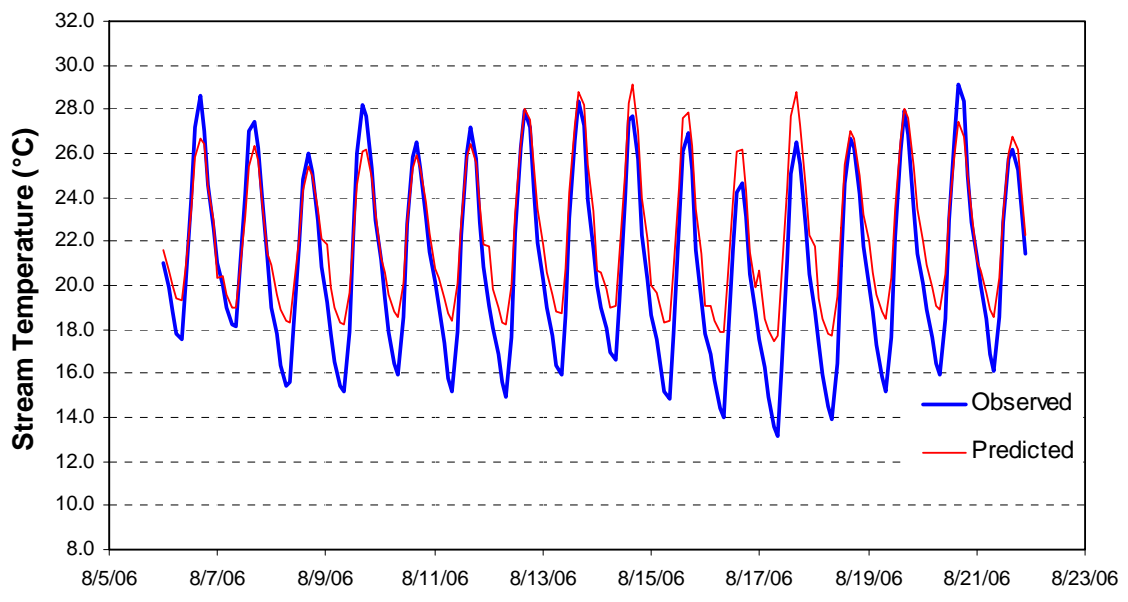


Figure 29-Diel temperature profile for site 15 (validation period)

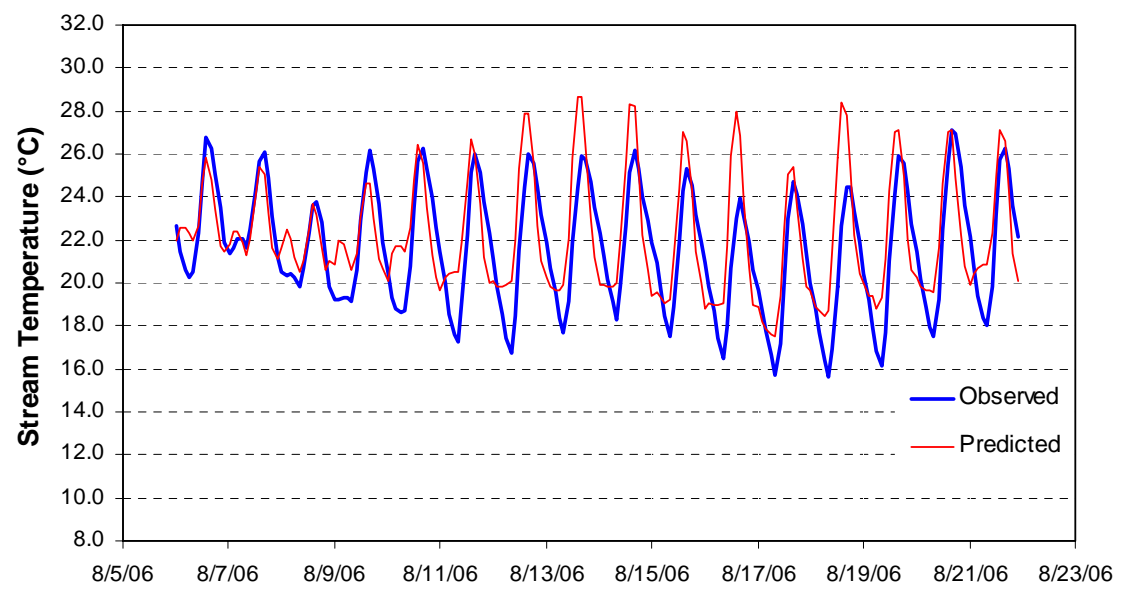


Figure 30-Diel temperature profile for site 19 (validation period)

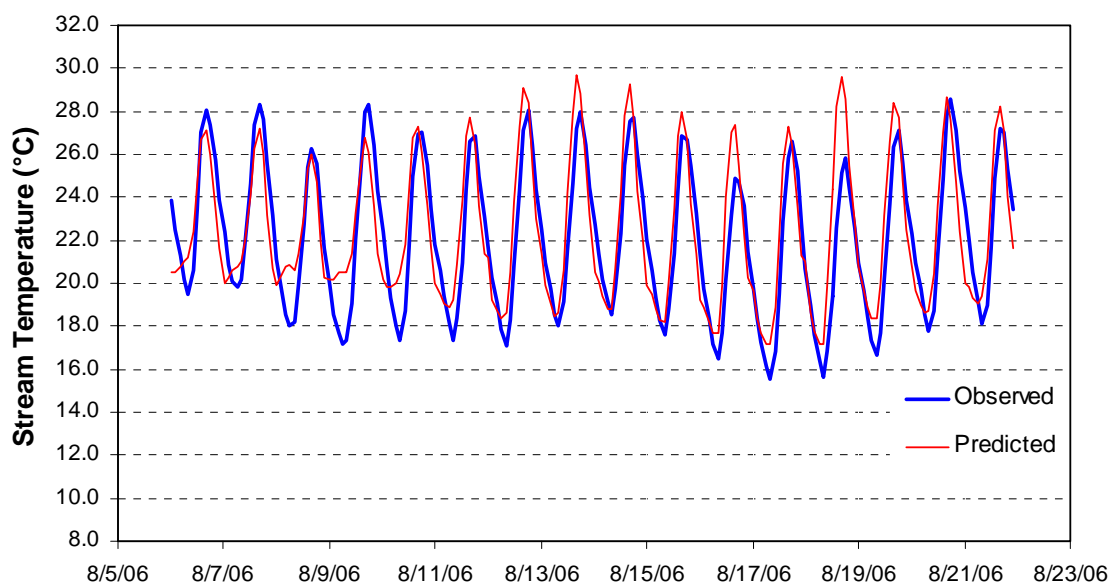


Figure 31-Diel temperature profile for site 22 (validation period)

Box and whisker plots of the daily maximum temperature range for the four validation sites are presented in Figure 32. At site 10 and 15, the difference in median value shows a general underprediction, but the range of daily maximum stream temperatures is similar. Site 19 shows a positive bias and a wider range of predicted daily maximums than was observed. The range of predicted daily maximums for Site 22 is more in line with what was observed during the validation period, but the maximum range is still slightly warmer than the observed range.

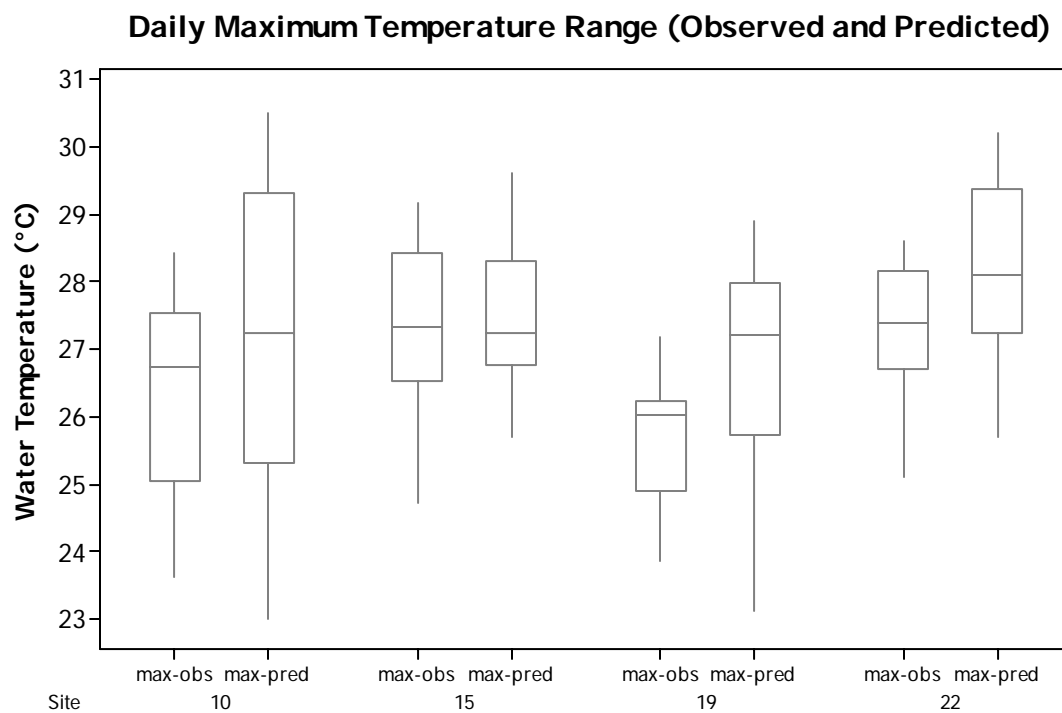


Figure 32-Box plots of the daily maximum temperature range for the four validation sites

4.2.2 Longitudinal Profiles

Longitudinal profiles of the model predictions are more informative than diel profiles when attempting to understand the spatial variation of model parameters and processes. The model produces a longitudinal output profile every two hours, resulting in 12 profiles per day. Including all of the profiles in this document was impractical, so only the best and worst-fits for the time steps representing the daily maximum temperature for the 16 day validation period are presented. Model fit was based on RMSE. Figures 33 and 34 show the best and worst-fit model predictions longitudinally downstream (red dots), along with the observed data (yellow dots), the distribution of atmospheric zones (upper row of colored blocks), accretion zones (lower row of colored blocks), locations of inflows (green dots), low head dams (blue dots), and the existing effective shade in the

model domain (red line at bottom of figure - refer to shading methodology section for definition of effective shade).

The best-fit scenario occurred on 8/8/06 at 4:00pm. Figure 33 shows the model did an excellent job (RMSE = 0.60°C) simulating stream temperature in the reach downstream of the last low head dam (stream km 28-Site 8) and in the reach downstream of Mexican Dam (stream km 9-Site 18).

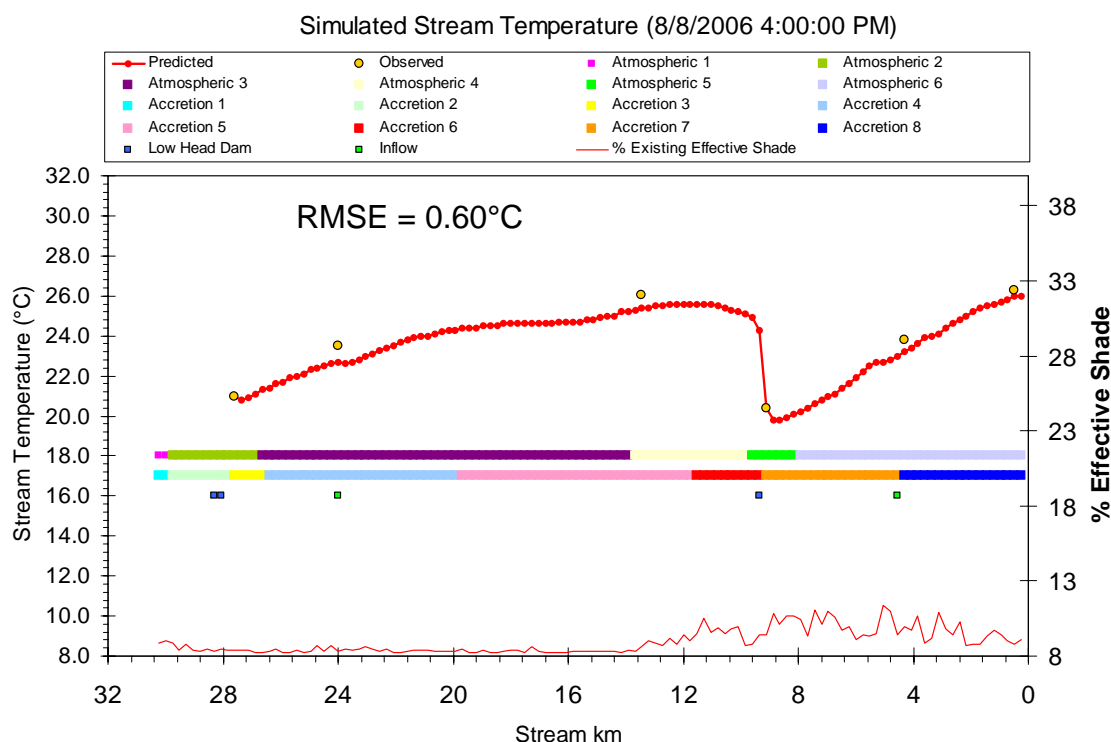


Figure 33-Longitudinal profile (best-fit scenario)

The worst-fit scenario, presented in Figure 34, occurred on 8/18/06 at 4:00pm. The figure shows that the model produces a similar level of accuracy as the best-fit scenario for the reach downstream of the last low head dam (stream km 28-Site 8), but the fit downstream of Mexican Dam (stream km 9-Site 18) is very poor. We attribute the poor fit in this reach of the model to poor hydraulic representation resulting from

uncertainty associated with withdrawals at the Mexican Dam (Site 18), and the returns at the Riverview park return flow (Site 19). For the selected time step, RMSE for the worst-fit scenario was 2.83°C, but nearly all of the error can be attributed to the poor fit below Mexican Dam.

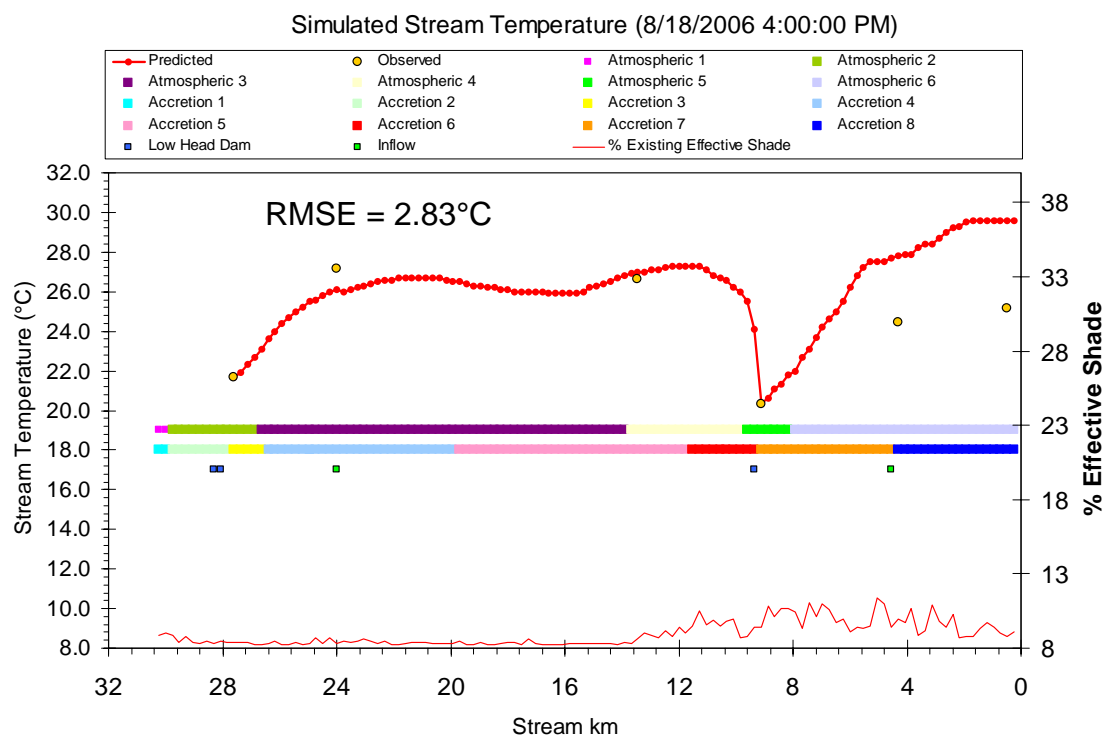


Figure 34-Longitudinal profile (worst-fit scenario)

4.2.3 Thermal Infrared Survey

The TIR survey acquired in the summer of 2006 was used as a second independent validation measure in assessing the accuracy of the HEATSOURCE model. The main limitation of the TIR survey as a validation tool is that it is merely a snapshot in time. However, it is still a valuable means to assess model error and determine the strengths and weaknesses of the model as a predictive tool. The portion of the survey covering the study area was acquired on 8/8/06 over the time period 1:40-2:19pm.

Luckily, this corresponded perfectly with the model's longitudinal profile for 2:00pm.

Figure 35 compares predicted stream temperatures to the TIR survey.

In terms of overall fit, it is apparent that there are reaches of the study area where the model predictions match the survey very well and other reaches where the model performed poorly. For discussion, the longitudinal profile in Figure 35 is labeled with 4 regions (A, B, C, and D) to highlight different aspects of the model's fit. In region A, the model underpredicts observed stream temperatures by an average residual error of 1.5°C. In contrast, region B fits the TIR data very well and the residual error shows an average residual of 0.3°C. In region C, the model overpredicts the TIR temperatures by an average residual error of 1.7°C and in region D the model fits TIR data very well with an average residual error of 0.3°C. It is encouraging that we did achieve a tight fit in regions B and D, since this was part of the reach of the river where revegetation would be simulated.

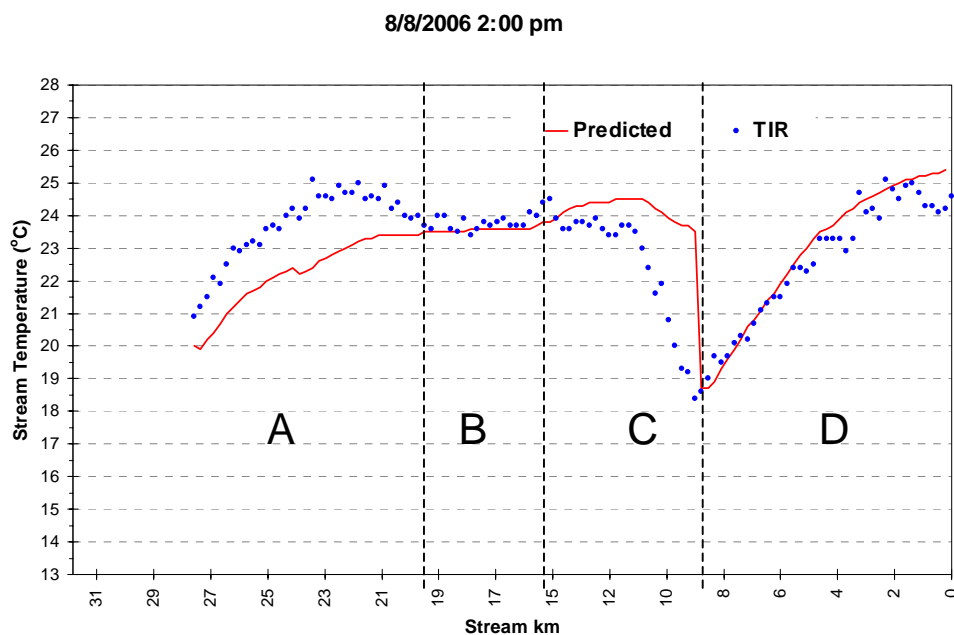


Figure 35-Comparison of predicted stream temperatures and the TIR survey temperatures

4.3 Simulating Revegetation Scenarios

The simulations of revegetation represented the maximum potential tree cover that could be expected in the revegetated reach. For revegetation analysis, we will focus only on the portion of the longitudinal profile where the revegetation would occur (stream km 27.84 to 13.68). The reach downstream of the simulated revegetation was more of a concern with respect to verifying that the existing canopy was being represented properly. The longitudinal profile showing the coolest daily maximum stream temperature was selected because it provides the most likely possibility that the 20°C threshold could be met. If the threshold temperature cannot be reached on the day of coolest maximum stream temperature, then it is unlikely that it could be reached for warmer model conditions. Figure 36 shows the longitudinal stream temperature predictions for the validated model with existing vegetation in red dots and simulated vegetation attributes in blue Xs. The blue line at the bottom of the figure corresponds to the effective shade produced by revegetation. The temperature predictions for the simulated vegetation clearly show a maximum reduction in stream temperature of 1.8°C at stream km 15 (upstream of MCT-Site 15). On average, increased tree cover reduced the temperature of the revegetated reach from 23.56°C to 22.49°C, with a maximum local change from 25.2°C to 23.4°C. Even with these levels of stream temperature reduction, the temperature is not reduced to $\leq 20.0^\circ\text{C}$ at any point in the revegetated reach.

Maximum daily temperature predictions (4:00pm) were checked for all days in the validation period to determine whether the goal of $\leq 20.0^\circ\text{C}$ was attained at any point in the revegetated reach. The results showed that the stream's maximum daily temperature was not reduced to $\leq 20^\circ\text{C}$ for any location in the revegetated reach. Since

the maximum potential revegetation scenario did not reduce temperatures to $\leq 20^{\circ}\text{C}$, no further variations of revegetation attributes were tested (e.g. shorter willow versus cottonwood canopy).

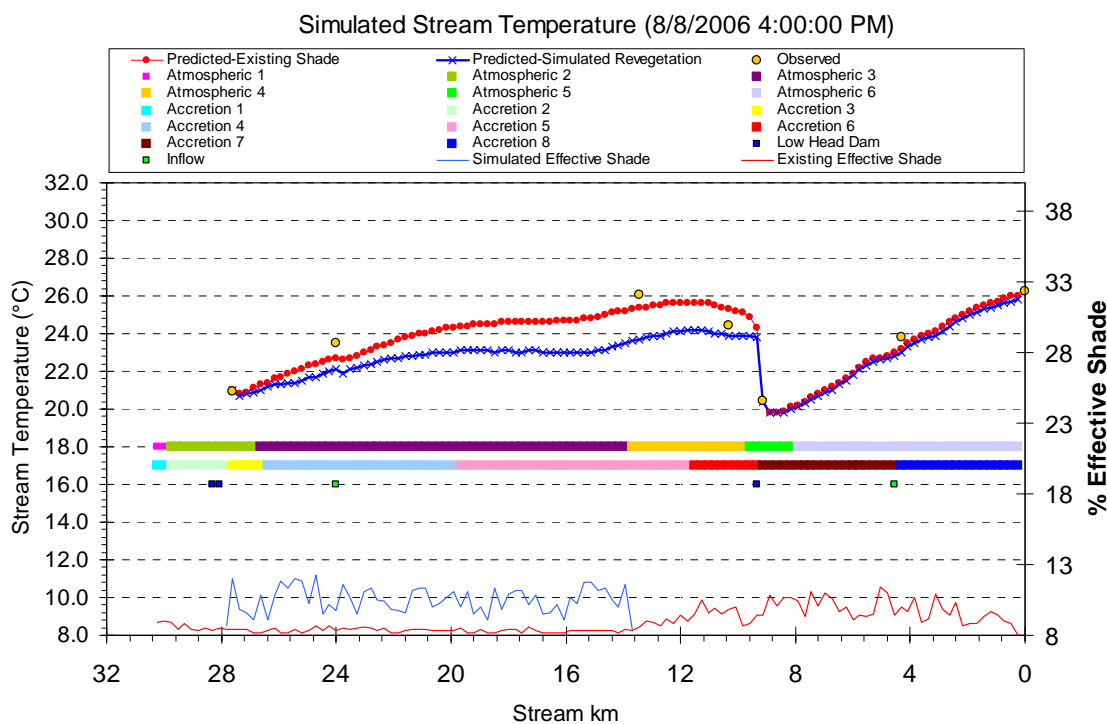


Figure 36-Comparison of predicted stream temperatures for existing vegetation (red dots) and simulated vegetation (blue Xs)

4.3.1 Change in Energy Components-Post Revegetation

The change in energy components after revegetation gives an indication of how the various fluxes were affected by increased riparian shade. To provide further illustration that the revegetation is having the intended effect, the diel profiles of each energy component for a single model node (stream km 15.84) upstream of the McTarnahan site (Site 15) in the revegetated reach are presented in Figures 37 through 42. This node was selected for its tight correspondence to the TIR survey and relatively strong temperature response.

Figure 37 shows the shortwave flux to the stream surface is reduced at the time of maximum solar exposure, but the greatest reductions in solar flux occur in the morning and afternoon as the low angle of incoming shortwave radiation allows more interception by the tree cover. Vegetation emits longwave energy in the form of radiant heat. In the unvegetated model, the stream radiates heat mostly into the air due to the absence of vegetation in these areas. When we introduced tree cover, the back-radiation leaving the stream now radiates energy into some ratio of vegetation to air and these materials have different emissivities. This causes a shift in the net balance of longwave energy (Figure 38). Figure 39 shows the evaporative flux from the stream has become more negative after the introduction of near-stream riparian vegetation. Evaporation could be influenced in this way by two processes: reduction in turbulence at the air water interface, or reduction because less evaporation occurs at cooler water temperature. We feel the reduction in evaporative cooling is more likely driven by reductions in wind speed associated with the simulated tree canopy. This supports the rationale for revegetating solely on the banks which could provide shading to the stream surface, and not on those banks which could offset reductions associated with revegetation. Overall, the convective flux became more positive (Figure 40). The increase is attributed to the larger heat gradient between the air and water that results from cooler stream temperature, which increases the rate of molecular heat exchange between the mediums. Heat transfer by conduction at the water streambed interface shows a response similar to the convective flux after revegetation, becoming more positive over the entire validation period. In this case, the increase is attributed to the larger heat gradient between the water and

streambed (Figure 41). Figure 42 shows that the net heat flux to the stream has decreased over the validation period, indicating the tree cover is having the desired effect.

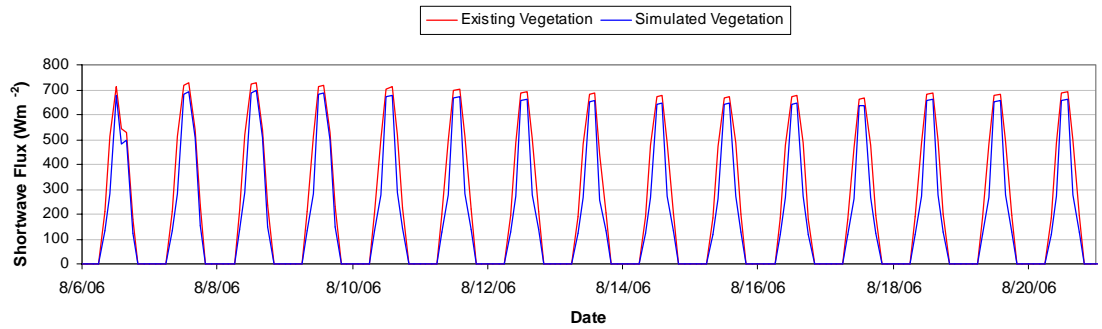


Figure 37-Shortwave flux for existing and simulated vegetation

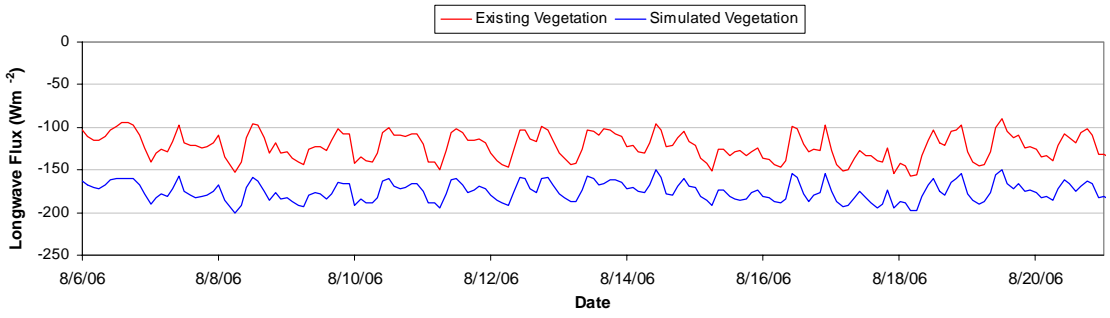


Figure 38- Longwave flux for existing and simulated vegetation

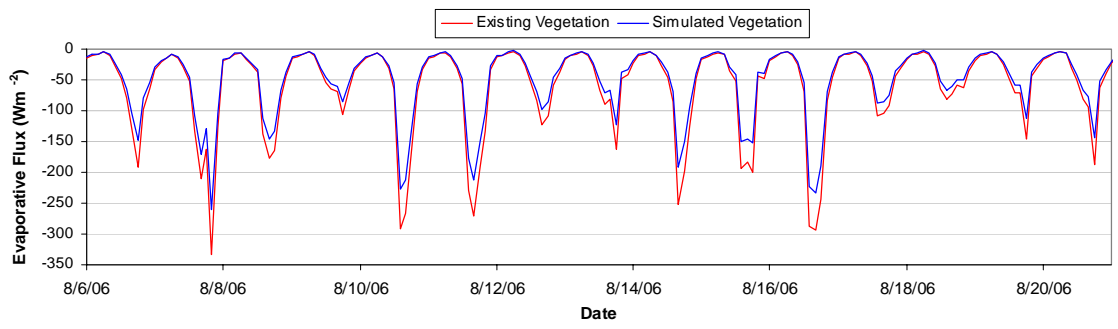


Figure 39- Evaporative flux for existing and simulated vegetation

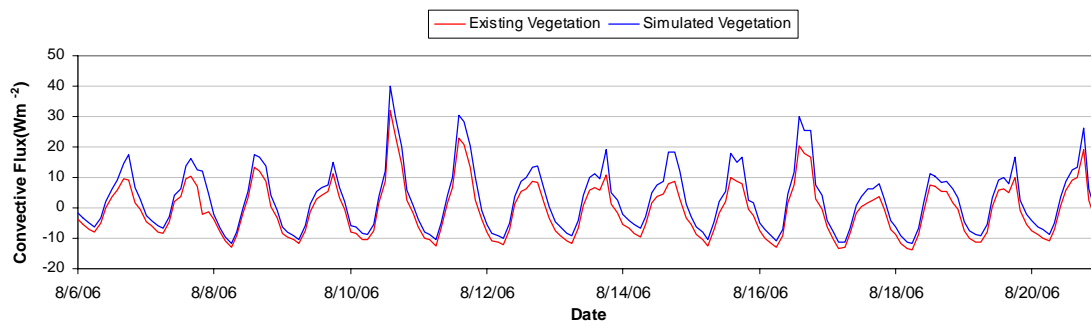


Figure 40- Convective flux for existing and simulated vegetation

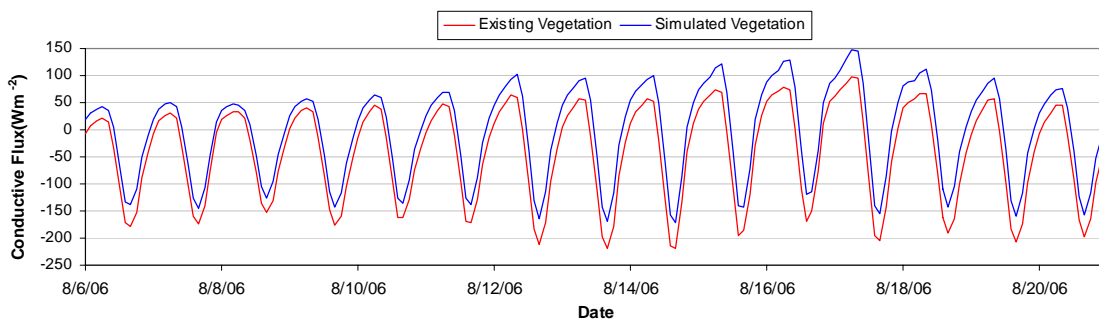


Figure 41- Conductive flux for existing and simulated vegetation

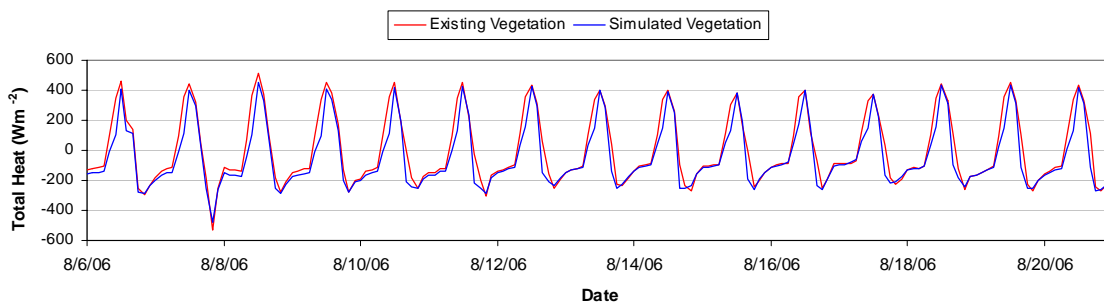


Figure 42- Total heat flux for existing and simulated vegetation

4.4 Increased Streamflow Scenarios

We performed two increased streamflow simulations to determine the importance of streamflow relative to other factors, such as revegetation. The first simulation was performed with existing vegetation and the second was performed with simulated vegetation. For the increased streamflow scenarios, we again focused on the revegetated

portion of the longitudinal profile from stream km 27.84 to stream km 13.68. Figure 43 shows the longitudinal profiles for the $15 \text{ m}^3 \text{ s}^{-1}$ streamflow simulations with existing vegetation (purple dots) and simulated vegetation (black dots). The results from the validated model (existing vegetation and actual flow) are shown with red dots for comparison. On average, increased streamflow with existing vegetation reduced the predicted temperature from 23.58°C to 21.33°C , and reduced the maximum temperature from 25.30°C to 22.20°C . Increased streamflow with simulated revegetation reduced the average temperature for the revegetated reach to 20.92°C , and the maximum temperature was reduced to 21.30°C .

For the increased flow scenarios, the simulated revegetation cooled temperatures by a maximum of 1°C compared to existing vegetation. The minimal difference between the two scenarios shows that the relative importance of riparian shade is overshadowed by the river's ability to maintain its temperature at higher flow levels. Temperatures remained close to the temperature of boundary condition inflows for both increased flow simulations, showing minimal warming regardless of vegetation. Longitudinally, the predicted temperatures follow a generally linear warming trend over the revegetated reach, never reaching the $\leq 20.0^\circ\text{C}$ threshold. The two increased flow scenarios showed that increased streamflow alone and increased streamflow with revegetation were not able to reduce temperatures to $\leq 20^\circ\text{C}$ if increased flow was not accompanied with a reduction in upstream temperature.

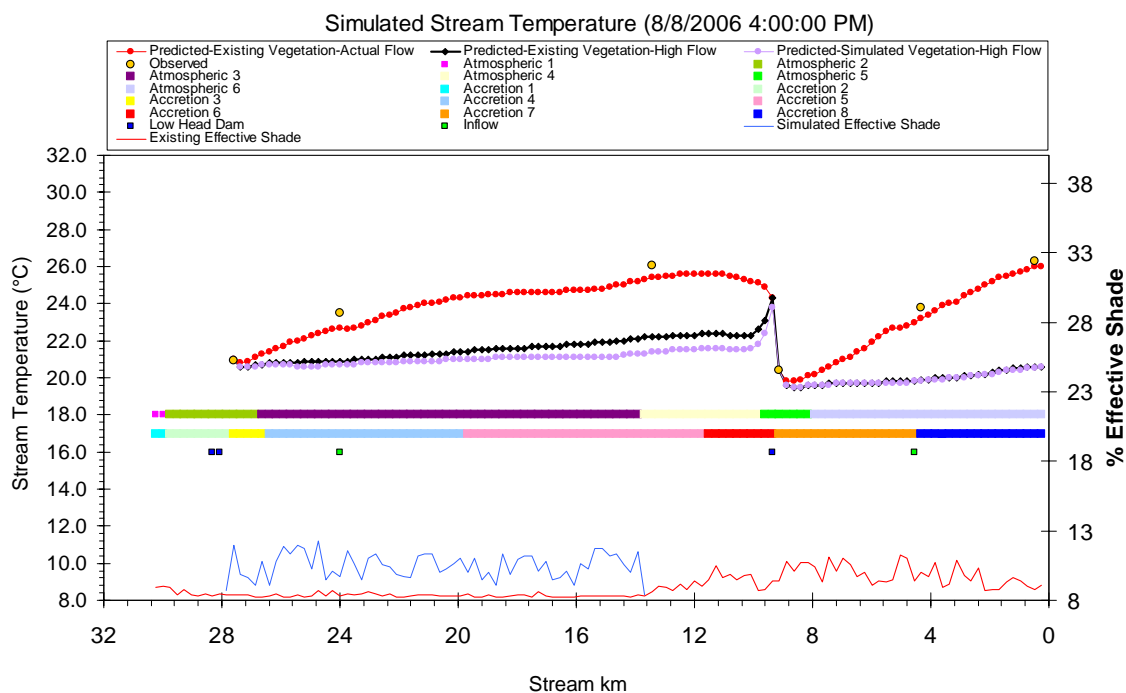


Figure 43-Longitudinal profiles for existing vegetation with actual flow (red dots), existing vegetation with high flow (black dots), and simulated vegetation with high flow (purple dots)

5 Discussion

The modified HEATSOURCE model showed that the maximum revegetation simulation produced maximum reductions in stream temperature of 1.8°C, but also demonstrated that there were no days over the entire validation period when the maximum daily stream temperature was $\leq 20^{\circ}\text{C}$ in the revegetated reach. The increased streamflow with existing vegetation, and increased streamflow with maximum revegetation scenarios, were also not able to maintain temperatures to $\leq 20^{\circ}\text{C}$ in the revegetated reach of the Carson River. The increased streamflow with existing vegetation scenario allowed the river to maintain a lower temperature, decreasing the average temperature of the revegetated reach from 23.56°C to 21.33°C and the maximum temperature from 25.30°C to 22.20°C. The increased streamflow with simulated

vegetation scenario also prevented the river from warming as rapidly, decreasing the average temperature of the revegetated reach from 23.56°C to 20.92°C and the maximum from 26.0°C to 21.30°C.

Field data for model calibration and validation were sampled at a high spatio-temporal resolution, and geospatial data complimented ground level measurements. Unfortunately, failure rates for iButton[®] model DS1922L temperature data loggers averaged 25% over the two years of data collection, which resulted in data gaps at many sites. We needed to monitor temperatures potentially above 30°C, which was the main reason for selecting this model iButton[®]. In hydrologic systems where water temperature does not exceed 27°C, iButton[®] model DS1921Z is a better option because the failure rate (8%) for this model is much lower than the rate we experienced for the DS1922L model (Johnson et al., 2005).

When developing data sampling protocols and sampling designs, it is difficult to anticipate all the problems that could potentially be encountered. The tendency of the Carson River's streambed to shift at different flow regimes resulted in burial of temperature stakes, which contributed additional uncertainty regarding water column temperatures at some sites in 2005. The stake design worked well overall, but when they were buried, we lost all confidence in the measurement of the water column temperature. The float and tether design that was used in 2006 resolved the burial issue. The temperature data logger in the float and tether design could not be buried, but that design did not allow measurement of streambed temperatures and had a different set of problems. For example, accumulation of algae on one float actually dragged the entire apparatus 50 yards downstream at one site. The stake design would be more suited to

rivers with a coarser substrate and more stable flow regime, whereas the float and tether design is better when quick deployments and infrequent return visits are desired.

Data gaps resulting from iButton failures, burials, and low head dam effects led to a high degree of uncertainty associated with some observed water temperature data. Uncertainty and data gaps reduced the number of sites available for calibration and the temporal extent of data available for the calibration period. Ideally, we would have preferred to calibrate and validate with more sites over a longer period of time, but with the uncertainty and data gaps this was not possible.

Some aspects of the original HEATSOURCE code were not entirely appropriate for representing the hydraulic and energy exchange processes in our study area. Portions of the model code were modified to better suit the system behavior, to make use of detailed geospatial data, and to correct programming errors. Of all the modifications to the HEATSOURCE model code, the most important was probably the implementation of the two-channel geometry. Use of the standard, single trapezoid setup in the original HEATSOURCE model was not believed to be a viable option because at low flow the Carson River recedes into a thalweg channel, which is not represented well by a single trapezoid. Latham et al. (2006) and Warwick et al. (1995) also encountered problems representing the complex channel geometry in the Carson River. In both studies, more detailed channel geometries were developed to represent the low flow condition. The LIDAR imagery and *simbanks* routine, along with the hyperspectral imagery and the field survey of maximum river depths, facilitated development of the two-channel configuration that allowed the model to simulate wetted channel dimensions more accurately, which resulted in more accurate estimation of heat fluxes.

Modifications to the conduction flux methods accounted for the effect that accreted water has on energy exchange in the streambed, and provided a more realistic estimation of the temperature of accreted water. In keeping with a deterministic approach, this modification better represented the streambed conduction term in the energy balance equation. We feel that the model changes to the conduction flux were an improvement, mostly because some previous temperature models have simplified or even ignored this term. Spatially distributed alluvium temperature zones allowed greater delineation of alluvium temperatures for the model domain. Due to low head dams and other complex subsurface flow processes in the study area, the spatial variation of alluvium temperatures is obviously much more complicated than the representation by three zones; however these zones provided greater flexibility in optimizing alluvium parameters during MOCOM calibration runs.

Another of the more important modifications was the derivation of shading attributes from the available high resolution LIDAR survey. Original HEATSOURCE methods were not used because they assume that large areas of riparian tree cover have been aggregated to polygons. The type of point sampling used in the Ttools method could not accurately capture the vegetation height and density from the LIDAR data, as it assumes a very high degree of generalization in the input vegetation data. As an alternative, we coded a program to sample the vegetation attributes directly from the LIDAR survey. The program provided a much more detailed representation of the height-density distribution of streamside vegetation and its shading of the river.

Calibrating the modified HEATSOURCE model was a two stage process. Model input parameters were originally developed based on a 30m nodal spacing, but were later

calculated at a 240m spacing. This resulted in a higher degree of averaging in the model output. There was good correspondence between the 240 meter model spacing and the point-based field measures despite the difference in scales. With the exception of the influence of return flows, we believe that temperature variations in the model domain were not substantial at the 30m scale. The TIR survey supports this contention, as spatial variations in temperature at the 240m scale are generally less than 0.5°C.

Low head dams posed the biggest problem in completing the manual calibration of the model. The use of a control depth in model segments immediately upstream of low head dams produced some improvement in the representation of dams, allowing an appropriate amount of streamflow to pass over the dams. However, the ponding effect of low head dams propagated much further upstream than could be adequately represented with a single control depth. This is apparent in the poor fit to the TIR data, specifically in region C upstream of the Mexican Dam (Site 18-Figure 35). We tried using multiple control depths, but the model had instability issues when multiple control depths were used. Overall, there is a general uncertainty associated with the representation of low head dams. It is not clear whether problems with the model's dispersion coefficient or control depths are to blame, but what is clear is that low head dam hydraulics are not being represented well by the model. As a result, the model cannot simulate longitudinal cooling or heating of the river as rapidly as it should upstream of dams.

Downstream of site 8 (last low head dam) in region A of Figure 35, the model underpredicted the TIR survey downstream to the Sun Ridge Golf Course site (Site 13). At site 9, located in region A, average predicted streamflow rates were offset from observed data by less than $0.05 \text{ m}^3 \text{ s}^{-1}$ during the calibration period. With current

calibration settings, confidence intervals derived using the GLUE method showed site 10 to be incapable of simulating stream temperatures any higher than those in the observed data from 2005. This is reflected in the underprediction observed relative to the TIR survey (Figure 35). Even though the hydraulics were reasonable at the rating curve site in 2005, it is possible that the travel time through this stretch of the river is too fast, not allowing the river sufficient time to heat up.

The manual calibration of the potential solar radiation flux to observed pyranometer data reduced error associated with this component of the model. The method we developed to estimate cloudiness factors incorporated the effect of cloud cover during the day-time hours, but since the method is based on pyranometer data, we have no information on cloud cover for the night time hours. This could be a source of error for the model because we are assuming no cloud cover at night, and the tendency for the atmosphere to retain or release heat is greatly influenced by cloud cover. However, at low flow we observed that water temperatures would equilibrate relatively quickly to ambient conditions, so it is unlikely that a night-time effect would propagate strongly to affect estimates of maximum daytime temperatures.

Dissolved and suspended loads on the Carson River are high compared to rivers in Oregon for which the original model was developed and calibrated. Because of this, the original empirical formulas in HEATSOURCE for estimating transmittance and absorbance of radiation in the water column and streambed were not representative of our study area. Modifications to these formulas were made using field observations of downwelling and upwelling PAR. The modifications produced more realistic characteristics for the attenuation of radiation in the water column and streambed.

MOCOM provided a computer-based method by which multiple parameters were optimized simultaneously with two objective measures. Substantial programming time was required to enable use of MOCOM with the modified HEATSOURCE model. We fitted to the calibration period (12:00-24:00) to allow a better opportunity of fitting to the observed daily maximum temperatures. This enhanced the fit during the period of interest, but may have diminished the fit in other portions of the diel profile. Despite fitting to this period, we still maintained a reasonable fit to the daily minimum temperatures. Overall, MOCOM performed well, producing a Pareto curve of solutions from which we selected the parameter set that suited our project goals best. The rectilinear shape of our Pareto solutions (Figure 59) from the final MOCOM calibration run showed that there was a definite global optimum with respect to the two objective functions. Further analysis of the solution curve showed the low precision in the model output, narrow range of error, and low sample size were the main contributors to the shape of the curve. The very narrow range of $|\%bias|$ and RMSE also showed that selection of lowest RMSE versus lowest $|\%bias|$ produced minimal difference in model output error. Therefore, a trade-off solution actually had little utility with respect to the best fit solution.

Bartholow (1991) used the SNTMP temperature model to assess the thermal regime of an urban sport fishery on the Cache la Poudre River in Colorado. That model was applied over a length of 31km, with mean annual flow of $11 \text{ m}^3 \text{ s}^{-1}$, and an extensive amount of irrigation diversions. The SNTMP model was used to calculate the mean daily water temperature, and although our model was used to calculate the daily maximum, a comparison of the results gives an indication of the modified

HEATSOURCE model's performance relative to a similar deterministic heat transfer model. For both models, error was assessed with bias, a 50% confidence limit, and the maximum overprediction over the calibration period. The SNTEMP model produced an average positive bias of 0.04°C , with 50% of the predictions within 0.47°C of the observations, and a maximum overprediction of 1.8°C during the calibration period (Bartholow, 1991). Our modified HEATSOURCE model produced an average positive bias of 0.16°C , with 50 % of model predictions within 0.62°C of the observations, and a maximum overprediction of 3.4°C . The calibration results from the modified HEATSOURCE model were somewhat higher, but still comparable to those obtained using the SNTEMP model.

Over the model validation period, predictions were biased differently depending on site. Sites 10 and 15 showed a negative temperature bias, indicating that our predictions of stream temperature are a conservative estimate because the actual temperatures in the unvegetated state are on average higher than our predictions. Sites 19 and 22 showed positive temperature bias. Given that these sites are in a reach of the river that already has relatively dense, mature tree cover and they are still overpredicted, it is possible that the cooling effect of riparian shade may be somewhat underestimated. The downstream reach of the study area has a north-south orientation that does not produce much effective shade during the period of maximum solar exposure. This orientation allowed only a maximum of 10% effective shade, which did not give a full estimate of the total shading potential. We felt that this reduced the flexibility of the MOCOM algorithm in fitting to observed data and could be a reason why our canopy shade factor showed minimal sensitivity. It is also quite possible that this bias in the downstream sites

may arise from uncertainties in the hydraulics. Unfortunately, given the complexities of factors influencing stream hydraulics and shading mechanics it was not possible to discern what part of the uncertainty is attributed to hydraulics versus error that is due to problems in the representation of the canopy. Maximum effective shade in the revegetated reach was higher (12%), but not out of the range of effective shade observed in the downstream reach (vegetation zone 2). This suggests that any error in the predictions for the revegetated reach would not be expected to exceed those observed in the downstream reach.

Longitudinal profiles of the best-fit and worst-fit scenarios of predicted stream temperature for the model validation period had a low RMSE in the revegetated reach. Comparison of the TIR survey to longitudinal stream predictions showed that the model effectively captured the general pattern of stream temperature fluctuations in the study area. While the fit for regions A and C (Figure 35) was less than optimal, the model fit the TIR survey very well in region B, and this is where the revegetation strategy was shown to have the greatest effect. Furthermore, the level of uncertainty in the validation period remained roughly equivalent to the level of uncertainty in the calibration period despite somewhat different flow and temperature conditions, providing confidence in the model's ability to represent a range of naturally occurring conditions.

One reach of the river was the most appropriate candidate for simulating revegetation (vegetation zone 2) because of a lack of existing tree cover, compatible land use, and an appropriate orientation of the river for shading. The revegetation scenario utilized the maximum potential tree cover that could be expected in the revegetated reach, based on the fact that the transplanted vegetation attributes represented a dense stand of

mature cottonwoods that actually exists in the study area. The revegetation scenario resulted in a maximum stream temperature reduction of 1.8°C at stream km 15.

Temperatures at the point of maximum reduction were near 23°C, still well above the 20°C limit for coldwater fisheries. Model predictions from the validation period showed an uncertainty in the range $\pm 1.0^\circ\text{C}$ to 2.0°C over the revegetated reach. Even with this level of uncertainty, the amount of reduction in stream temperature for the revegetation scenario presented here still would not be expected to make the temperature threshold attainable. The inability of the maximum potential revegetation scenario to cool stream temperatures to $\leq 20^\circ\text{C}$ indicates that revegetation alone is not sufficient to meet the specified goal. It should be noted that the water years for 2005 and 2006 were large water years for the Carson River Basin. Thus, if the 20°C threshold cannot be reached for such high volume water years, then the probability is low for reaching the goal during normal or drought conditions.

To understand the relationship between boundary condition streamflow and the thermal regime of the study area, we ran the model with existing vegetation and simulated vegetation at an increased flow of $15\text{m}^3\text{ s}^{-1}$. Both flow scenarios showed that the river did not heat up as rapidly and the difference between the two increased flow scenarios was small, showing that at higher flow, the relative contribution of revegetation to stream temperature cooling is minimal. This demonstrates that at higher flow, the river's temperature has a tendency to remain near the condition at which it entered the reach, whereas at lower flow, the river has a greater capacity to be warmed or cooled. Thus, at higher flow, the river's thermal regime is more influenced by boundary

condition temperature, whereas at lower flow the amount of riparian vegetation is more of a factor.

We feel the level of uncertainty associated with the modified HEATSOURCE model is acceptable and that we accomplished the goal of establishing the potential for revegetation to reduce temperatures in the study reach of the Carson River to $\leq 20^{\circ}\text{C}$. The revegetation scenarios did show that the threshold temperature was unattainable even with maximum shade. Increased flow alone and increased flow with maximum shade also proved incapable of reaching the threshold, assuming the boundary condition temperature is not reduced. Since a streamflow of $15 \text{ m}^3 \text{ s}^{-1}$ does not ordinarily occur at this time of year, there is a large amount of uncertainty regarding what the temperature of such a flow would be even if it could be attained. Based on the minimal amount of upstream storage in the basin, the snowpack dependence of streamflow, and the current negotiated water use upstream of our study area, it is very unlikely that a minimum flow of this magnitude could be maintained throughout a summer.

Future work on the study area portion of the river might include investigations of the importance of channel morphology (e.g. reductions in channel width) on stream temperature and the geometry of riparian shade. There are upstream riparian areas on the East and West Forks of the Carson River that have complete to near-complete canopy closure over the channel. Most often, the areas of highest canopy closure corresponded to those areas of more natural morphology.

The main conclusion to be reinforced is that changes in boundary condition temperature and streamflow would be required to produce further stream cooling over this reach, which would require changes in the current land and water use in the portion

of the basin upstream of our study area. If a quantitative analysis was to expand the model to include such changes in the upstream portion of the watershed, a great deal of complexity would be added to the analysis. Difficulties would arise because there are multiple forks, including East Fork, West Fork, and two forks of the Brockliss Slough, which would have to be modeled, and in places, the East and West Fork channels are nearly dry for the low flow condition. Furthermore, numerous low head dams and irrigation diversions are present. Overcoming the HEATSOURCE model's struggles with impoundments and ensuring accurate flow rates and temperatures downstream from diversions would be challenging given the sheer number of diversions and lack of data on flows. The LIDAR and hyperspectral imagery are available for the area upstream of the study area to the California border. These data sources would enable high resolution characterization of tree cover and the model modifications we made here could be applied, but even with these improvements, quantifying the temporal and spatial flow variations resulting from irrigation diversions would prove difficult. The TIR survey we used for model validation extended upstream to the Nevada-California state line. Water temperatures in the West and East forks as they pass the state line were recorded at or near 20°C. Thus, even if the hydraulics could be effectively modeled, we hypothesize that maintaining this temperature level through Carson Valley and up to the boundary condition site for our model without maintaining higher flow volumes would be improbable. However, future work including this portion of the basin in subsequent temperature modeling efforts would have to be performed before this could be confirmed.

6 Literature Cited

- Bartholow, J.M. (1991). A modeling assessment of the thermal regime for an urban sport fishery. *Environmental Management*, 15(6), 833-845.
- Bartholow, J.M. (1993). Sensitivity of the U.S. Fish and Wildlife Service's Stream Network Temperature Model. Pages 247-257 *in* Morel-Seytoux, ed., *Proceedings of the Thirteenth Annual American Geophysical Union Hydrology Days*. Fort Collins, CO.
- Bartholow J.M. (2000) Estimating cumulative effects of clearcutting on stream temperatures. *Rivers*, 7, 284–297.
- Boyd, M., B. Kasper (2002). TTools Users Manual, Oregon Department of Environmental Quality, Portland, Oregon.
- Boyd, M., B. Kasper (2004). Analytical methods for dynamic open channel heat and mass transfer, methodology for the HEATSOURCE model Version 7.0. Watershed Sciences, Portland, Oregon.
- Brock, J.T. and C.L. Caupp, (2004). Application of DSSAMt water quality model: Truckee River, Nevada Technical Report No. RCR96-1.1.
- Caissie, D. (2006) The thermal regime of rivers: a review. *Freshwater Biology* 51:8, 1389-1406.
- Caissie, D., El-Jabi, N., and St-Hilaire, A. (1998). Stochastic modeling of water temperatures in a small stream using air to water.
- Chen, Y.D., R.F. Carsel, S.C. McCutcheon and W.L. Nutter (1998). Stream temperature simulation of forested riparian areas: I. Watershed-scale model development. *Journal of Environmental Engineering*, April 1998, pp 304-315.
- Coutant, C. C. (1976). Thermal effects on fish ecology. Pages. 891–896. *Encyclopedia of Environmental Engineering*. Volume 2 W & G Baird, Northern Ireland, UK.
- Crisp D.T. & Howson G. (1982) Effect of air temperature upon mean water temperature in streams in the north Pennines and English Lake District. *Freshwater Biology*, 12, 359–367.
- Eaton, J. G., and others. (1995). A field information-based system for estimating fish temperature tolerances. *Fisheries* 20(4): 10-18.

- Goldberg, D.E., (1989). Genetic algorithms in search, optimization, and machine learning. Addison-Wesley Publishing Co., Reading, MA, pp. 412.
- Gu, R., S. Montgomery and T. Austin. (1998). Quantifying the effects of stream discharge of summer river temperature. *Hydrological Science Journal* 43(6):885-894.
- Halliday D. and R. Resnick. (1988). *Fundamentals of Physics*. 3rd Edition. John Wiley and Sons, New York. pp. 472-473.
- Horvath, M. (1996). Quantification of non-point source nutrient pollution, impacts along the Carson River, Nevada. *Hydrologic Sciences*. Reno, University of Nevada, Reno: 88.
- Jeppesen E. & Iversen T.M. (1987) Two simple models for estimating daily mean water temperatures and diel variations in a Danish low gradient stream. *Oikos*, 49, 149–155.
- Jobson, H.E. (1977). Bed conduction computation for thermal models. *Journal of Hydraulic Engineering Div., ASCE*, 103(HY10), pp 1213-1216.
- Johnson F.A. (1971) Stream temperatures in an alpine area. *Journal of Hydrology*, 14, 322–336.
- Johnson, A.N., B.R. Boer, W.W. Woessner, J.A. Stanford, G.C. Poole, S.A. Thomas, and S.J. O'Daniel, (2005). Evaluation of an inexpensive, small diameter temperature logger for documenting groundwater – river interactions. *Ground Water Monitoring and Remediation*. 25(4): 68-74.
- Jourdonnais J.H., Walsh R.P., Pickett F. & Goodman D. (1992) Structure and calibration strategy for a water temperature model of the lower Madison River, Montana. *Rivers*, 3, 153–169.
- Latham, Z.B. (2005). Dissolved oxygen dynamics in the Carson River, Nevada *Hydrologic Sciences*. Reno, University of Nevada, Reno.
- Loheide II, S. P. and S.M. Gorelick. (2006). Quantifying stream-aquifer interactions through analysis of remotely sensed thermographic profiles and in-situ temperature histories. *Environment, Science and Technology*, 40, p. 3336-3341
- Marcotte, N. & Duong V.L. (1973) Le calcul de la température de l'eau des rivières. *Journal of Hydrology*, 18, 273–287.
- Maurer, D.K., Berger, D. L., Tumbusch M. L., and Johnson, M. J. (2006), Rates of evapotranspiration, recharge from precipitation beneath selected areas of native

vegetation, and streamflow gain and loss in Carson Valley, Douglas County, Nevada, and Alpine County, California : U.S. Geological Survey Scientific Investigations Report 2005-5288.

- Mohseni O., Stefan H.G. & Erickson T.R. (1998) A nonlinear regression model for weekly stream temperatures. *Water Resources Research*, 34, 2685-2692.
- Morin, G. and D. Couillard. (1990). Predicting river temperatures with a hydrological model. Chapter 5. *Encyclopedia of Fluid Mechanics: Surface and Groundwater Flow Phenomena*. Volk Gulf Publishing Company, Houston, Texas. pp. 171-209.
- National Resource Council (NRC) Assessing the TMDL Approach to water quality management; National Academy Press: Washington, D.C., 2001.
- Neumann, D. W., Rajagopalan, B., and Zagona, E. A. (2003). Regression model for daily maximum stream temperature. *Journal of Environmental Engineering*, 129:7 pp. 667.
- Nevada Division of Wildlife, July (1999). Memo from Bob McQuivey, Chief of Habitat to Gene Weller, Chief of Fisheries, Historical Records for the Carson River Fisheries.
- Nevada Department of Wildlife, May 2000. East Carson River Draft Fisheries Management Plan.
- Nevada Division of Environmental Protection (NDEP) Carson River Non-point Source Management Plan Carson City, NV. 2003.
- Nevada Division of Environmental Protection (NDEP) Carson River Watershed Project Plan Carson City, NV. 2004.
- Oke, T. R. (1978). *Boundary layer climates*. Maethuen and Company, Ltd. London, England. pp. 372.
- Pahl, R. (2004). History of Carson River water quality standards- A supporting document for the Carson River report card. Carson City, NV, Nevada Division of Environmental Protection, Bureau of Water Quality Planning: 20.
- Parker, F.L. and P.A. Krenkel. (1969). *Thermal pollution: Status of the Art*. Rep. 3. Department of Environmental and Resource Engineering, Vanderbilt University, Nashville, TN.
- Rutherford, J. C., S. Blackett, C. Blackett, L. Saito, R. J. Davies-Colley; (1997): Predicting the Effects of Shade on Water Temperature in Small Streams. *New Zealand Journal of Marine and Freshwater Research* 31:101-121.

- Sinokrot B.A. & Stefan H.G. (1993) Stream temperature dynamics: measurements and modeling. *Water Resources Research*, 29, 2299–2312.
- Smith K. (1981) The prediction of river water temperatures. *Hydrological Sciences Bulletin*, 26, 19–32.
- Stallman, R.W., (1965), Steady one-dimensional fluid flow in a semi-infinite porous medium with sinusoidal surface temperature: *Journal of Geophysical Research*, v. 70, no. 12, p. 2821-2827.
- Stefan H.G. & Preud'homme E.B. (1993) Stream temperature estimation from air temperature. *Water Resources Bulletin*, 29, 27–45.
- Stonestrom, D.A., and J. Constantz, (2003). Heat as a tool for studying the movement of ground water near streams. USGS Circular 1260. USGS.
- Strahler, A.N., and A.H. Strahler. (1973). *Environmental geoscience: Interaction between natural systems and man*. Hamilton Publishing, Santa Barbara, CA.
- Sullivan, K., J. Tooley, K. Doughty, J.E. Caldwell, and P. Knudsen. (1990). Evaluation of prediction models and characterization of stream temperature regimes in Washington. *Timber/Fish/Wildlife Rep. No. TFW-WQ3-90-006*. Washington Department of Natural Resources, Olympia, Washington. 224 pp.
- Suzuki, S., (1960), Percolation measurements based on heat flow through soil with special reference to paddy fields: *Journal of Geophysical Research*, v. 65, no. 9, p. 2883-2885.
- U.S. Environmental Protection Agency. *Federal Water Pollution Control Act: Section 303(d)*, 1972.
- Warwick, J.J., and Heim, K.J., (1995): Hydrodynamic modeling of the Carson River and Lahontan Reservoir, Nevada, *Water Resources Bulletin*, vol. 31(1), p. 67-77.
- Webb B.W. and Nobilis F. (1997) A long-term perspective on the nature of the air-water temperature relationship: a case study. *Hydrological Processes*, 11, 137–147.
- Winter, T. C., Harvey, J.W., Franke, O.L., and Alley, W.M., (1998), *Ground water and surface water, a single resource*, U.S. Geological Survey Circular 1139, 79 p.
- Yapo, P. O., H. V. Gupta, and S. Sorooshian, (1998), Multi-objective global optimization for hydrologic models, *Journal of Hydrology*, 204 83-97.

7 Appendix A-Figures from Parameter Estimation Procedure

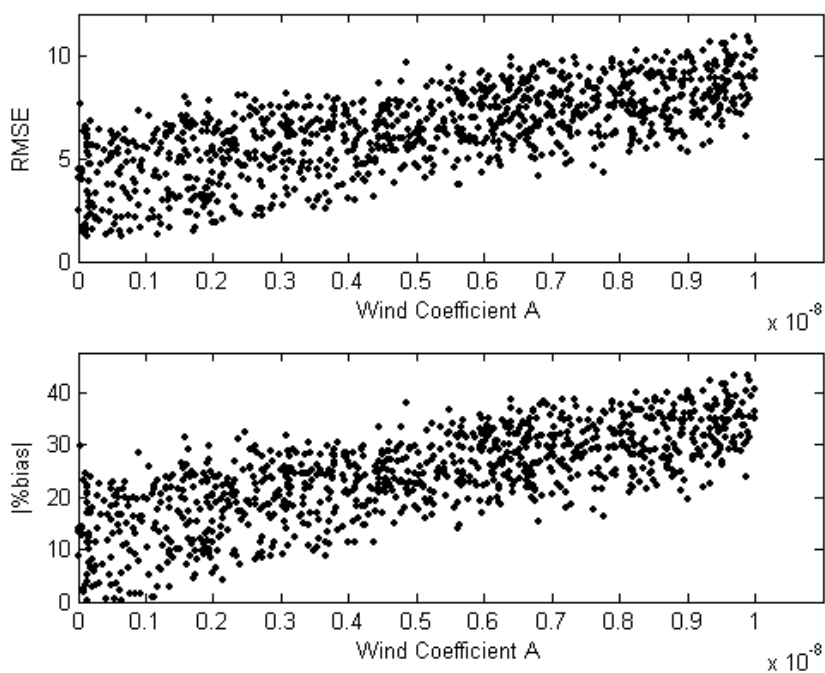


Figure 44-Sensitivity of wind coefficient A

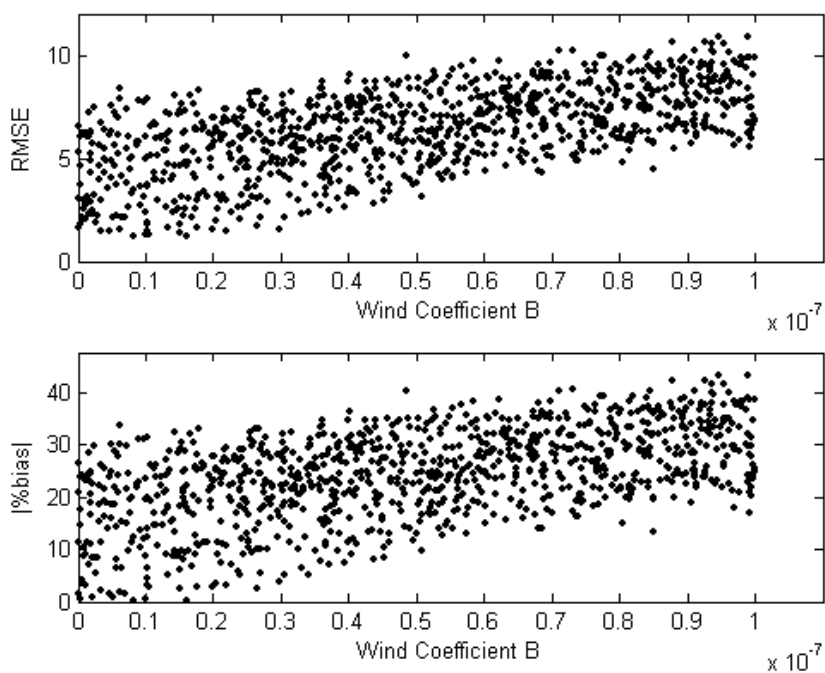


Figure 45-Sensitivity of wind coefficient B

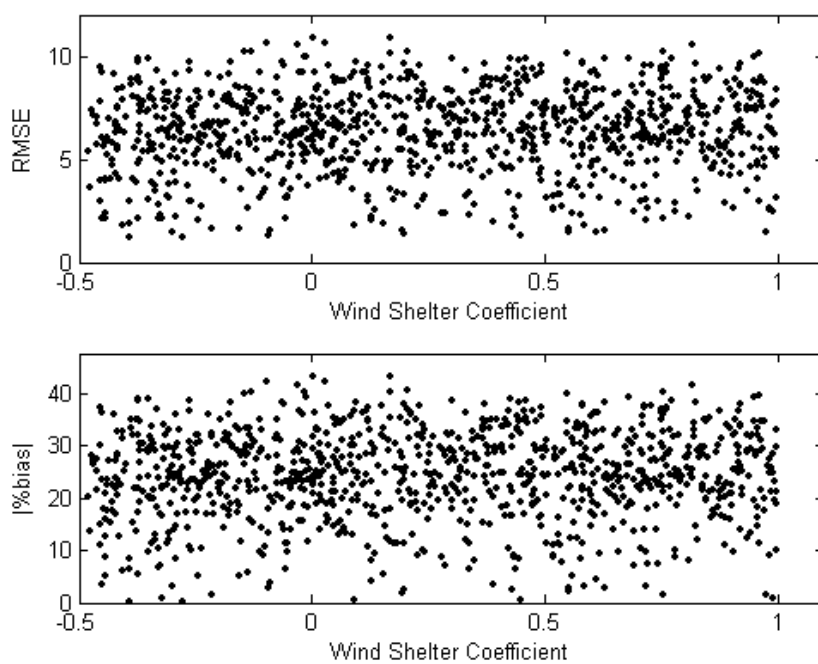


Figure 46-Sensitivity of wind shelter coefficient

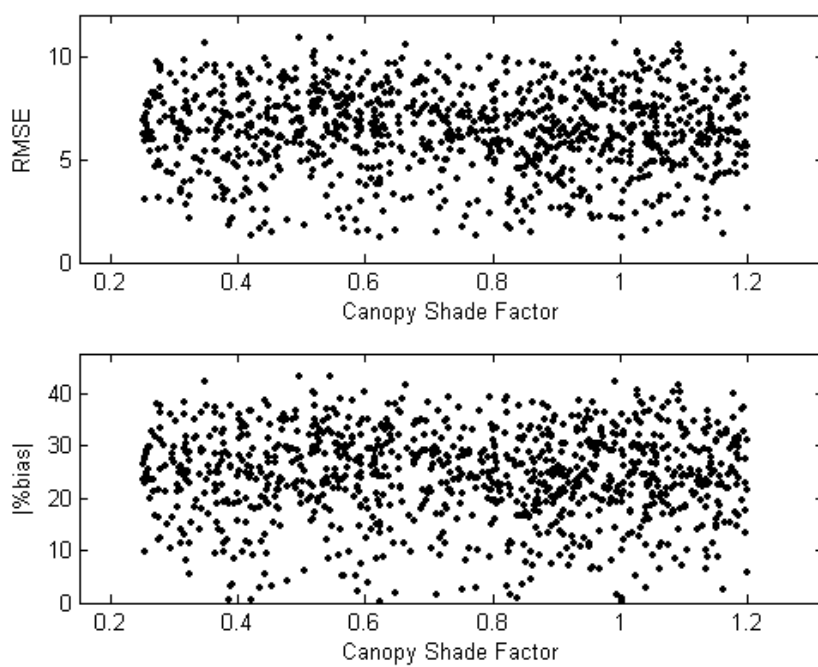


Figure 47-Sensitivity of canopy shade factor

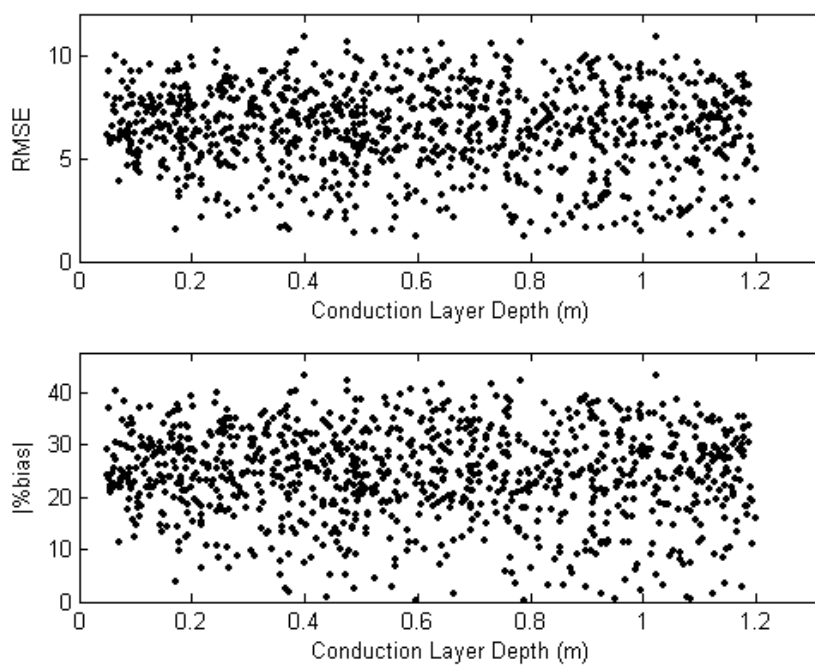


Figure 48-Sensitivity of conduction layer depth

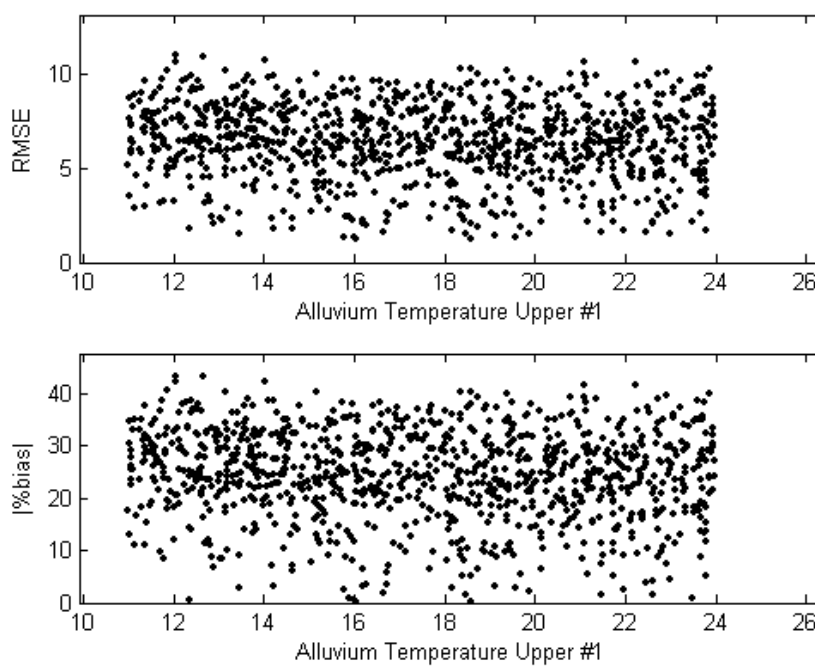


Figure 49-Sensitivity of alluvium temperature upper #1

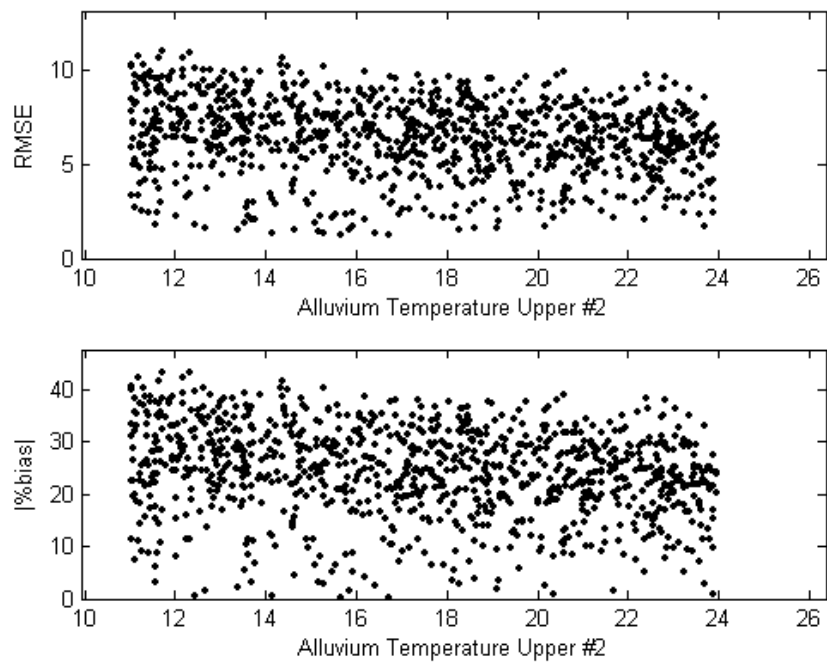


Figure 50-Sensitivity of alluvium temperature upper #2

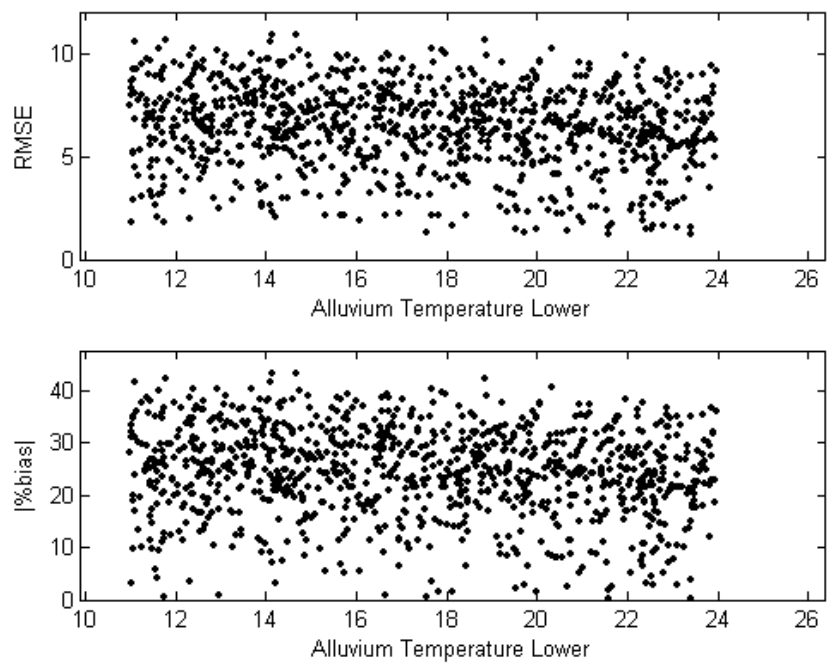


Figure 51-Sensitivity of alluvium temperature lower

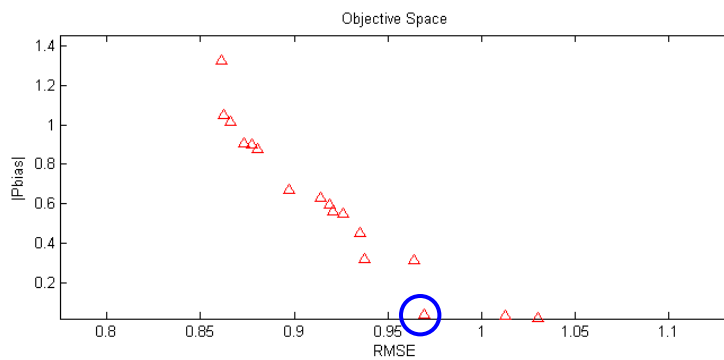


Figure 52-MOCOM solution for WCA and WCB

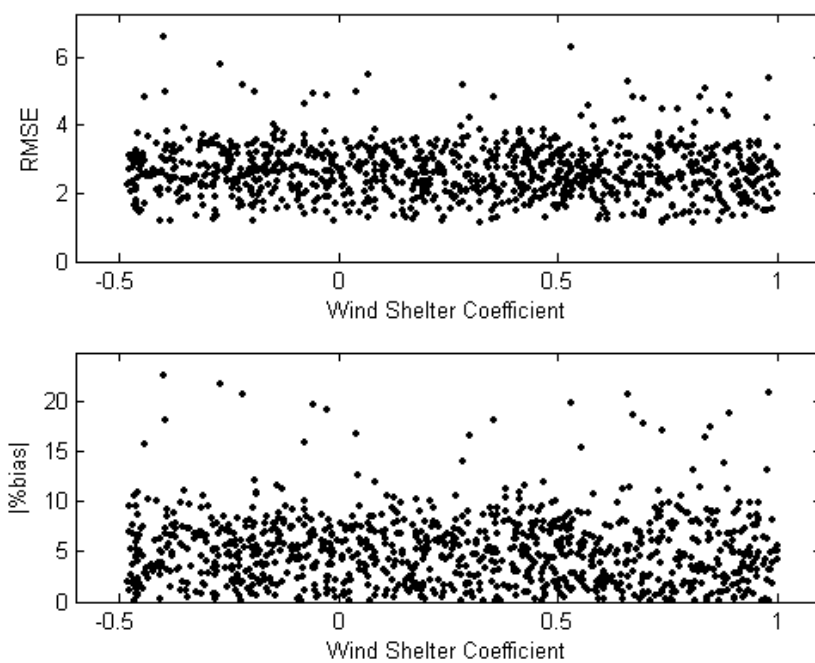


Figure 53-Sensitivity of wind shelter coefficient (2nd sensitivity)

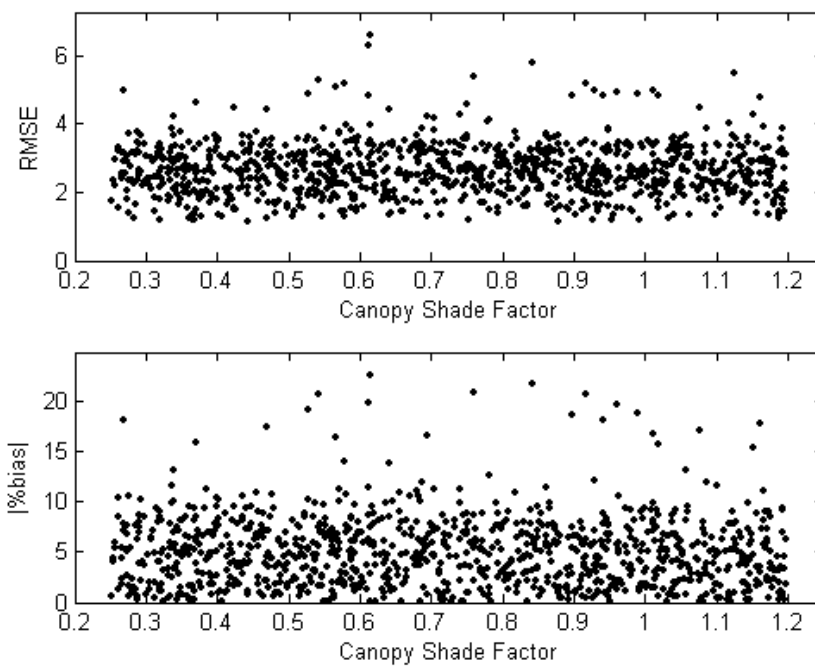


Figure 54-Sensitivity of canopy shade factor (2nd sensitivity)

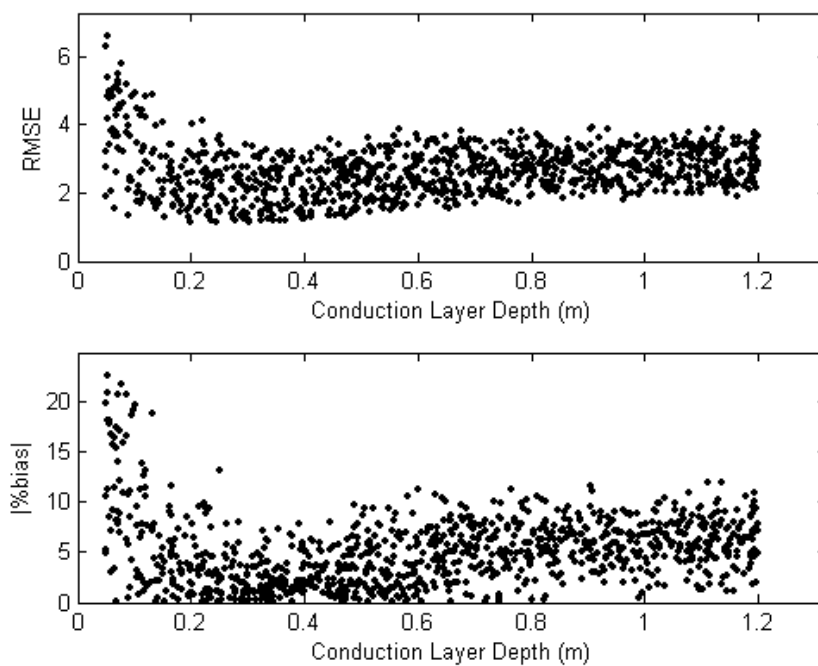


Figure 55-Sensitivity of conduction layer depth (2nd sensitivity)

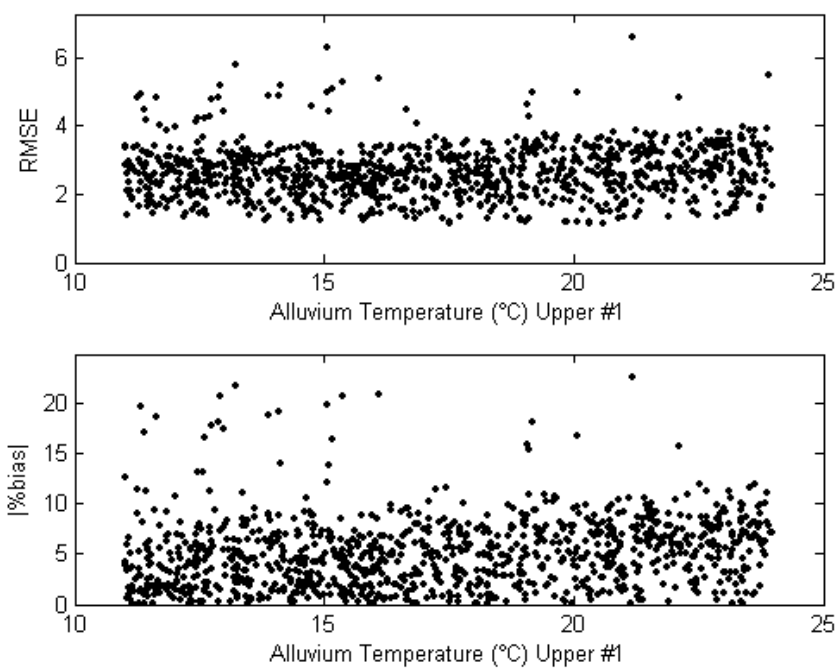


Figure 56-Sensitivity of alluvium temperature upper #1 (2nd sensitivity)

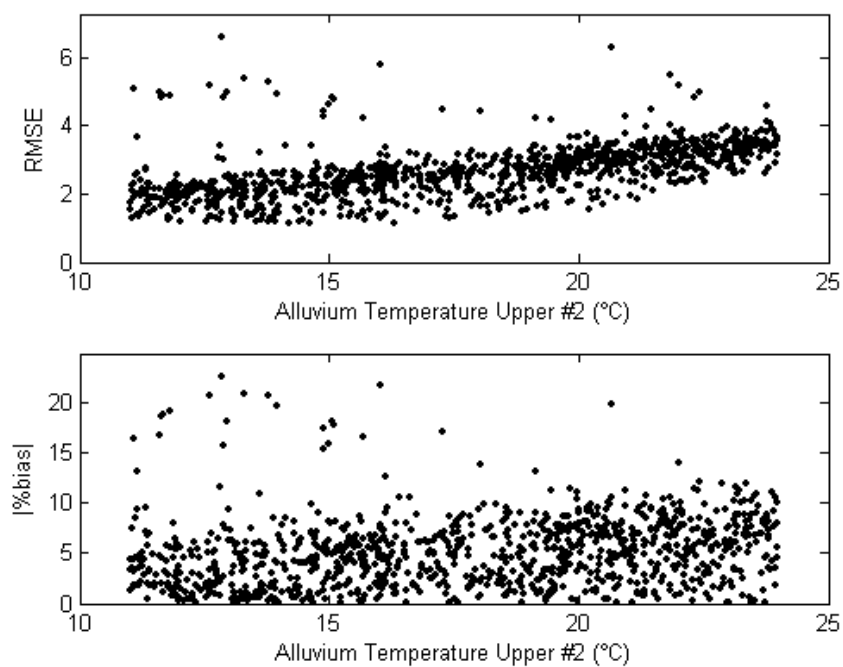


Figure 57-Sensitivity of alluvium temperature upper #2 (2nd sensitivity)

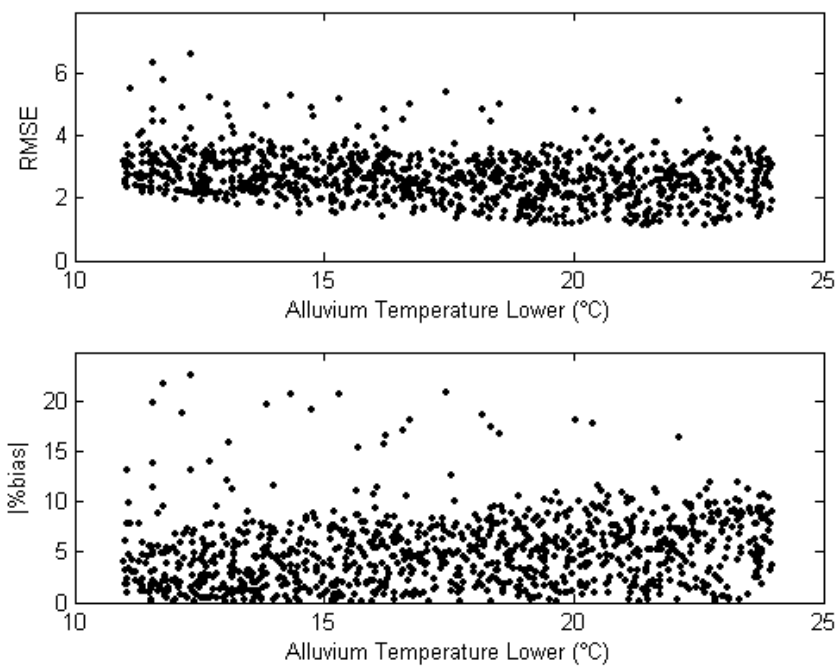


Figure 58-Sensitivity of alluvium temperature lower (2nd sensitivity)

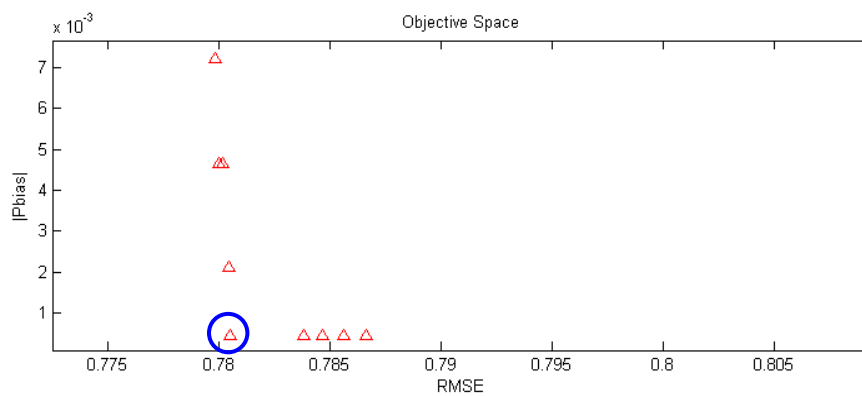


Figure 59- Final MOCOM calibration solution (circled)

8 Appendix B-Water and Streambed Temperature Data (2005)

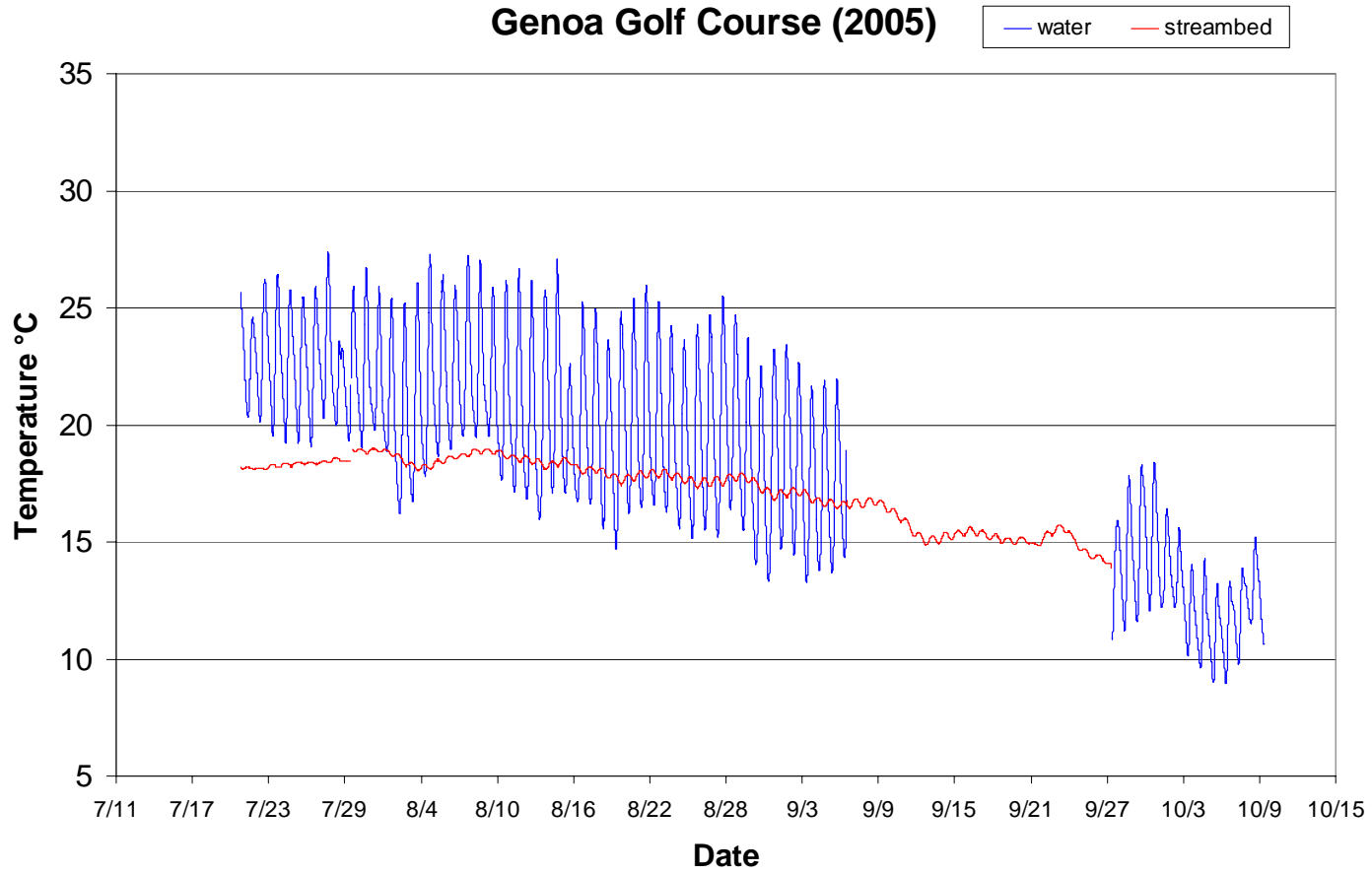


Figure 60-Water and streambed temperatures for Genoa Golf Course (Site 4)

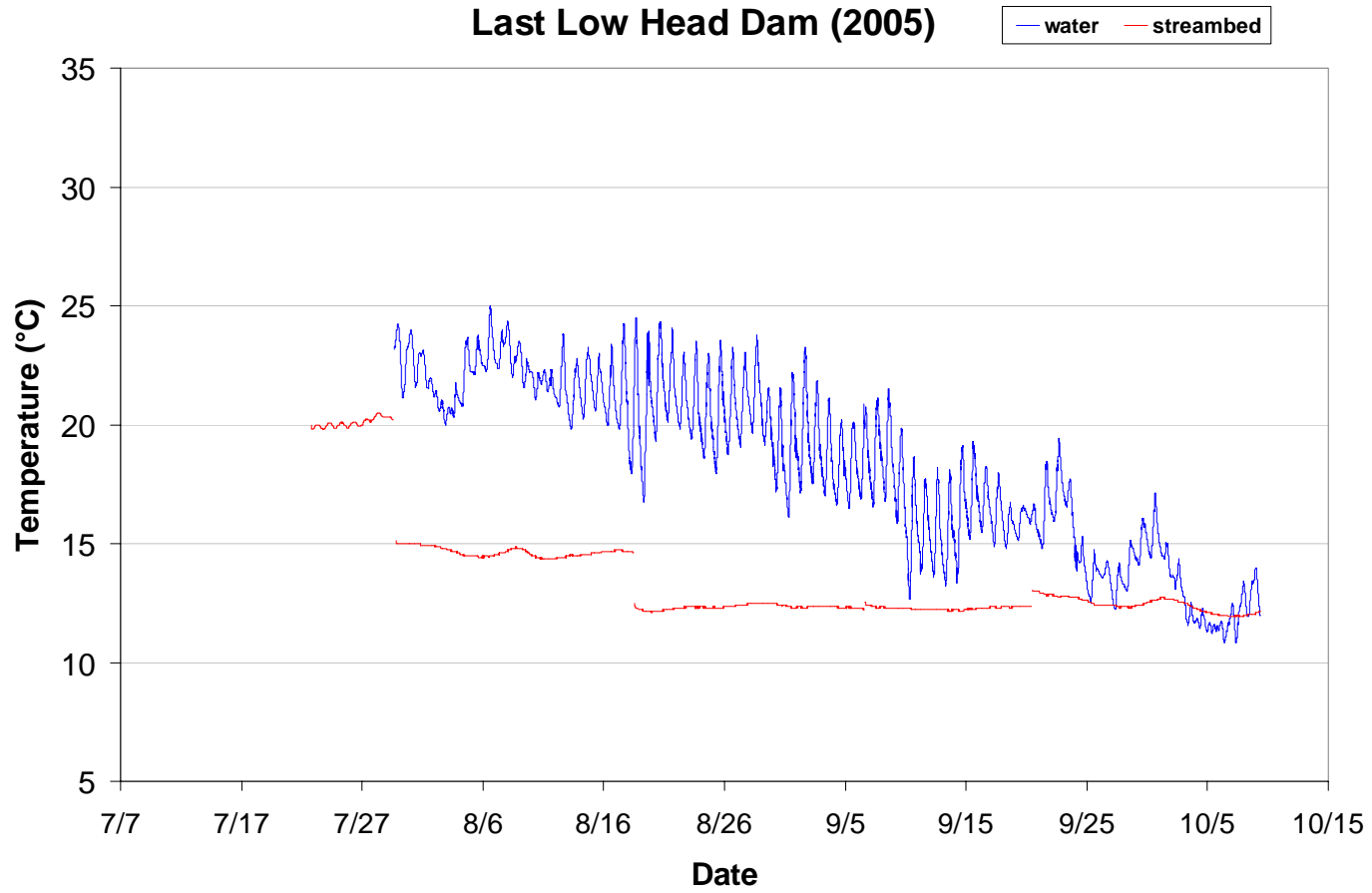


Figure 61-Water and streambed temperatures for last Low Head Dam (Site 8)

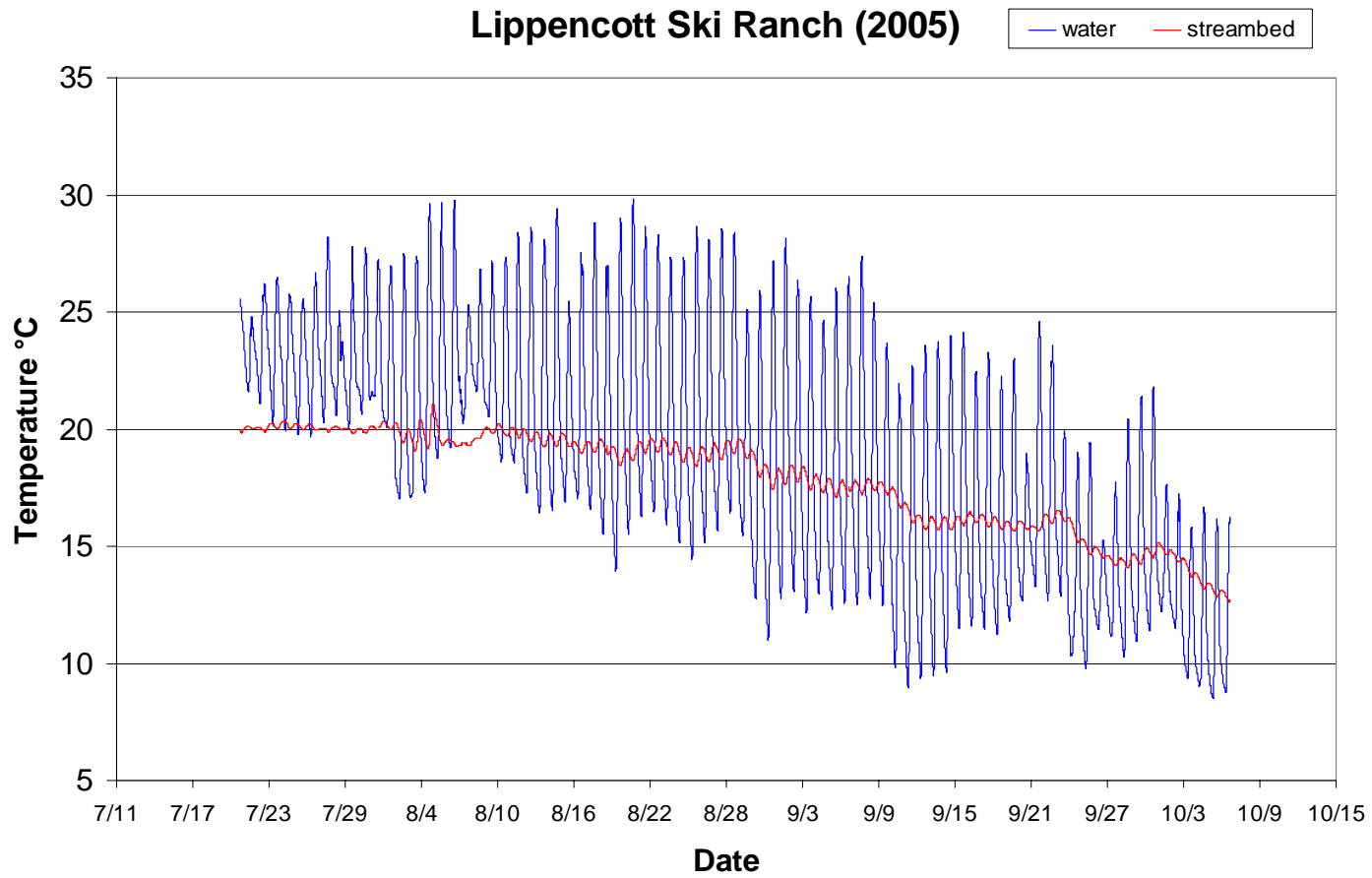


Figure 62-Water and streambed temperatures for Lippencott Ski Ranch(Site 10)

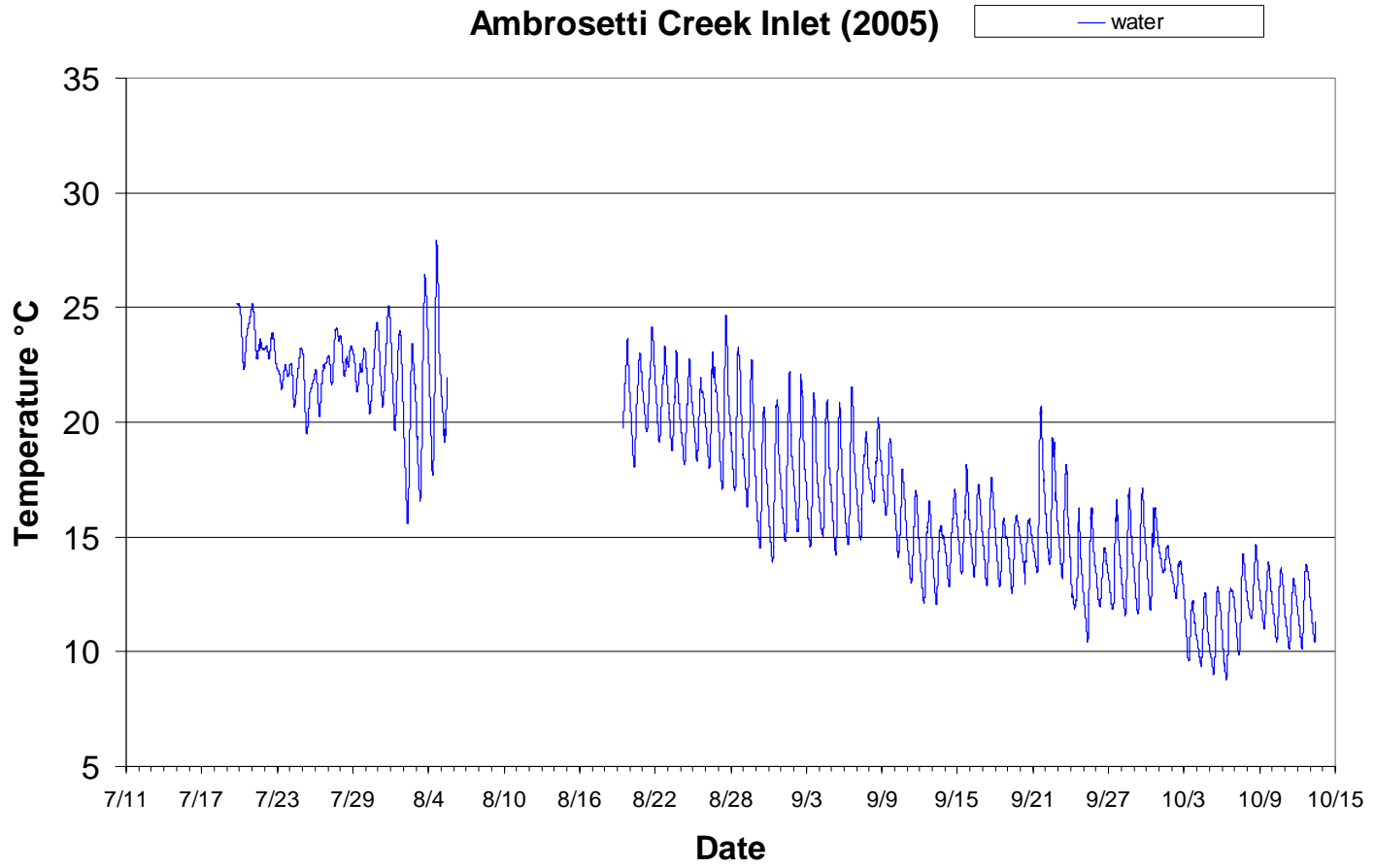


Figure 63-Water and streambed temperatures for Ambrosetti Creek Inlet (Site 11)

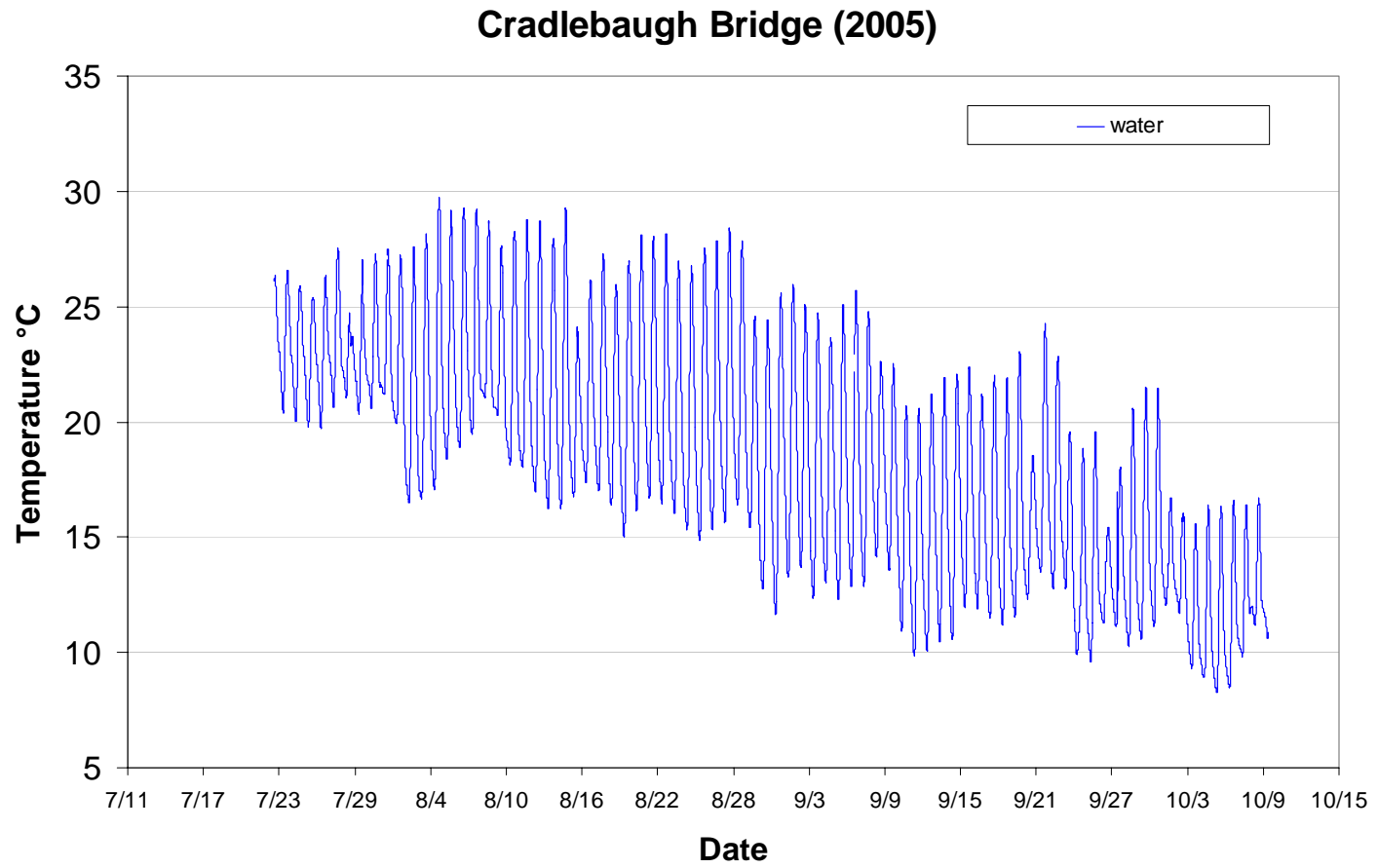


Figure 64-Water and streambed temperatures for Cradlebaugh Bridge (Site 12)

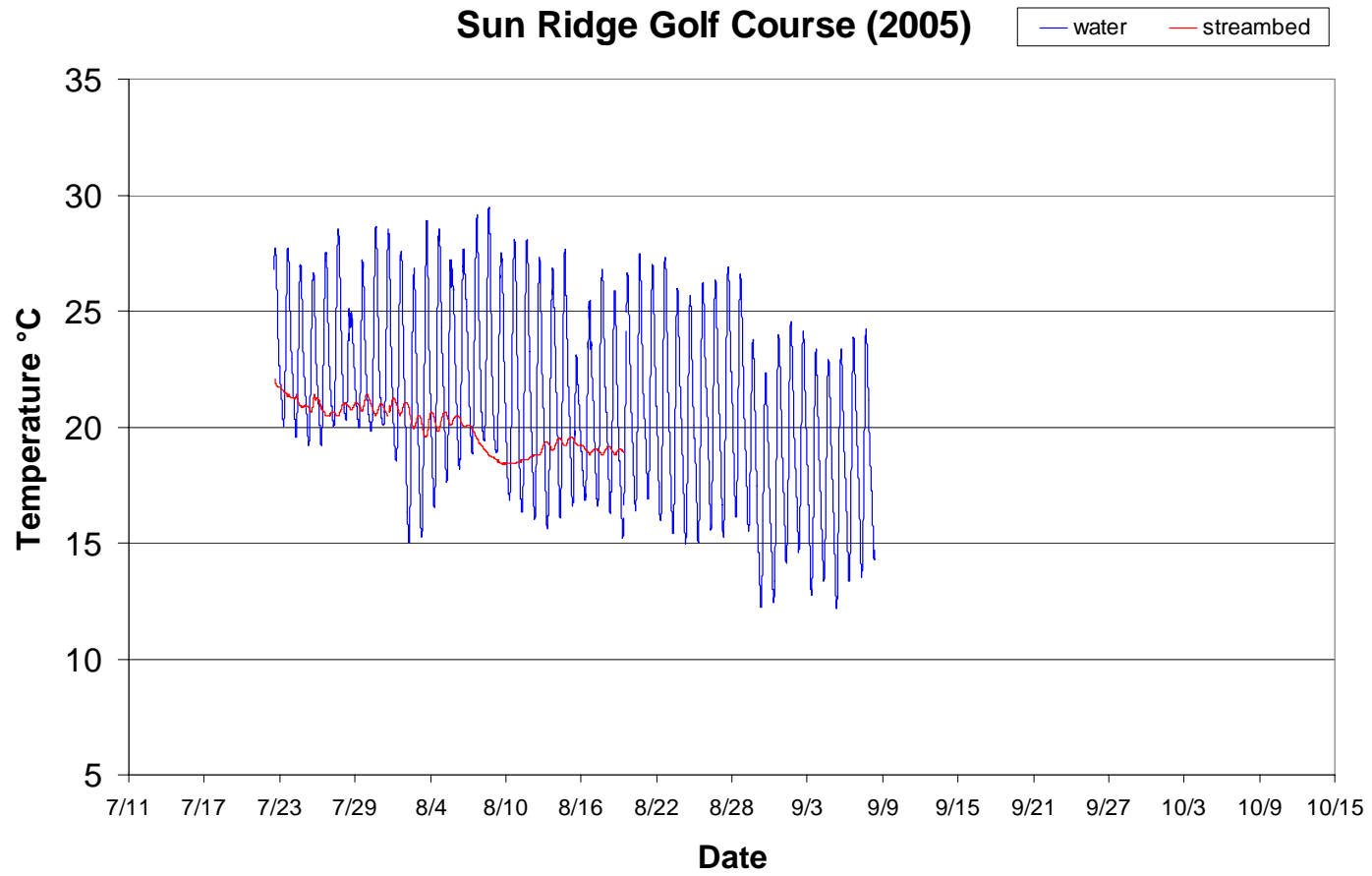


Figure 65-Water and streambed temperatures for Sun Ridge Golf Course (Site 13)

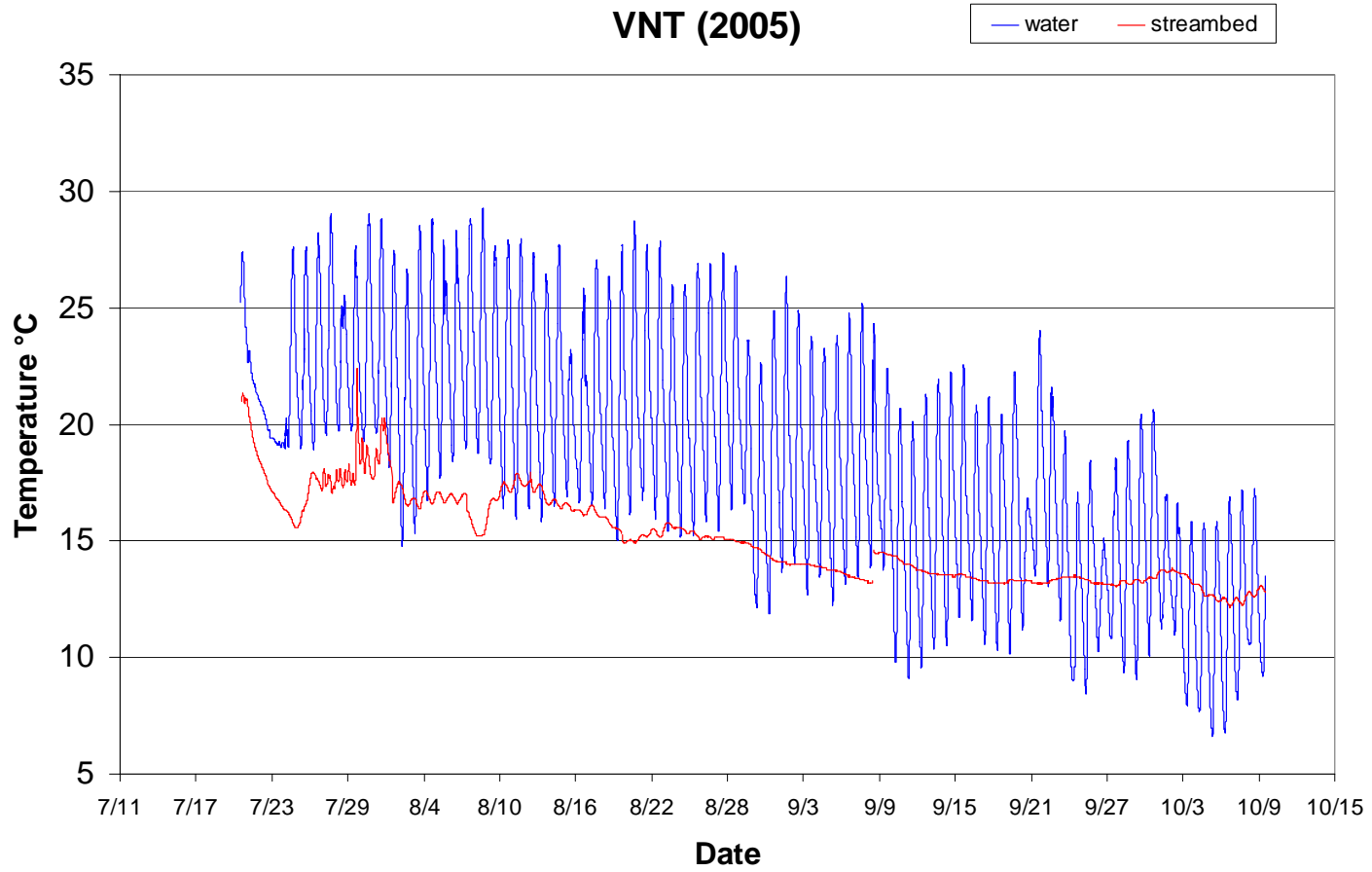


Figure 66-Water and streambed temperatures for VNT (Site 14)

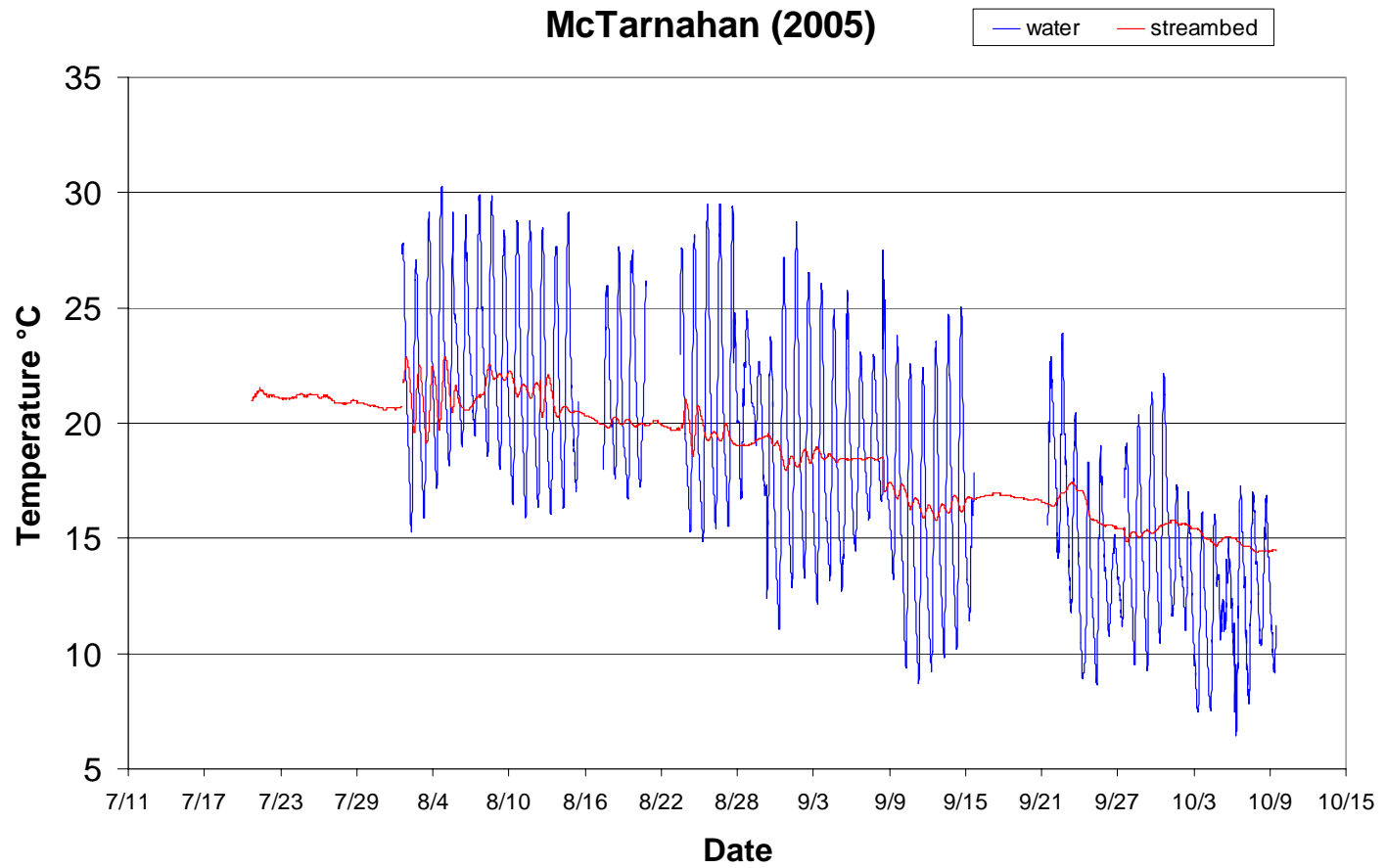


Figure 67-Water and streambed temperatures for McTarnahan (Site 15)

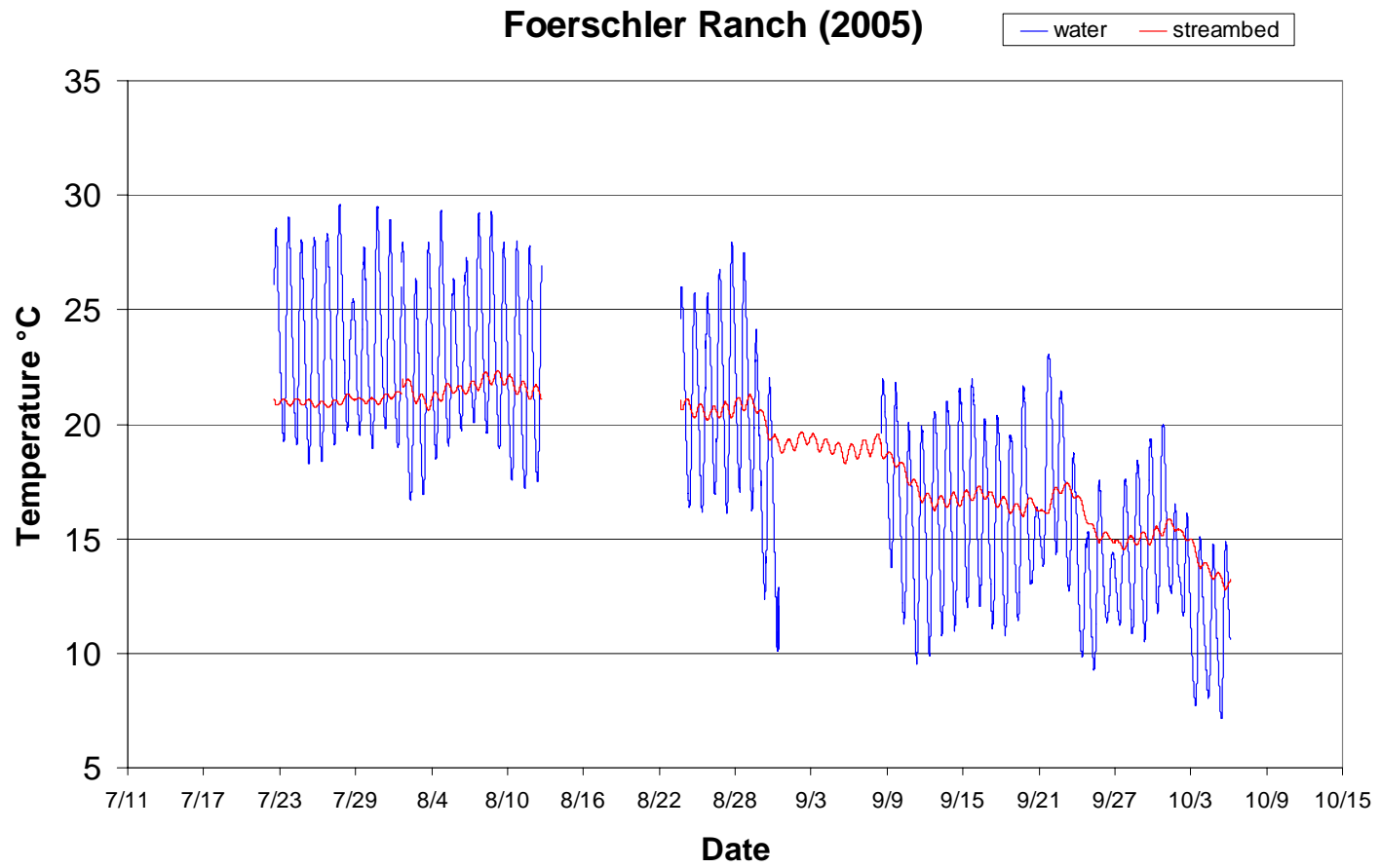


Figure 68-Water and streambed temperatures for Foerschler Ranch (Site 17)

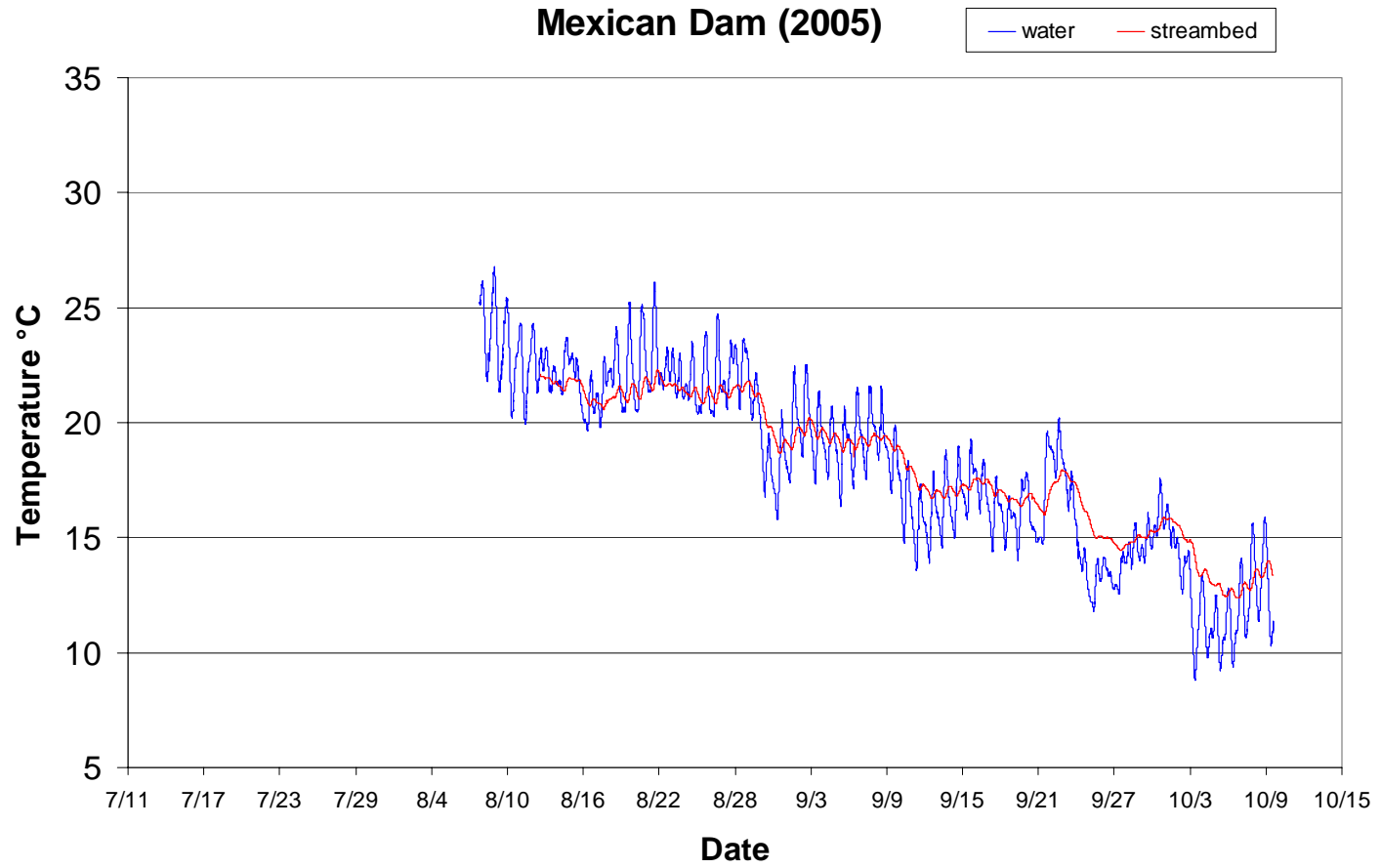


Figure 69-Water and streambed temperatures for Mexican Dam (Site 18)

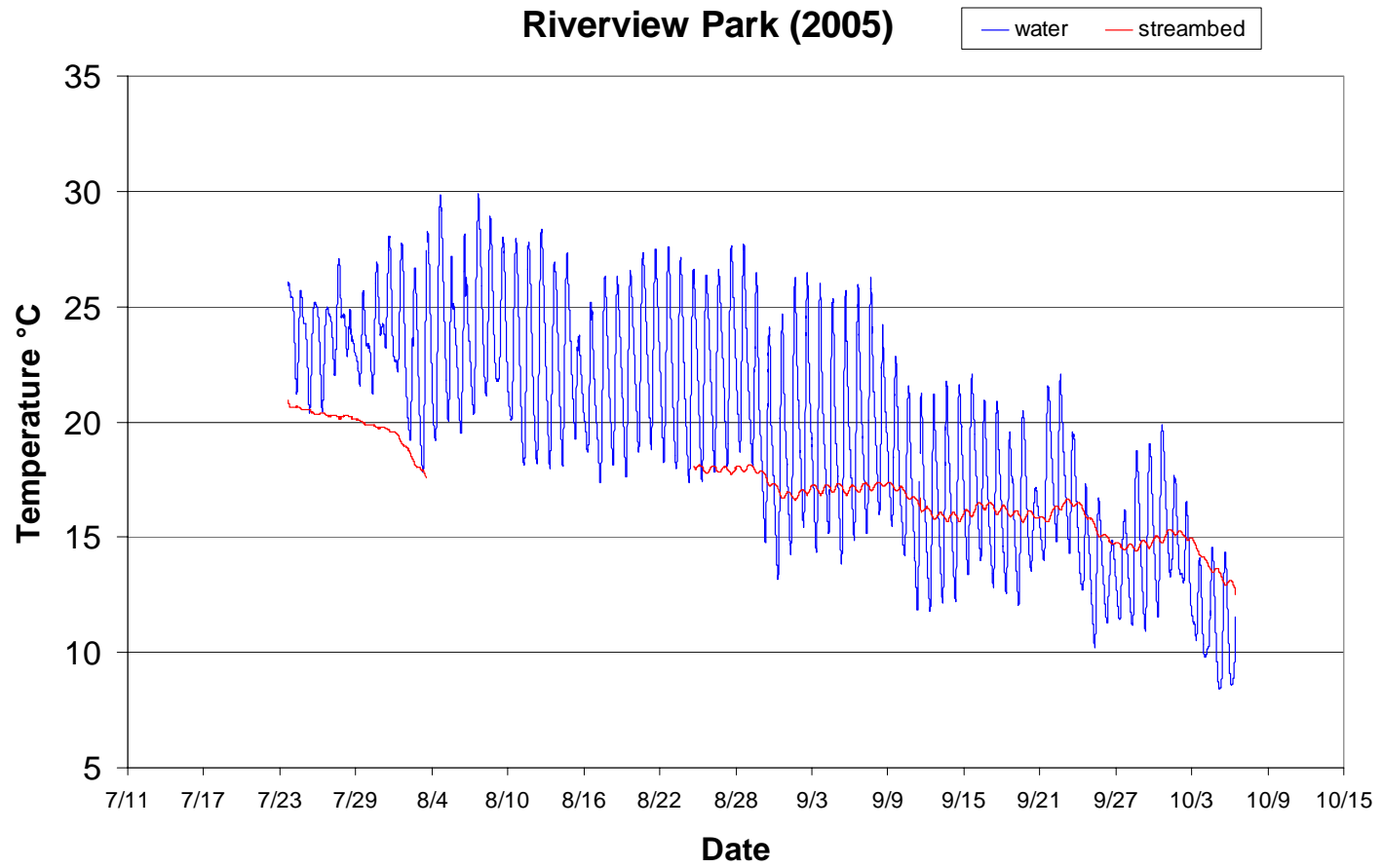


Figure 70-Water and streambed temperatures for Riverview Park (Site 19)

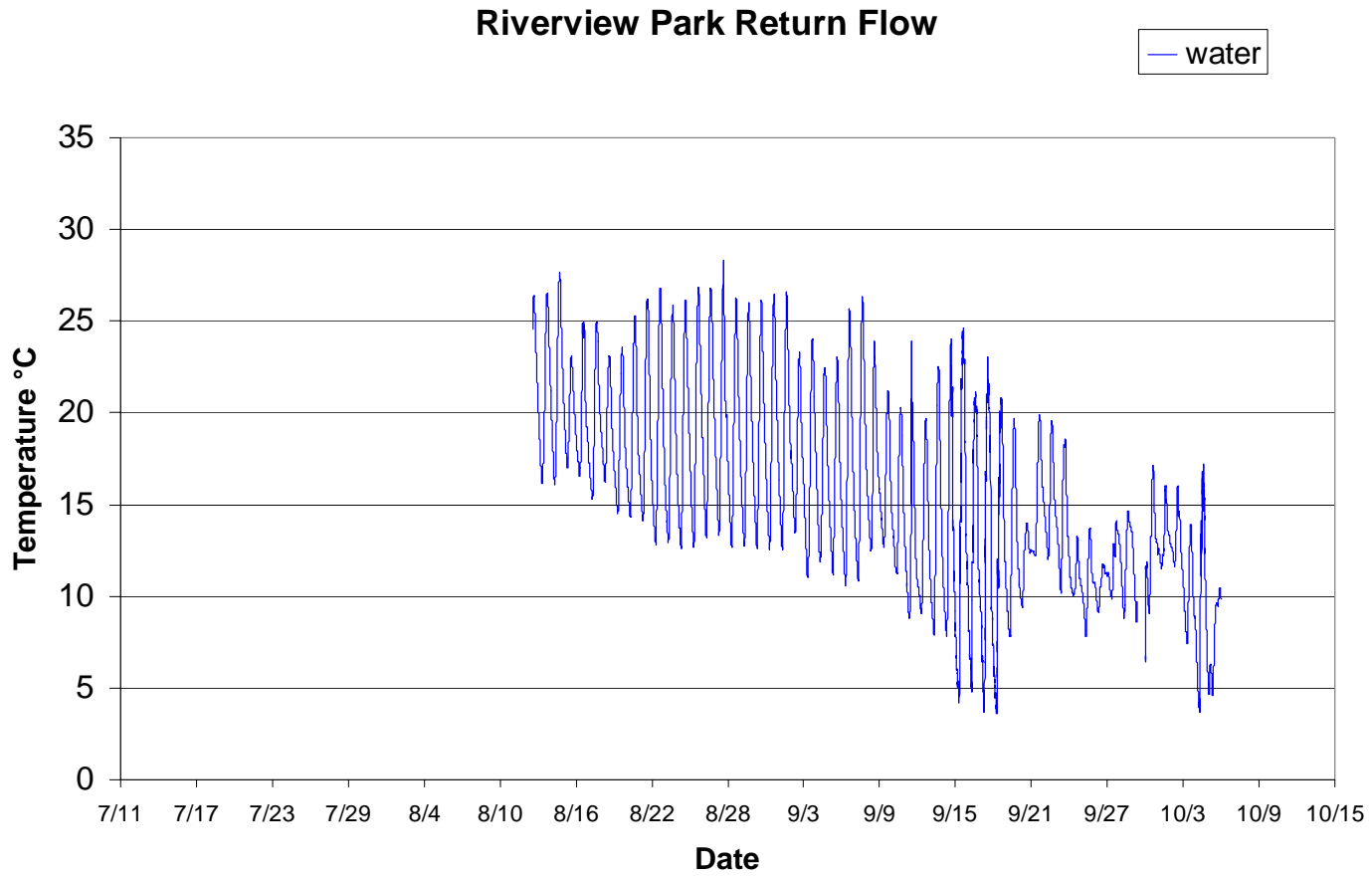


Figure 71-Water and streambed temperatures for Riverview Park return flow (upstream of Site 19)

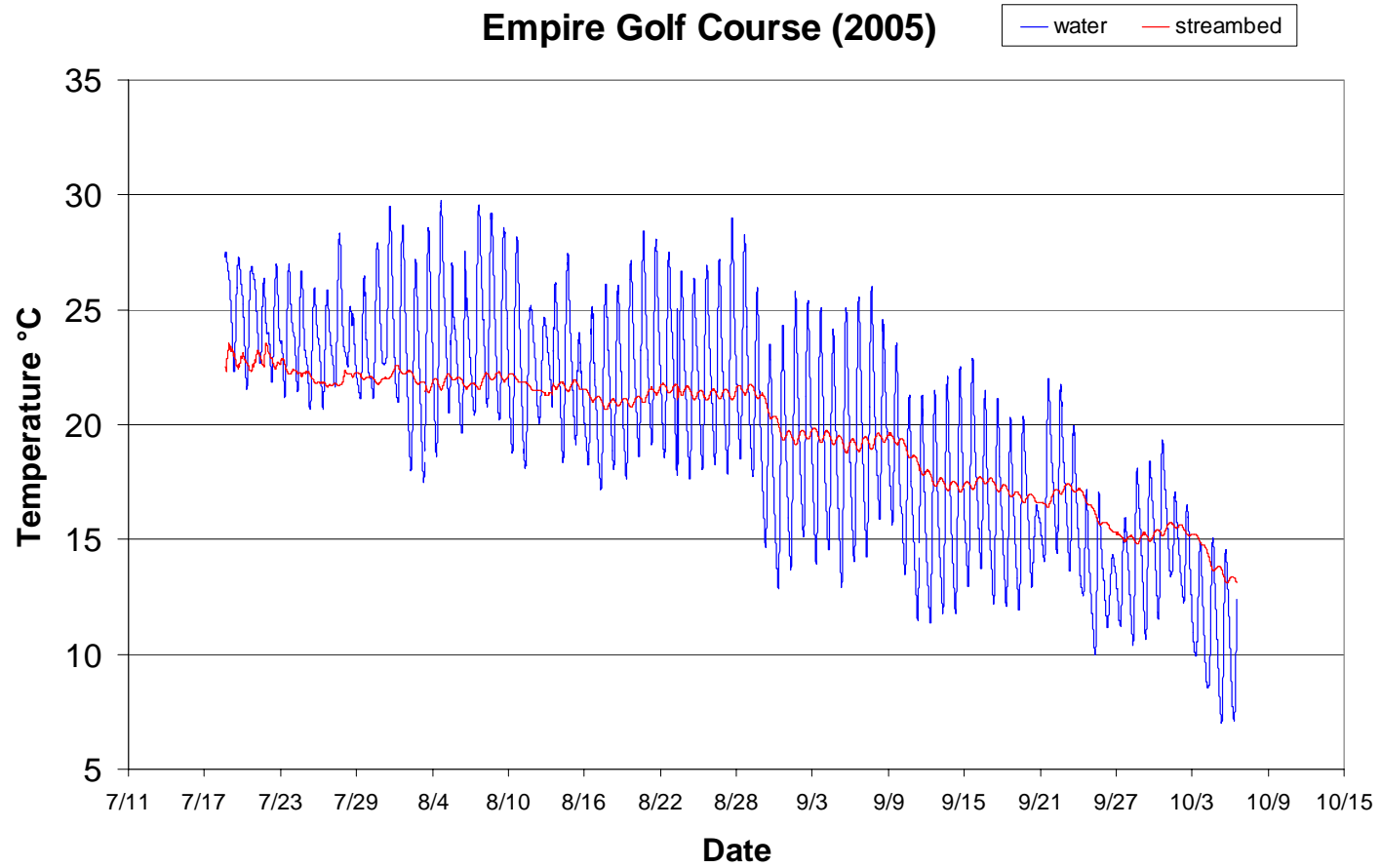


Figure 72-Water and streambed temperatures for Empire Golf Course (Site 20)

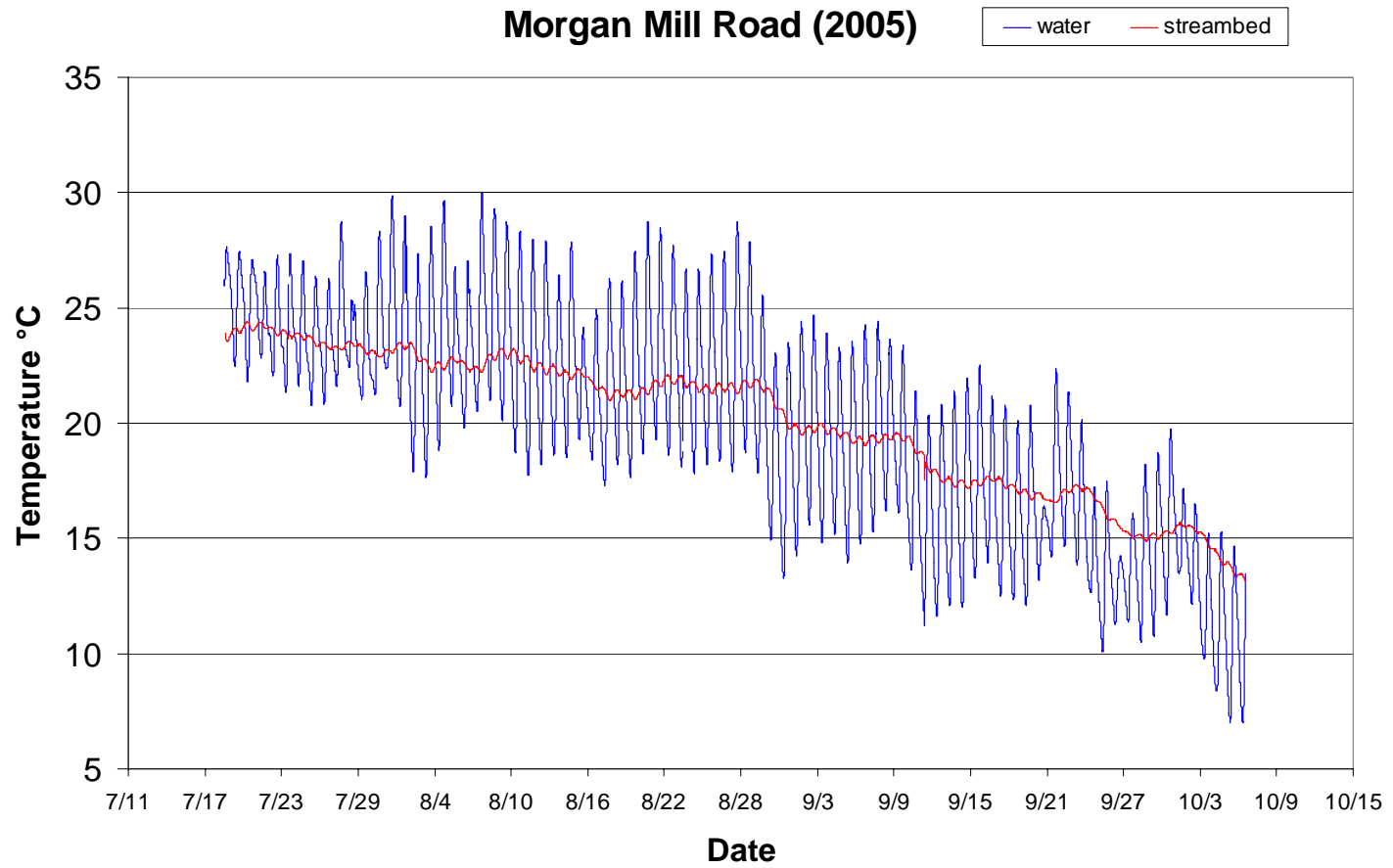


Figure 73-Water and streambed temperatures for Morgan Mill Road (Site 21)

9 Appendix C-Water Temperature Data (2006)

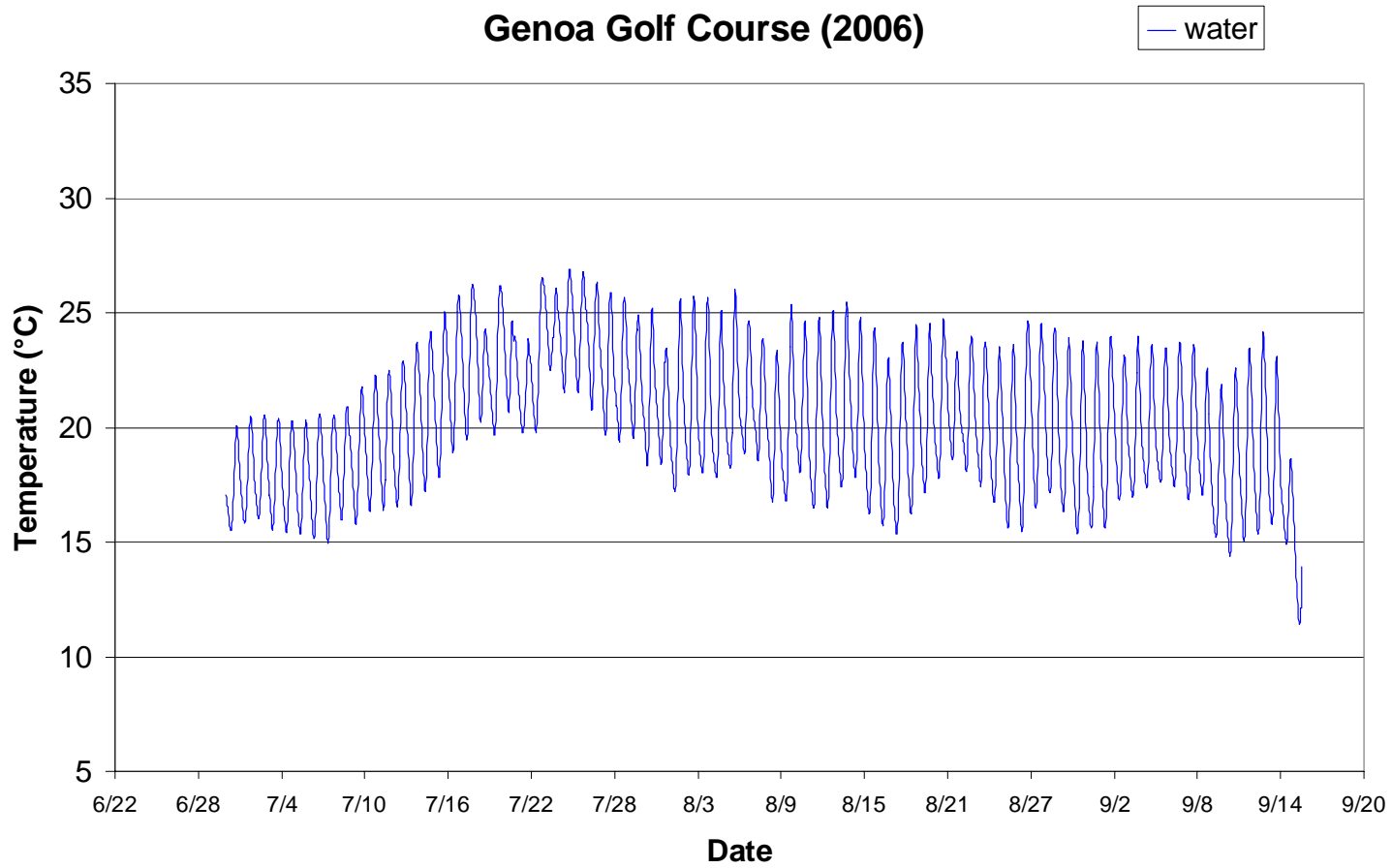


Figure 74-Water temperatures for Genoa Golf Course (Site 4)

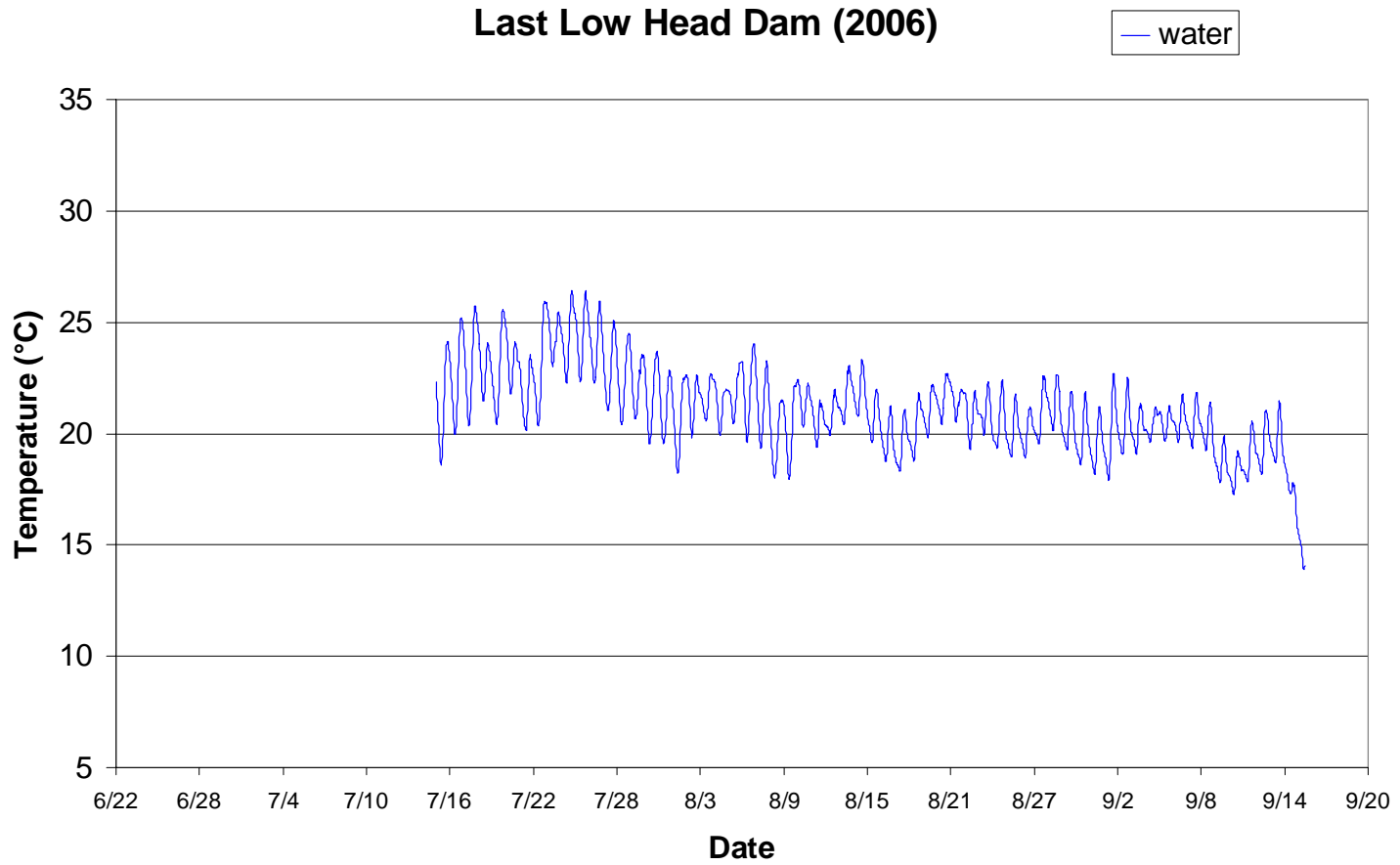


Figure 75-Water temperatures for Last Low Head Dam (Site 8)

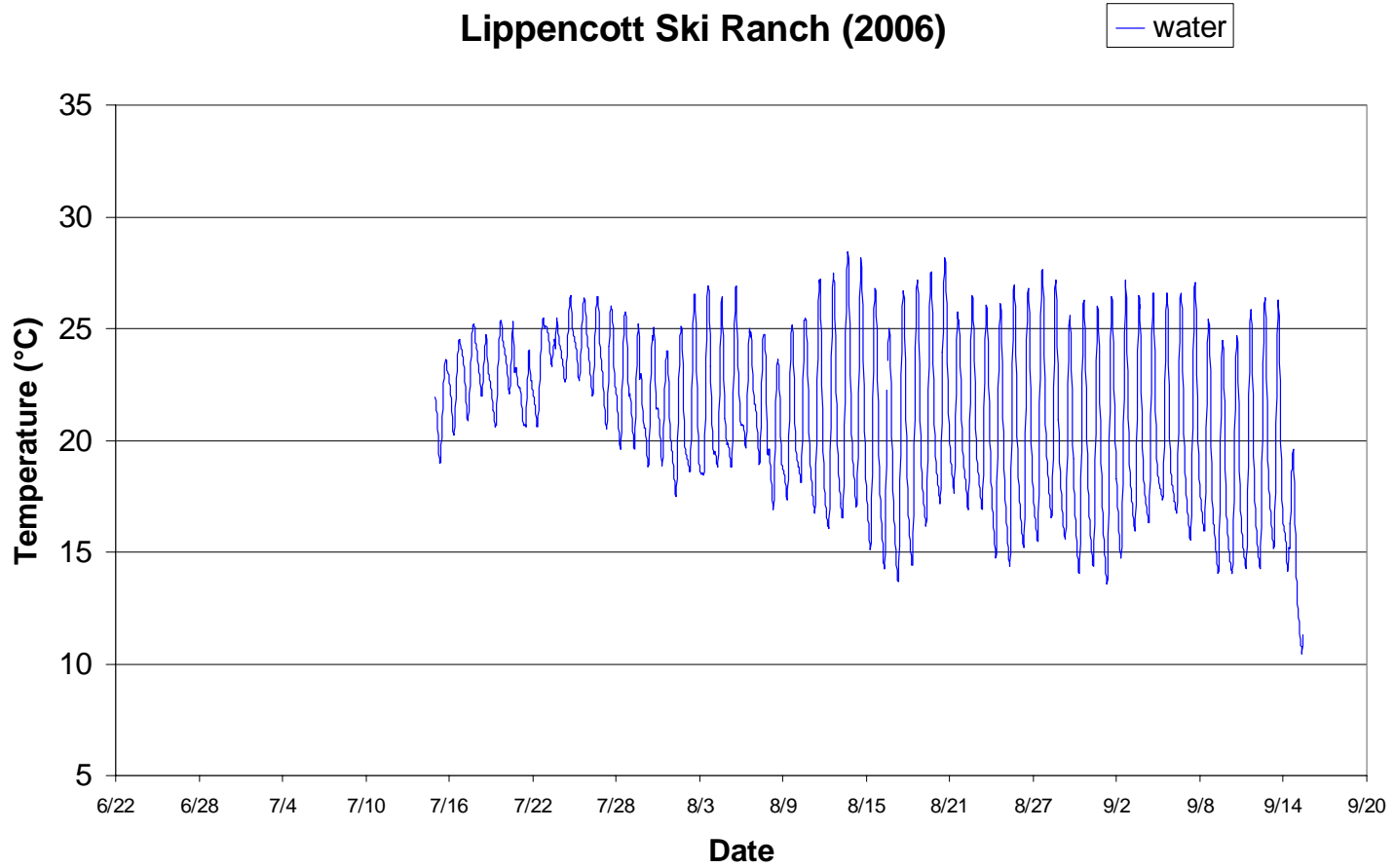


Figure 76-Water temperatures for Lippencott Ski Ranch (Site 10)

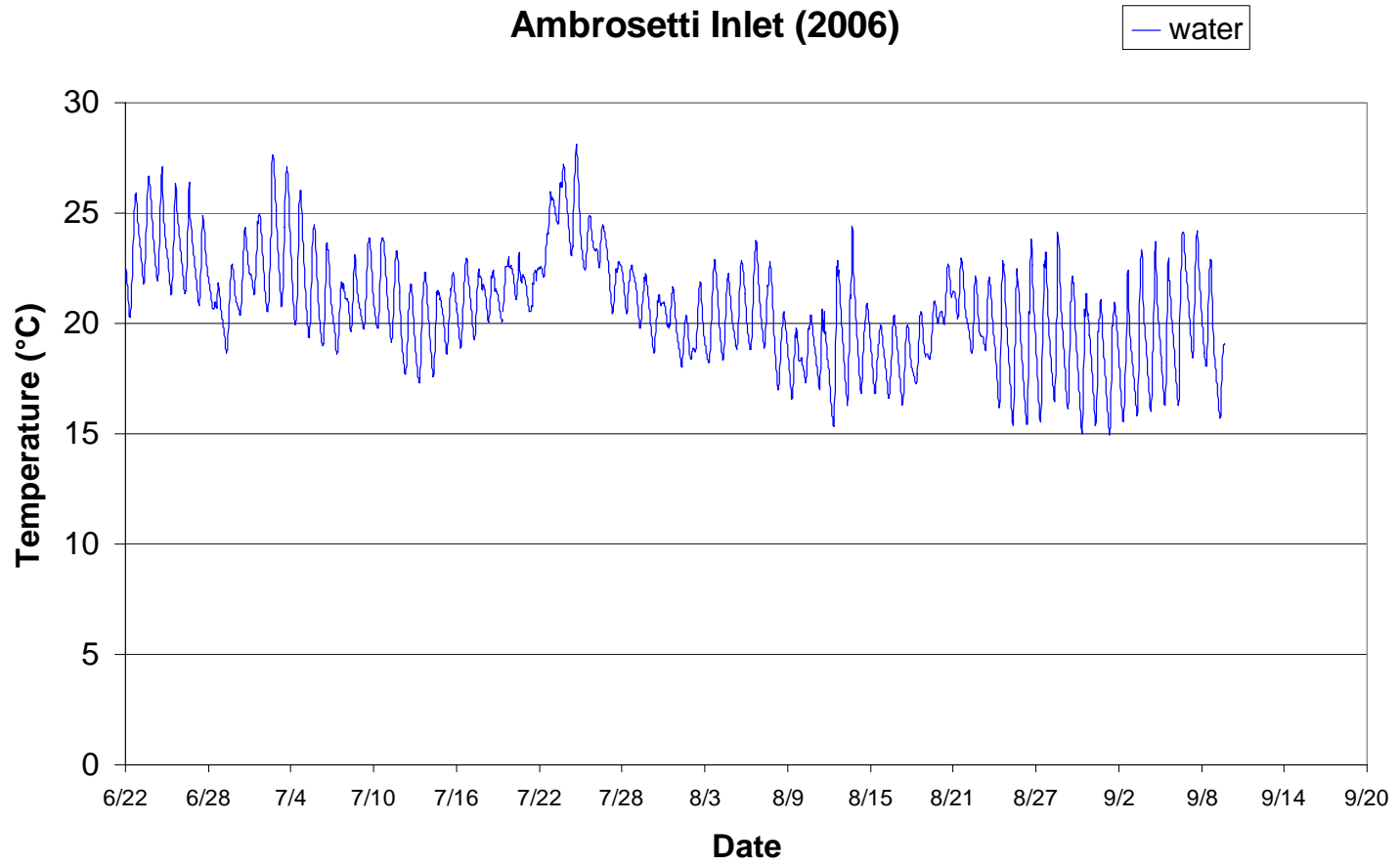


Figure 77-Water temperatures for Ambrosetti Creek Inlet (Site 11)

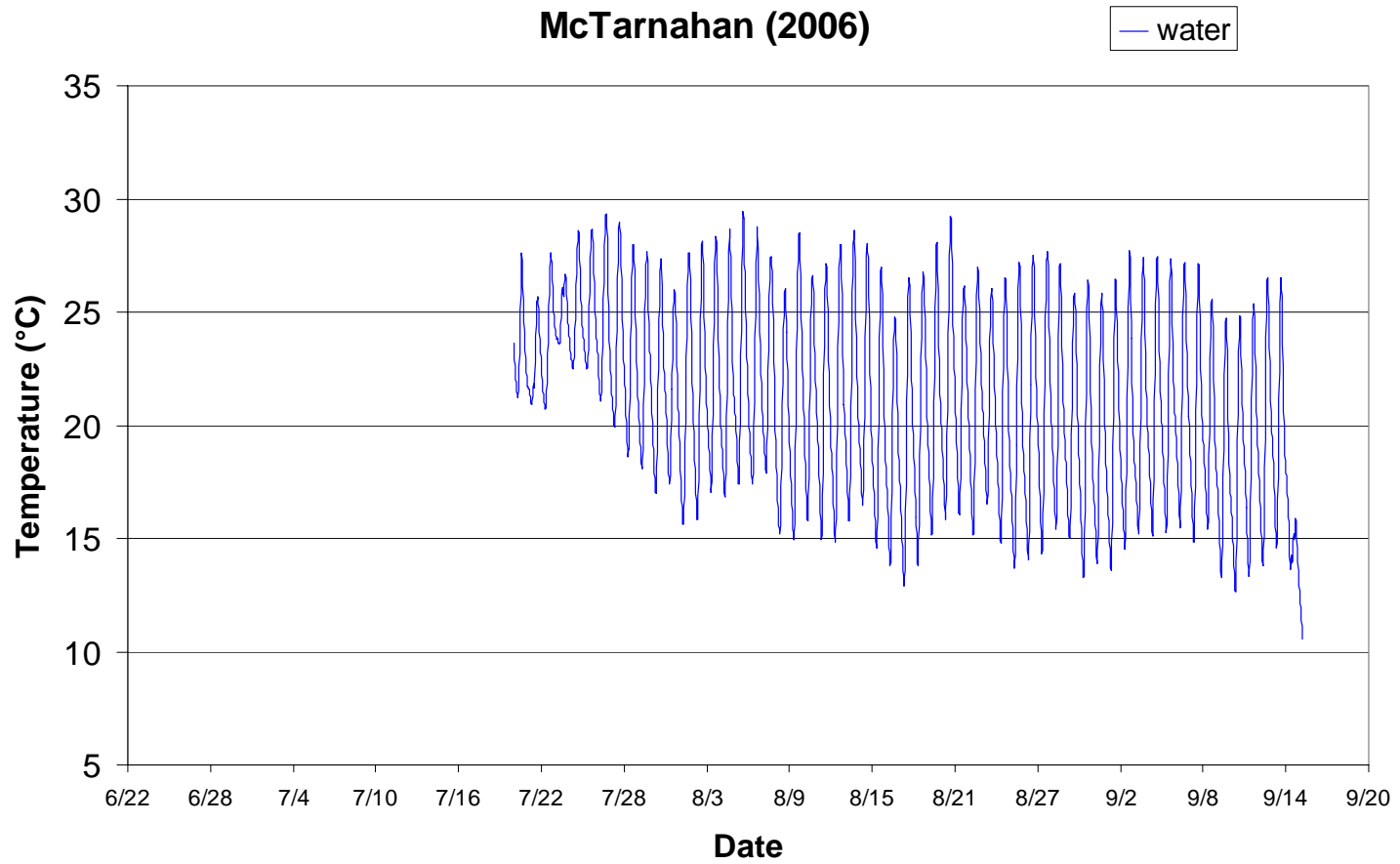


Figure 78-Water temperatures for McTarnahan (Site 15)

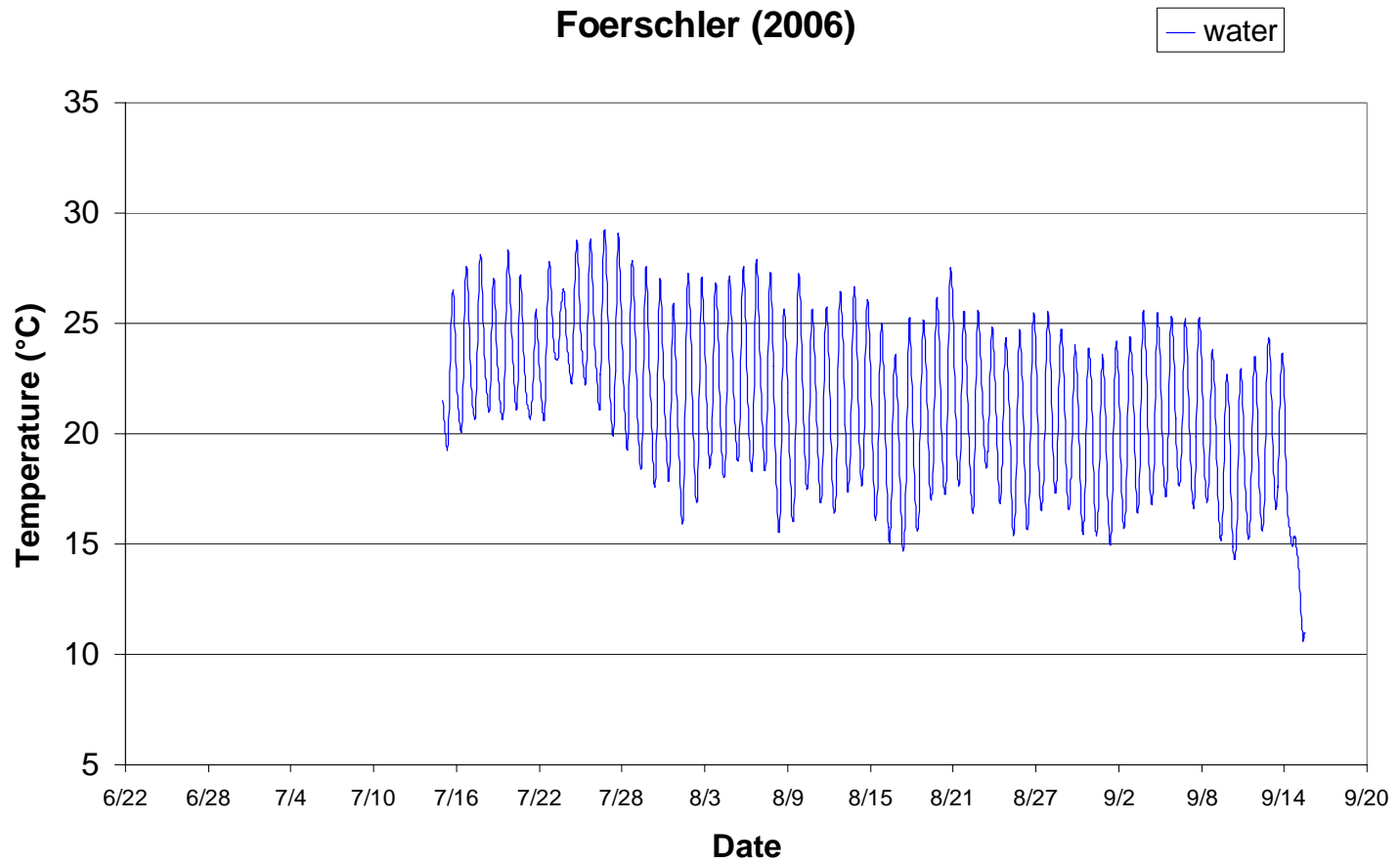


Figure 79-Water temperatures for Foerschler Ranch (Site 17)

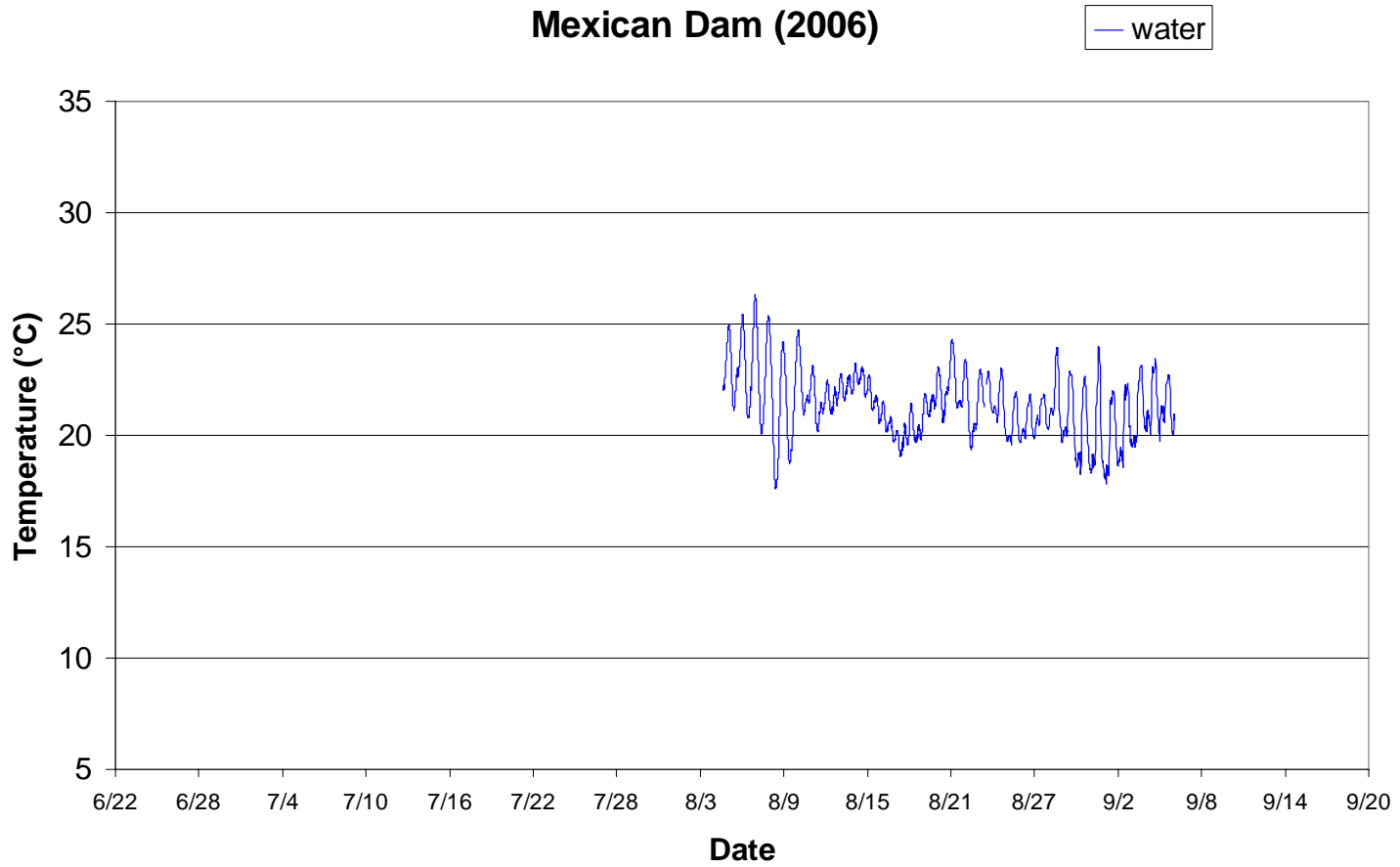


Figure 80-Water temperatures for Mexican dam (Site 18)

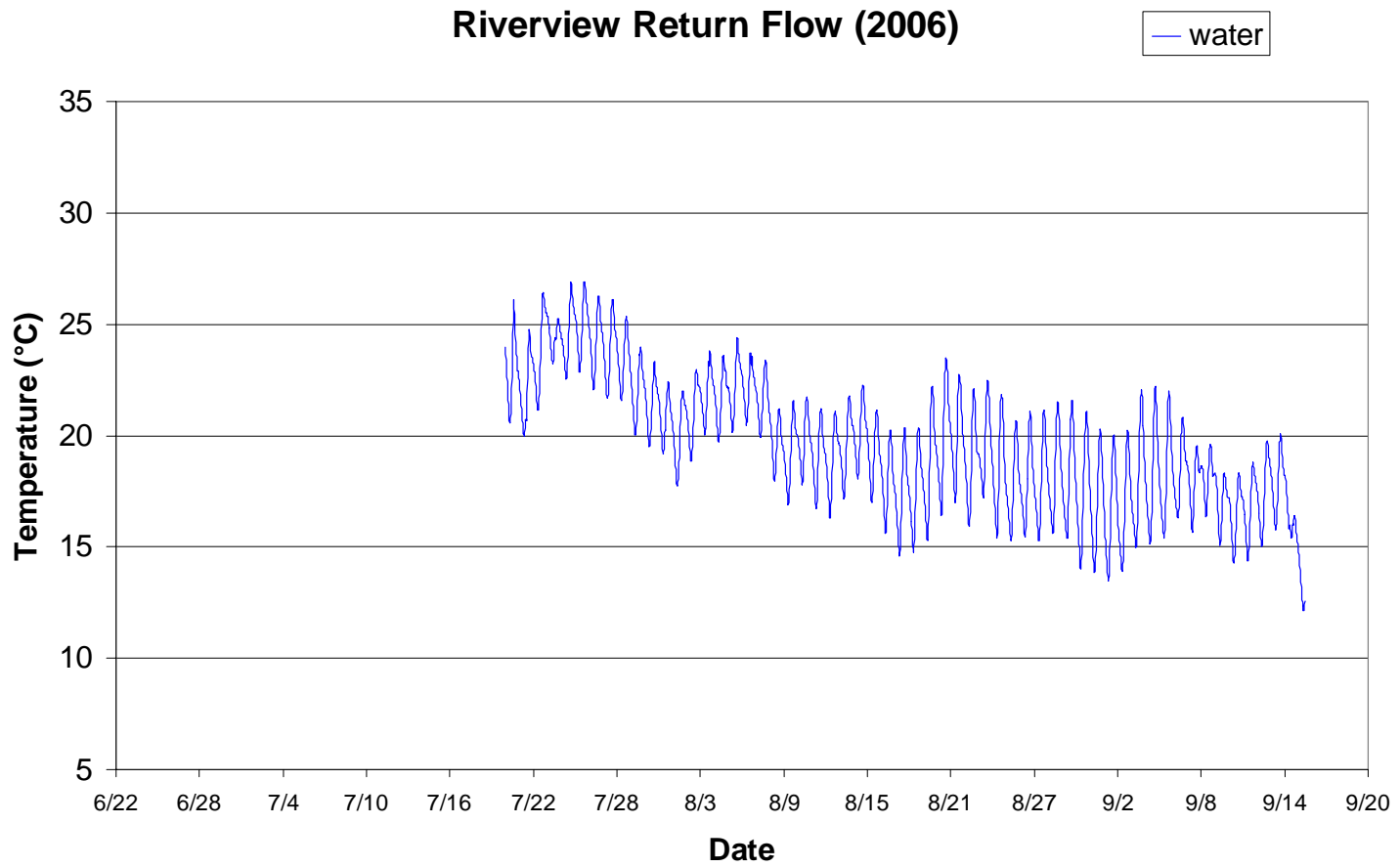


Figure 81-Water temperatures for Riverview park return flow (downstream of Site 19)

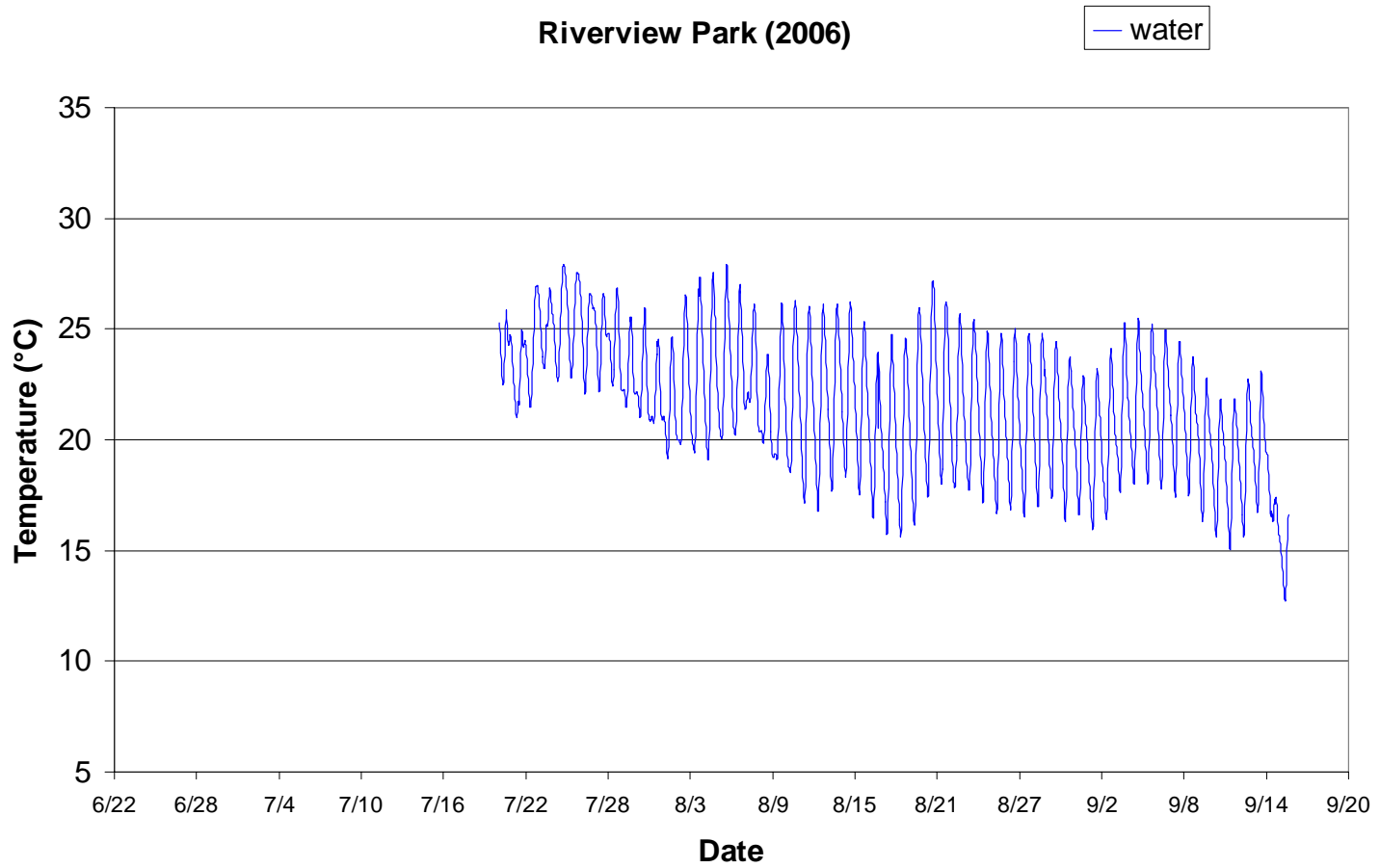


Figure 82-Water temperatures for Riverview Park (Site 19)

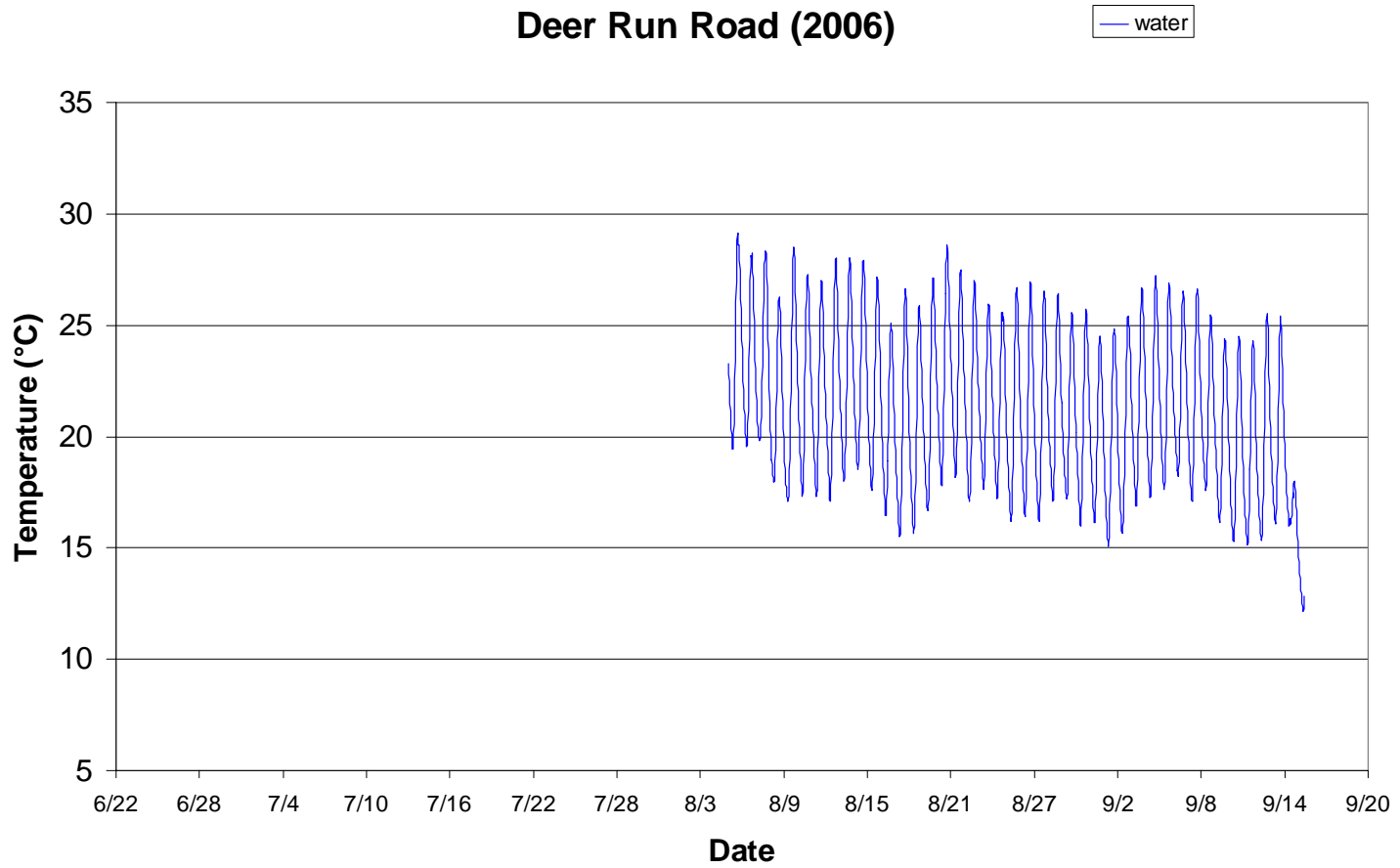


Figure 83-Water temperatures for Deer Run Road (Site 22)